Utrecht University

Master Thesis

Mathematical Sciences

Inverse Schrödinger Scattering for Seismic Imaging

Author
Kemal Raik

Supervisor
Dr. Tristan van Leeuwen

Second Reader
Dr. Paul Zegeling

August 14, 2017

Preface

The use of inverse scattering methods in seismic exploration is rapidly expanding. This generally involves classical wave equations which describe the traversion of waves through acoustic media. In particular, one may recover data of an inhomogeneous penetrable medium in the subsurface of the Earth by first probing it with an incident field and then measuring the reflected waves from some observation position. The data, however, is scattered and the objective of inverse scattering methods is thus to reconstruct the scattering potential of waves traversing the aforementioned scattering medium.

In my thesis, I treat the inverse Schrödinger scattering problem whereby we attempt to reconstruct the scattering potential of a medium from measurements of the medium response to a harmonic exitation which can be formulated by the Schrödinger equation. In quantum physics, this problem has been well treated and I draw parallels between the Schrödinger equation, for which there exist exact inversion methods[8], and the classical wave equation for which, in three dimensions at least, no exact inversion methods exist. Moreover, the inverse Schrödinger scattering problem is configured and thus generalised to the setting of seismic imaging.

In particular, I compare fast layer stripping algorithms which recursively reconstruct the scattering potential under the assumption of weak scattering and otherwise alongside integral equation based methods and also sampling schemes for reconstructing the potential in the frequency domain.

Acknowledgements

Firstly, I would like to express my gratitude to Dr. van Leeuwen for his guidance and assistance as my supervisor. This thesis begun from a paper he suggested (namely reference [7]) thus, over the subsequent months, pathing the way for me to become acquainted with the field of inverse problems. I would also like to thank Dr. Zegeling for being my second reader.

This thesis could not have been written without the company of my friends during the countless coffee breaks in between writing this thesis. Indeed, to quote the honourable Paul Erdős, *a mathematician is a machine for turning coffee into theorems.*[1] I also express my sincerest thanks to my family for their continual and endearing support, in spite of the distance.

My time in Utrecht, amidst the periods of intense studying, is littered with pleasant memories and I am grateful for my time here.

[1] *Alfréd Rényi*, `http://www-history.mcs.st-andrews.ac.uk/Biographies/Renyi.html`

Contents

Chapter 1

Preliminaries

1.1 Introduction

Scattering theory is the study of the effects of an inhomogeneous medium on an incident particle or wave. It is fundamental in computed tomography (CT) and other forms of medical imaging and also in physics and can, for example, answer questions such as "why is the sky blue?"; see *Rayleigh scattering*.

The theory of scattering consists of the direct scattering problem and the inverse scattering problem. In particular, a wave may be decomposed as $u = u_{\text{inc}} + u_{\text{sc}}$, where u_{inc} is the incident wave and u_{sc} is the scattered wave. The direct scattering problem is to determine u_{sc} given the incident wave u_{inc} and the governing equation of motion. The inverse scattering problem, on the other hand, is to determine the nature of the inhomogeneity given knowledge of the asymptotic behaviour of the scattered wave u_{sc}.

In the inverse scattering problem in seismic imaging, we are interested in determining properties of either a penetrable inhomogeneous medium or a bounded impenetrable obstacle. In order to retrieve this information, seismic surveys are conducted, for which we provide an illustration below

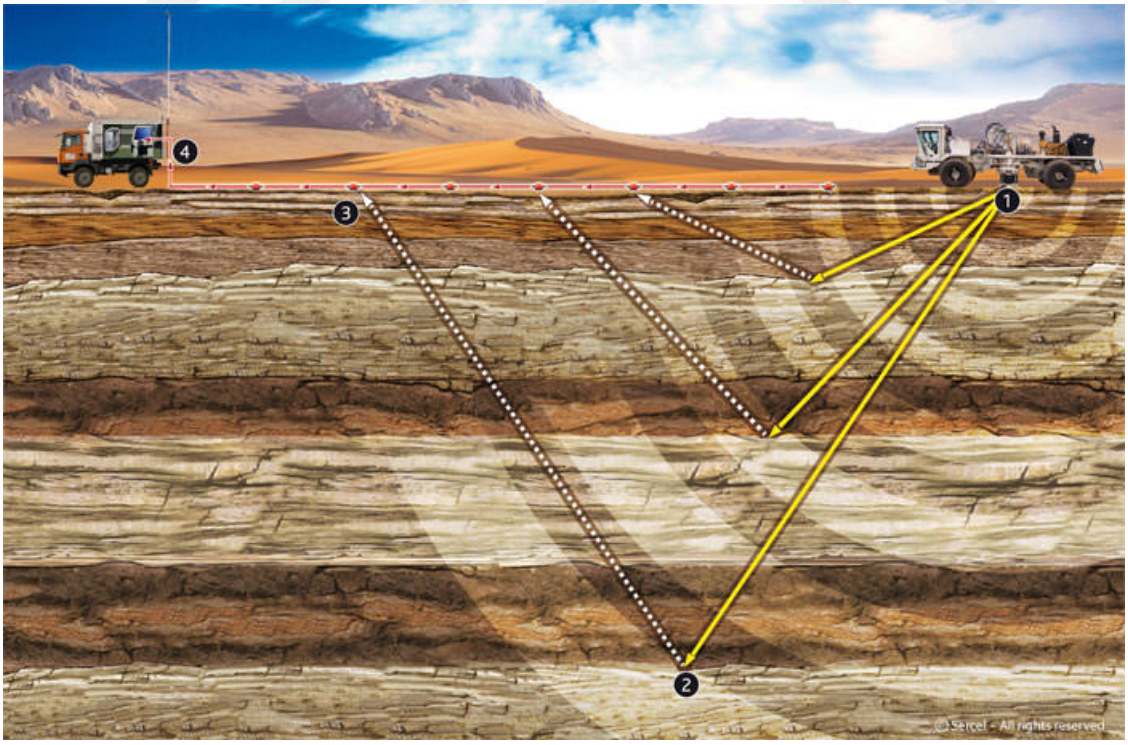

Figure 1.1: (1) source; (2) domain of the medium ; (3) receiver.

In particular, a seismic survey consists of an array *receivers* and a *source*. If the seismic survey is conducted on land, then the receivers are geophones and the source may be a thumper truck (as in the illustration) or the more rudimentary dynamite. If conducted on water, then the receivers and sources are generally hydrophones

and air guns respectively. The source emits a wave which traverses the medium and the receiver(s) measure the subsequently reflected waves.

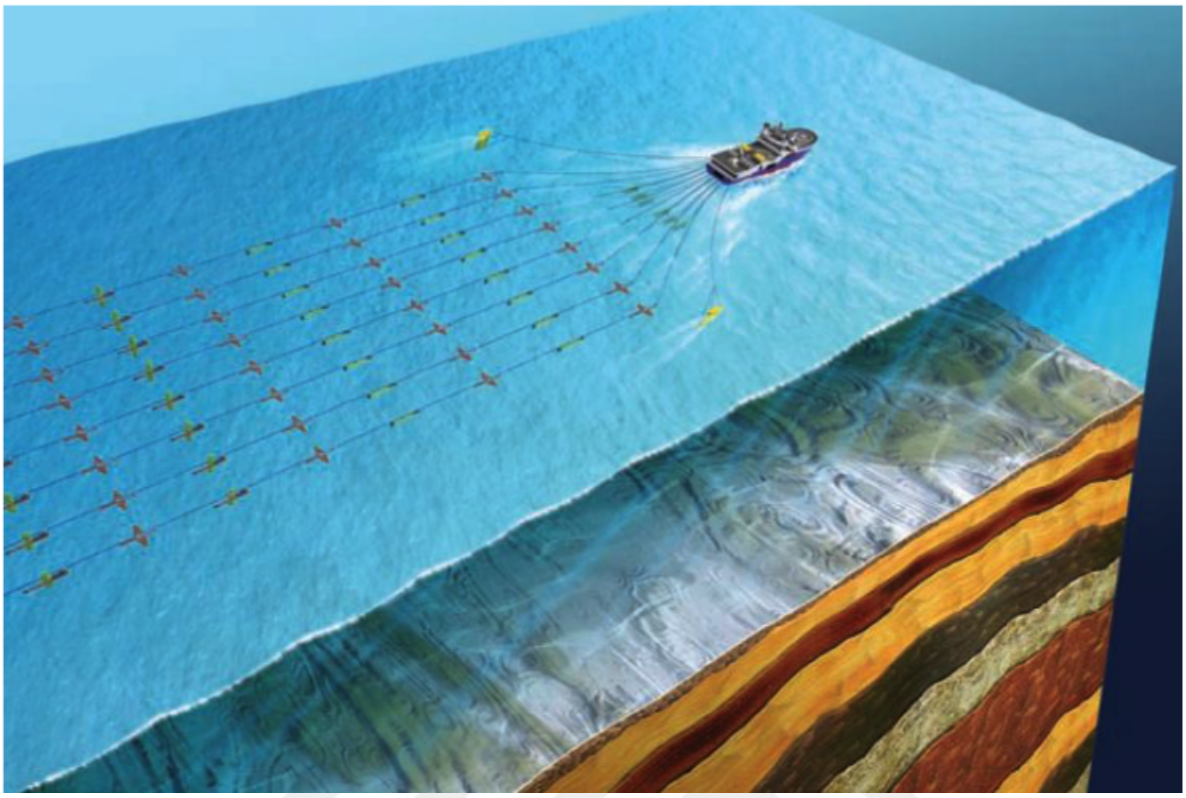

Figure 1.2: The above illustration is of a seismic survey conducted over sea. This generally consists of a tugboat which pulls air guns firing incident waves into the surface beneath the water and arrays of receivers which record the reflections. In this image, the silver objects closest to the boat would be the air guns and the hydrophones are the remaining objects supported by the buoys.

In this thesis, we concern ourselves with retrieving the scattering of waves traversing an inhomogeneous penetrable medium with compact support. In our model, we assume that there is a single source and receiver respectively whereby the source emits only a single incident wave field.

In classical inverse scattering for seismic imaging, the governing equation of motion for the waves is the acoustic wave equation (1.7). In this thesis, however, we wish to solve an inverse *Schrödinger* scattering problem in the context of seismic imaging whereby we try to reconstruct the scattering potential of an inhomogeneous isotropic acoustic medium from surface measurements of the medium response to a harmonic excitation which can be formulated by the Schrödinger equation:

$$(\Delta + \omega^2 m(x) - r(x))\hat{u}(\omega, x) = 0, \qquad (\omega \in \mathbb{R}_+, x \in \mathbb{R}^n) \tag{1.1}$$

where $\hat{u} : \mathbb{R}_+ \times \mathbb{R}^n \to \mathbb{R}$ is the wave field, $m \in C^\infty(\mathbb{R}^n)$ describes the speed of sound travelling through the medium, ω is the temporal frequency and $r \in C_c^\infty(\mathbb{R}^n)$ is the real valued compactly supported and smooth scattering potential. We also refer to $\mathbb{D} := \operatorname{supp} r$ as the domain of the scatterer.

In general, one cannot speak about inverse problems without referring to ill-posedness, as the great majority of inverse problems are indeed ill posed.

Definition 1 (Hadamard Well-Posed)**.** *A problem is said to be well-posed if*

(a) a solution exists;

(b) the solution is unique;

(c) the solution depends continuously on the data.

If a problem is not well-posed then it is called ill-posed.

In operator theoretic terms, the above may be restated as

Definition 2. *Let $A : U \subset X \to V \subset Y$ be an operator from a subset U of a normed space X into a subset V of a normed space Y. Then the equation*

$$A(\psi) = f$$

is called well-posed if $A : U \to V$ is bijective and the inverse operator $A^{-1} : V \to U$ is continuous. Otherwise the equation is called ill-posed. [9]

Note that here we interpret A as the operator for the governing equation of motion, ψ is the unknown and f is the data. Thus an inverse problem can be interpreted as follows: given $f \in Y$, find $\psi \in X$ such that $A(\psi) = f$. The solution of $A(\psi) = f$, however, need not be close to the solution of $A(\psi) = f^\varepsilon$ if $\|f - f^\varepsilon\| \leq \varepsilon$, where $\varepsilon > 0$ is the measurement error.

A regularisation scheme is then a family of bounded linear operators $R_\lambda : Y \to X$, with $\lambda > 0$, such that $(R_\lambda A)(\psi) \to \psi$ as $\lambda \to 0$ for all $\psi \in X$, i.e. $R_\lambda \to A^{-1}$ as $\lambda \to 0$ pointwise. In general, one regularises to make sure that small errors in the data will cause only small errors in the solution. There exist various regularisation schemes in the literature, most notably, perhaps, *Tikhonov regularisation* (which, incidentally, is known to produce smooth reconstructions). We do not state the scheme here and instead refer the reader to reference [2].

The solution of the inverse Schrödinger scattering problem in one dimension is not unique if there are *bound states*. For the one dimensional case, we provide a brief discussion of bound states in the form of Proposition 10. The same is true in three dimensions. We will not define bound states explicitly, as the definition is rather involved, but it is normally enough for the wave fields to decay rapidly enough so that they are integrable. According to reference [8], it is normally enough to assume that $r \geq 0$ and this is indeed the assumption which we make throughout the thesis. Consequently we do not concern ourselves with questions of ill-posedness in this thesis and refer the interested reader to reference [8] for a more in-depth discussion of the well-posedness of the inverse Schrödinger scattering problem.

In the proceeding section, i.e. §1.2, we set up the forward scattering problem.

§2 assumes single scattering (i.e. the *Born approximation*) and the setting of §2.1 is one dimensional homogeneous media. In this setting, we derive the data function in §2.1.1 and then in §2.2.2 solve the inverse scattering problem of acquiring the scattering potential. We also give the *Shannon-Nyquist interpolation formula* for reconstructing the scattering potential if the data function is sampled (i.e. discrete). We derive the scattering potential via a single pass of the *layer stripping* algorithm, which is a fast method and finally we provide numerical simulations for the aforementioned algorithms.

The setting for §2.2 is then three dimensional homogeneous media and we acquire the data function (in the frequency domain) in §2.2.1 using a *far field* approximation. Then in §2.2.2 we explore various sampling schemes through which we attempt to reconstruct the scattering potential via interpolation methods in the frequency domain and again provide numerical simulations. In §2.2.3 we adopt a depth migration model and introduce the *double square root equation*.

§3 no longer assumes single scattering, inducing the *Born series*. The setting of §3.1 is one dimensional homogeneous media and in fact we do not stray from this setting throughout the chapter. In §3.1.1 we introduce the layer stripping algorithm and in §3.1.2 provide numerical simulations which implement various interpretations of the aforementioned algorithm for when we assume the *very weak scattering condition* (i.e. single scattering) and otherwise. We also test numerically the Shannon-Nyquist interpolation formula from the previous chapter on multiply scattered data.

1.2 Mathematical Model

The wave field $u = u_{\text{inc}} + u_{\text{sc}}$ may be decomposed in $\mathbb{R}^n$ as the superposition of an incident wave field and a scattered wave field which satisfy

$$\begin{cases} (\Delta + \omega^2 m(x))\hat{u}_{\text{inc}}(\omega, x) = 0, \\ (\Delta + \omega^2 m(x))\hat{u}_{\text{sc}}(\omega, x) = r(x)\hat{u}(\omega, x), \\ \lim\limits_{\|x\|\to\infty} \|x\|^{\frac{n-1}{2}} \left(\dfrac{\partial}{\partial\|x\|}\hat{u}_{\text{inc/sc}}(\omega, x) - \dfrac{i}{\omega\sqrt{m(x)}}\hat{u}_{\text{inc/sc}}(\omega, x) \right) = 0, \end{cases}$$

uniformly for all directions $\xi = x/\|x\| \in \mathbb{S}^{n-1}$, where the partial differential equations are homogeneous and inhomogeneous Helmholtz equations respectively.[9] We also have the boundary condition at infinity, which is

called the Sommerfeld radiation condition. This ensures the uniqueness of the wave field u in an unbounded domain and subsequently also u_{inc} and u_{sc}. The incident wave field $u_{\text{inc}} : \mathbb{R}_+ \times \mathbb{R}^n \to \mathbb{R}$ is the part of the wave field which is undisturbed by the scatterer and the scattered field $u_{\text{sc}} : \mathbb{R}_+ \times \mathbb{R}^n \to \mathbb{R}$ constitutes the rest of the wave field. In particular, we probe the medium with the plane waves $\hat{u}^{\pm}_{\text{inc}}(\omega, x) = e^{\pm i\omega x\sqrt{m(x)}}$ for $n = 1$ and $\hat{u}^{\pm}_{\text{inc}}(\omega, x) = e^{\pm i\omega\xi\cdot x\sqrt{m(x)}}$ for $n = 3$, where $\xi \in \mathbb{S}^2$ is directed towards the scattering medium.

The response $\widehat{G}\big|_{x-x'}$ of the scattering medium at the location $x = x'$ may be formulated as:

$$\begin{cases} (\Delta + \omega^2 m(x))\widehat{G}\big|_{x-x'} = \delta_{x-x'}, \\ \lim\limits_{\|x\|\to\infty} \|x\|^{\frac{n-1}{2}} \left(\dfrac{\partial}{\partial\|x\|}\widehat{G} - \dfrac{i}{\omega\sqrt{m(x)}}\widehat{G} \right) = 0, \end{cases}$$

uniformly in all directions ξ, where $\delta_{x-x'}$ represents an impulse at the location $x = x'$ and $\widehat{G}$ is the response of this impulse satisfying the Sommerfeld radiation condition, ensuring that the waves are outward propagating.

Remark. *Note that $\delta \in \mathcal{S}'(\mathbb{R}^n)$ is a tempered distribution as opposed to a function and we opt to treat this in a particularly rigorous manner. For the reader who is unacquainted with the language of distributions (a.k.a. generalised functions), we refer to the appendix.*

Definition 3 (Helmholtz Operator)**.** *The Helmholtz operator*

$$\begin{aligned} \mathcal{L} : \mathcal{S}'(\mathbb{R}_+ \times \mathbb{R}^n) &\to \mathbb{C} \\ E &\mapsto (\Delta - \omega^2 m(x))E, \end{aligned}$$

is a linear partial differential operator acting a priori on the space of tempered distributions.

Definition 4 (Fundamental Solution)**.** *A fundamental solution of the Helmholtz operator $\mathcal{L} : \mathcal{S}'(\mathbb{R}_+ \times \mathbb{R}^n) \to \mathbb{C}$ is a tempered distribution $E \in \mathcal{S}'(\mathbb{R}_+ \times \mathbb{R}^n)$ which satisfies*

$$\mathcal{L}E = \delta,$$

where δ is the Dirac measure at the origin.

Thus we may observe that $\widehat{G} \in \mathcal{S}'(\mathbb{R}_+ \times \mathbb{R}^n)$ is a fundamental solution of the Helmholtz operator. Moreover, since it is defined in the frequency domain, we may assume that it has a well defined Fourier transform and for that reason we have been able to assume that it is at least of the tempered distribution class (since fundamental solutions belong a priori to the general class of distributions). In fact, $\widehat{G}$ is the *Green's function* of the Helmholtz operator. Note that Green's functions are defined to be fundamental solutions plus additional boundary conditions. In this case, the boundary condition is the aforementioned Sommerfeld radiation condition. For example, one may note that in homogeneous media (i.e. for constant m), the Green's functions for the three dimensional Helmholtz operator is a spherical waves which propagates with velocity equal to the wave speed profile of the medium. We will derive this explicitly in the subsequent text.

Since the Helmholtz operator $\mathcal{L}$ is a linear partial differential operator, we may infer the scattered field $\hat{u}_{\text{sc}}$ in terms of a convolution with the Green's function:

Proposition 5. *The scattered wave field is given by*

$$\hat{u}_{sc} = \widehat{G} *_x r\hat{u}, \tag{1.2}$$

where $*_x$ denotes convolution with respect to the x variable.

Proof. For all test functions $\phi \in C_c^\infty(\mathbb{R}^n)$, we may compute

$$\begin{aligned} \langle \mathcal{L}\hat{u}_{\text{sc}}, \phi\rangle &= \langle \mathcal{L}(\widehat{G} *_x r\hat{u}), \phi\rangle \\ &= \langle (\mathcal{L}\widehat{G}) *_x r\hat{u}, \phi\rangle \\ &= \langle \delta *_x r\hat{u}, \phi\rangle \\ &= \langle r\hat{u}, \phi\rangle, \end{aligned}$$

which is precisely equation the governing equation for the scattered field. □

The total wave field may therefore be rewritten as

$$\hat{u} = \hat{u}_{\text{inc}} + \widehat{G} *_x r\hat{u} \qquad \text{in } \mathbb{R}^n, \tag{1.3}$$

which is called the *Lippmann-Schwinger equation*. Moreover, this holds inside and outside the support of the scattering potential, thus in all $\mathbb{R}^n$. This is clear, since the support of r, which we called $\mathbb{D}$, is compact.

Proposition 6. *The Green's function of the n-dimensional Helmholtz operator in homogeneous media (e.g. $m(x) = c^{-2}$ for all $x \in \mathbb{R}^n$) is given by*

$$\boxed{\widehat{G}(\omega, x - x') = -\frac{i}{4}\left(\frac{\omega}{2\pi c\|x - x'\|}\right)^{n/2-1} H^{(1)}_{n/2-1}\left(\frac{\omega\|x - x'\|}{c}\right)} \tag{1.4}$$

where $H^{(1)}_{n/2-1}$ is the Hankel function of the first kind of order $n/2 - 1$.[1]

Note that in inhomogeneous media, we cannot necessarily analytically derive the Green's function. In this thesis, however, we consider only the case whereby the medium is homogeneous.

In particular, since $\widehat{G}$ is in fact a function for all $n \in \mathbb{N}$, we may rewrite the equation for the scattered field as

$$\boxed{\hat{u}_{\text{sc}}(\omega, x) = \int_{\mathbb{R}^n} \widehat{G}(\omega, x - x')r(x')\hat{u}(\omega, x')\,\mathrm{d}x'} \tag{1.5}$$

where the above thus describes the surface measurements at a point x of the medium response to an excitation.

We measure the scattered field at any given observation position and thus, having derived an explicit representation, we can now define our data function:

Definition 7 (Data Function)**.** *For a fixed observation position $x_0 \in \mathbb{R}^n \setminus \mathbb{D}$, the data is given by*

$$\begin{aligned} &d : \mathbb{R}_+ \to \mathbb{R} \\ &\quad t \mapsto u_{sc}(t, x_0) = \mathcal{F}^{-1}\left\{\hat{u}_{sc}(\cdot, x_0)\right\}(t) = \mathcal{F}^{-1}\left\{\int_{\mathbb{R}^n} \widehat{G}(\cdot, x_0 - x')r(x')\hat{u}(\cdot, x')\,\mathrm{d}x'\right\}(t), \end{aligned} \tag{1.6}$$

The inverse scattering problem is then to recover r from the data. In this thesis, I aim to provide answers for whether we can retrieve the scattering potential from scattered data in various settings. I will compare two algorithms, namely Fourier inversion and *layer stripping* (also referred to as *downward continuation* in seismic literature) on a series of model problems of increasing complexity: single scattering in one dimension, *2.5D* and multiple scattering in one dimension, *etcetera*, and for various measurements.

Note that deducing (1.5) is the *forward scattering problem*, which is computationally expensive to solve and is to be derived before tackling the inverse problem. The layer stripping algorithm is a *fast* algorithm which exploits the Toeplitz or Hankel structure of the kernels of the Gelfand-Levitan (3.5) and Marchenko equations for quantum scattering respectively which, incidentally, are both integral equations. In reference [15], it is shown that the aforementioned equations may be reduced to differential equations (3.8) which require significantly fewer computations to solve. In particular, the layer stripping algorithm (3.10) solves these differential equations recursively and reconstructs r with greater efficiency than via more conventional means.[7]

Definition 8 (Toeplitz Matrix)**.** *An $N \times N$ matrix $\mathrm{A} = (t_{k,\ell})_{k,\ell=1}^N$ is said to be Toeplitz if it is constant along all its diagonals, i.e. if there exist numbers $\tau_{-N+1}, \tau_{-N+2}, \cdot, \tau_0, \cdots, \tau_{N-1}$ such that*

$$t_{k,\ell} = \tau_{k-\ell}, \qquad k, \ell = 1, 2, ..., N.$$

[14]

The numerical performance of these algorithms appear yet to be examined and I hope to draw conclusions through comparisons with more conventional methods. In particular, I compare interpolation formulae which reconstruct r from sampled d and finite difference schemes for the layer stripping method. Note that in the subsequent text, we define what it means for a function to be *sampled*.

[1] This derivation is courtesy of the user `Mark Viola` at `math.stackexchange.com` which can be found on: `https://math.stackexchange.com/questions/2254939/fundamental-solution-for-helmholtz-equation-in-higher-dimensions`

1.3 Additional Preliminaries

The time domain version of the Schrödinger equation (1.1) is the *plasma wave equation*

$$\left(\Delta - m(x)\frac{\partial^2}{\partial t^2} - r(x)\right) u(t,x) = 0, \tag{1.7}$$

which, incidentally, models the propagation of electromagnetic waves in the ionosphere.[13]

Solutions of (1.7) are related to those of (1.1) by an inverse Fourier transform with respect to time and we observe that (1.7) is a hyperbolic equation. We will switch freely between the frequency domain and the time domain, and back again.

We may also (partially) infer equation (1.1) from the *acoustic wave equation*, which is the governing equation for waves travelling through an acoustic medium

$$\left(\Delta - m(x)\frac{\partial^2}{\partial t^2}\right) u(t,x) = 0, \tag{1.8}$$

where m, again, describes the speed through which waves traverse the medium.

In particular, we may apply the Fourier transform with respect to t, which yields the following:

$$\begin{aligned}
&(\Delta + \omega^2 m(x))\hat{u}(\omega,x) = 0 \\
\iff &(\Delta + \omega^2 m(x) + \omega^2 - \omega^2)\hat{u}(\omega,x) = 0 \\
\iff &(\Delta + \omega^2 m(x) - \omega^2)\hat{u}(\omega,x) = -\omega^2\hat{u}(\omega,x) \\
\iff &(\Delta + \omega^2 (m(x) - 1))\hat{u}(\omega,x) = -\omega^2\hat{u}(\omega,x) \\
\iff &(\Delta + \omega^2 (-r(x)))\hat{u}(\omega,x) = -\omega^2\hat{u}(\omega,x) \\
\iff &(\omega^2 r(x) - \Delta)\hat{u}(\omega,x) = \omega^2\hat{u}(\omega,x),
\end{aligned}$$

where $r(x) = 1 - m(x)$.

We observe that this equation resembles (1.1), except that $r(x)$ is replaced by $\omega^2 r(x)$ and $\omega^2\hat{u}(\omega,x)$ is replaced by $\omega^2 m(x)\hat{u}(\omega,x)$. If $r(x)$ is replaced by a function that depends on ω (e.g. $\omega^2 r(x)$), then all the following results that do not refer to high frequency asymptotics or completeness still hold. This can be seen by simply replacing $\omega^2 r(x)$ by $r_0 := \omega_0^2 r(x)$, so that r_0 is independent of ω and is consistent with $\omega^2 r(x)$ at $\omega = \omega_0$. However, for high frequency asymptotics, this will be quite different and the results at this time are not fully known.[8]

Since waves propagating through acoustic media are modelled via the acoustic wave equation, the observation above is particularly insightful with regards to formulating the analogy between Schrödinger scattering and seismic scattering.

Chapter 2

Single Scattering

We may linearise the inverse scattering problem by utilising the single scattering approximation, also known as the *Born approximation*:

Definition 9 (Born Approximation)**.** *Approximating the total wave field as $u \approx u_{inc}$ for all $x' \in \mathbb{D}$ yields the Born approximation.*

Note that in the following text we abuse notation by writing "$u = u_{\text{inc}}$".

2.1 Homogeneous media in one dimension

The simplest setting for the inverse scattering problem is that of a one dimensional homogeneous medium. As noted in reference [1], *one dimensional models have historically played an important role in mathematical physics by providing a starting point for solving higher dimensional problems*, so this is how we will employ them here. For homogeneous media, m is constant, so we let $m(x) = c^{-2} > 0$ for all $x \in \mathbb{R}$.

Let $r \in C_c^\infty(\mathbb{R})$ be supported on a compact interval, say $[-M, M] \subset \mathbb{R}$. Then consider the plasma-wave equation

$$\left(\Delta - \frac{1}{c^2}\frac{\partial^2}{\partial t^2}\right) u(t,x) = r(x)u(t,x), \qquad x,t \in \mathbb{R}, \tag{2.1}$$

for the wave field $u : \mathbb{R}_+ \times \mathbb{R} \to \mathbb{R}$.

Notice that if $r(x) = 0$ for all $x \in \mathbb{R}$, then we would have the acoustic wave equation and would thus have general solutions of the form

$$u(t,x) = f(x - ct) + g(x + ct),$$

for arbitrary $f, g \in C^2(\mathbb{R})$, where $f(x - ct)$ and $g(x + ct)$ are leftward and rightward moving waves respectively with constant velocity. One can verify this quite easily by simply plugging $u(t,x)$ into the equation.

If $r(x) \neq 0$ for all $x \in \mathbb{R}$; then in the region outside the support of r, we have solutions of the form

$$u^-(t,x) = f^-(x - ct) + g^-(x + ct) \qquad \text{and} \qquad u^+(t,x) = f^+(x - ct) + g^+(x + ct)$$

for $x \leq -M$ and $x \geq M$ respectively, for some $f^-, f^+, g^-, g^+ \in C^2(\mathbb{R})$.

For the region $-M \leq x \leq M$, we introduce some assumptions so that the plasma-wave equation has no *bound states*, which implies, in particular, that $u(t,x) \to 0$ as $t \to \pm\infty$ for any fixed x and any reasonable u (e.g. square integrable).

Remark. *This is equivalent to the assertion that $\sigma_p(\mathcal{H}) = \emptyset$, where $\mathcal{H}$ is the Schrödinger operator $\mathcal{H} := r - \Delta$ and σ_p refers to the point spectrum (i.e. the set of eigenvalues).[10]*

Proposition 10. *Let $u : \mathbb{R} \times \mathbb{R} \to \mathbb{R}$ be a solution of the plasma wave equation. Then $u(t,x) \to 0$ as $t \to \pm\infty$ if and only if $\sigma_p(\mathcal{H}) = \emptyset$ in $L^2(\mathbb{R})$.*

Proof. First, assume that $u(t,x) \to 0$ as $t \to \pm\infty$ and let $v \in L^2(\mathbb{R})$ satisfy the equation $\mathcal{H}v = \lambda v$. Since $\mathcal{H} \geq 0$, we also have that $\lambda \geq 0$. Then $u(t,x) = e^{i\sqrt{\lambda}t}v(x)$ is a solution of the plasma wave equation. Observe that $t \mapsto \|u(t)\|_{L^2(\mathbb{R})} < \infty$ and from our assumption, we must have that $v = 0$, which implies that $\sigma_p(\mathcal{H}) = \emptyset$. For the "$\Leftarrow$"direction, we refer to reference [10] which in fact states the theorem. □

Moreover, $u(t,x) = f^-(x-ct) + g^+(x+ct)$ for $t \ll 0$, then transitions to interact with the scattering potential r and then $u(t,x) = f^+(x-ct) + g^-(x+ct)$ for $t \gg 0$.

Note that $r(x) = 0$ for all $x \in \mathbb{R}$ implies that $f^+ = f^-$ and $g^+ = g^-$. When $r(x) \neq 0$, the relationship between f^-, f^+, g^-, g^+ involves the *reflection* and *transmission coefficients* of r. In the proceeding section, we provide explicit representations for these.

2.1.1 Forward Scattering

The forward scattering problem in one dimensional homogeneous media may be formulated as the boundary value problem

$$\begin{cases} u = u_{\text{inc}} + u_{\text{sc}}, \\ \left(\Delta + \dfrac{\omega^2}{c^2}\right) \hat{u}_{\text{inc}}(\omega, x) = 0, \\ \left(\Delta + \dfrac{\omega^2}{c^2}\right) \hat{u}_{\text{sc}}(\omega, x) = r(x)\hat{u}_{\text{inc}}(\omega, x), \\ \dfrac{\partial}{\partial x}\hat{u}_{\text{inc/sc}}(\omega, x) \mp \dfrac{ic}{\omega}\hat{u}_{\text{inc/sc}}(\omega, x) \to 0 \quad \text{as } x \to \pm\infty, \end{cases} \tag{2.2}$$

which includes the Sommerfeld radiation condition in $\mathbb{R}$ and also the Born approximation in the equation for the scattered field.

Lemma 11. *The Green's function of the Helmholtz equation in homogeneous media, $\widehat{G} \in \mathcal{S}'(\mathbb{R}_+ \times \mathbb{R})$, satisfying*

$$\begin{cases} \left(\Delta + \dfrac{\omega^2}{c^2}\right) \widehat{G} = \delta, \\ \dfrac{\partial}{\partial x}\widehat{G}(\omega, x) \mp \dfrac{ic}{\omega}\widehat{G}(\omega, x) \to 0 \qquad \text{as } x \to \pm\infty \end{cases} \tag{2.3}$$

is given by

$$\widehat{G}(\omega, x) = \frac{ic}{2\omega} e^{i\omega|x|/c}. \tag{2.4}$$

Proof. We prove this via a heuristic argument. In particular, we may deduce that

$$\begin{aligned} & P(k)\mathcal{F}\widehat{G}(\omega, k) = 1 \\ \iff & \left(\frac{\omega^2}{c^2} - k^2\right) \mathcal{F}\widehat{G}(\omega, k) = 1 \\ \iff & \mathcal{F}\widehat{G}(\omega, k) = \frac{1}{\left(\frac{\omega}{c} + i\varepsilon\right)^2 - k^2}, \end{aligned}$$

where $0 < \varepsilon \ll 1$ is arbitrarily small so as to avoid a singularity when we invert the Fourier transform. In particular, an application of the inverse Fourier transform yields

$$\begin{aligned} & \mathcal{F}^{-1}\{\mathcal{F}\widehat{G}(\omega, \cdot)\}(x) = \lim_{\varepsilon \downarrow 0} \frac{1}{2\pi} \int_{-\infty}^{\infty} \frac{e^{ix\cdot k}}{\left(\frac{\omega}{c} - i\varepsilon\right)^2 - k^2} \, \mathrm{d}k \\ \iff & \widehat{G}(\omega, x) = \lim_{\varepsilon \downarrow 0} \frac{1}{4\pi} \int_{-\infty}^{\infty} \frac{e^{ix\cdot k} - e^{-ix\cdot k}}{\left(\frac{\omega}{c} + i\varepsilon\right)^2 - k^2} \, \mathrm{d}k \\ \iff & \widehat{G}(\omega, x) = \frac{ic}{2\omega} e^{i\omega|x|/c}, \end{aligned}$$

which is what we wanted to show. □

The impulse response of the medium at $x = x'$ is $\widehat{G}(\omega, x - x') = ic\exp(i\omega|x - x'|/c)/2\omega$, thus we may use the above result to write the scattered wave field as

$$\hat{u}_{\text{sc}}(\omega, x') = \frac{ic}{2\omega} \int_{-\infty}^{\infty} e^{i\omega|x-x'|/c} r(x')\hat{u}(\omega, x') \, \mathrm{d}x',$$

which is a *Fredholm integral equation of the first kind*. The part of the integrand excluding $r(x')$ is the kernel of the integral operator. It is worth noting that, in general, there is no guarantee that a Fredholm integral equation of the first kind will have a stable inverse. However, a class of integrals which does have stable inverses are Fourier transforms and their extensions; namely pseudo-differential operators and Fourier integral

operators with their inverses being the inverse Fourier transform, the inverse pseudo-differential operator and the pseudo-inverse Fourier integral operator respectively. In addition to being analytically stable, these inverse operators are also numerically stable.

Since the Green's functions for the Helmholtz operator contain factors of complex exponentials, the consequential scattered wave fields are Fourier transform-like integrals. Although Fourier transforms have stable inverses, care must be taken with band-width and spatial range so that the solution of the inverse transform is not degraded.[1]

Incidentally, the equation for the total wave field (1.3) is a Fredholm integral equation of the second kind. For a more comprehensive overview of *Fredholm theory* (which constitute the study of such equations) and, in particular, its applications to inverse scattering theory, we refer the reader to reference [17].

We now employ the Born approximation, i.e. $u = u_{\text{inc}}$ (recalling our abuse of notation), so that our scattered wave field is in fact given by

$$\hat{u}^{\pm}_{\text{sc}}(\omega, x) = \frac{ic}{2\omega} \int_{-\infty}^{\infty} e^{i\omega|x-x'|/c} r(x') \hat{u}^{\pm}_{\text{inc}}(\omega, x') \, \mathrm{d}x', \tag{2.5}$$

Proposition 12. *The functions $\hat{u}^{\pm}_{inc}(\omega, x) = e^{\pm i\omega x/c}$ are solutions of the Helmholtz equation*

$$\left(\Delta + \frac{\omega^2}{c^2}\right) \hat{u}_{inc}(\omega, x) = 0.$$

Proof. This follows via a simple verification. □

Remark. Indeed, the homogeneous Helmholtz equation has more general plane wave solutions

$$\hat{u}_{\text{inc}}(\omega, x) = \frac{1}{c}\hat{f}(\omega) e^{-i\omega x/c} + \frac{1}{c}\hat{g}(\omega) e^{i\omega x/c},$$

for arbitrary $f, g \in C^2(\mathbb{R})$. However, we will opt to proceed with the incident wave field described by the fixed amplitude plane wave solutions $\hat{u}^{\pm}_{\text{inc}}(\omega, x) = e^{\pm i\omega x/c}$.

We probe the medium from the left and right with the plane waves $\hat{u}^{\pm}_{\text{inc}}(\omega, x) = e^{\pm i\omega x'/c}$ and get

$$\begin{aligned} \hat{u}^{\pm}_{\text{sc}}(\omega, x) &= \frac{ic}{2\omega} \int_{-\infty}^{\infty} r(x') e^{i\omega|x-x'|/c} \cdot e^{\pm i\omega x'/c} \, \mathrm{d}x' \\ &= \frac{ic}{2\omega} \int_{-\infty}^{\infty} r(x') e^{i\omega(|x-x'|\pm x')/c} \, \mathrm{d}x', \end{aligned} \tag{2.6}$$

where the $\pm$ sign represents waves coming from the left and right side respectively.

Lemma 13. *Measuring the data from $x_0 = 0$ for plane waves reflected from the left yields the data function*

$$\boxed{d(t) = u^{+}_{sc}(t, 0) = -\frac{c^2}{4} \int_0^t r(cs/2) \, \mathrm{d}s} \tag{2.7}$$

Proof. In order to solve the integral (2.9) equation for r, we can measure the result away from the scattering centre, i.e. for $x \in \mathbb{R} \setminus \mathbb{D}$. In doing so, we find that, since $x \ll 0$ implies that $|x - x'| = -(x - x') = x' - x$ and $x \gg 0$ implies $|x - x'| = x - x'$, we get the following four integral equations:

$$\hat{u}^{+}_{\text{sc}}(\omega, x) = \begin{cases} \dfrac{ic}{2\omega} e^{-i\omega x/c} \displaystyle\int_{-\infty}^{\infty} r(x') e^{2i\omega x'/c} \, \mathrm{d}x', & x \ll 0, \\ \dfrac{ic}{2\omega} \displaystyle\int_{-\infty}^{\infty} r(x') e^{i\omega x/c} \, \mathrm{d}x', & x \gg 0, \end{cases} \tag{2.8}$$

$$\hat{u}^{-}_{\text{sc}}(\omega, x) = \begin{cases} \dfrac{ic}{2\omega} \displaystyle\int_{-\infty}^{\infty} r(x') e^{-i\omega x/c} \, \mathrm{d}x', & x \ll 0, \\ \dfrac{ic}{2\omega} e^{i\omega x/c} \displaystyle\int_{-\infty}^{\infty} r(x') e^{-2i\omega x'/c} \, \mathrm{d}x', & x \gg 0. \end{cases}$$

We recognise these four contributions as the transmitted and reflected responses from the left and right. We may thus introduce the *transmission* and *reflection coefficients* as

$$\begin{aligned} T(\omega) &:= \int_{-\infty}^{\infty} r(x')\,\mathrm{d}x' = \hat{r}(0), \\ R_{\pm}(\omega) &:= \int_{-\infty}^{\infty} r(x') e^{\pm 2i\omega x'/c}\,\mathrm{d}x' = \hat{r}(\pm 2\omega/c), \end{aligned} \tag{2.9}$$

respectively.

Hence we can rewrite our transmitted and reflected responses as

$$\hat{u}^{+}_{\mathrm{sc}}(\omega, x) = \begin{cases} \left(e^{-i\omega x'/c}, \dfrac{ic}{2\omega} e^{-i\omega x/c} \cdot R_{+}(\omega) \right), & x \ll 0, \\ \left(\dfrac{ic}{2\omega} e^{i\omega x/c} \cdot T(\omega), 0 \right), & x \gg 0, \end{cases}$$

$$\hat{u}^{-}_{\mathrm{sc}}(\omega, x) = \begin{cases} \left(0, \dfrac{ic}{2\omega} e^{-i\omega x/c} \cdot T(\omega) \right), & x \ll 0, \\ \left(\dfrac{ic}{2\omega} e^{i\omega x/c} \cdot R_{-}(\omega), e^{i\omega x'/c} \right), & x \gg 0. \end{cases}$$

These are called the *Jost solutions* to (1.1).

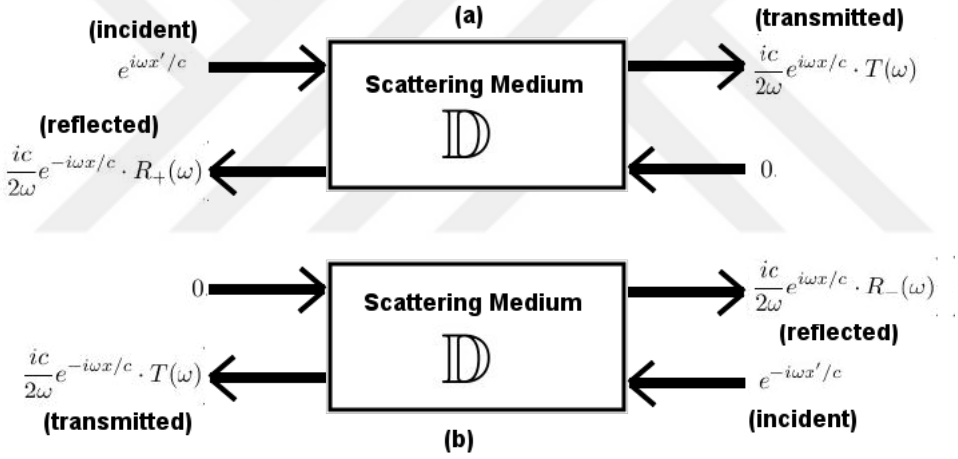

Figure 2.1: (a) is an illustration of the reflection problem probing from the left and (b) of the reflection problem probing from the right.

Physically, we can think of the solution $\hat{u}^{+}_{\mathrm{sc}}(\omega, x)$ resulting from a problem in which the scattering potential is probed from the left, in the $+x$ direction, and $\hat{u}^{-}_{\mathrm{sc}}(\omega, x)$ resulting from a problem in which the probing takes place from the right, in the $-x$ direction, which results in a *transmitted wave* $ic/2\omega \exp(i\omega x/c) T(\omega)$ and a *reflected wave* $ic/2\omega \exp(-i\omega x/c) R_{+}(\omega)$. Note that $T(\omega)$, by reciprocity, is the same for both solutions.

Notice also that we have rewritten our solutions so that the first component of each solution is the rightward traveling wave, and the second component is the leftward traveling wave.

Thus one may observe, in fact, that we have $u^{+} = f^{-} + g^{+}$ for $t \ll 0$ and $u^{+} = f^{+} + g^{-}$ for $t \gg 0$, where $f^{-} = \delta_{x-ct}$, $g^{+} = 0$, f^{+} is the reflected wave and g^{-} is the transmitted wave; and similarly for u^{-}.

We now take measurement at $x = 0$ of the reflection response; That is, we consider

$$\hat{u}^{+}_{\mathrm{sc}}(\omega, 0) = \frac{ic}{2\omega} R_{+}(\omega) = \frac{ic}{2\omega} \hat{r}(2\omega/c).$$

We may also assume, without loss of generality, that $\mathbb{D} = \operatorname{supp} r \subset (0, \infty)$.

Then it follows by the above and an application of the Fourier inverse transform that

$$\begin{aligned} d(t) &= u_{\text{sc}}^{+}(t,0) \\ &= \mathcal{F}^{-1}\{\hat{u}_1^{+}(\cdot,0)\}(t) \\ &= c\mathcal{F}^{-1}\left\{\frac{i}{2\cdot}\hat{r}(2\cdot/c)\right\}(t) \\ &= c\pi\mathcal{F}^{-1}\left\{\frac{i}{2\pi\cdot}\hat{r}(2\cdot/c)\right\}(t) \end{aligned}$$

Now, if $H \in \mathcal{S}'(\mathbb{R})$ is the Heaviside step function, then its Fourier transform is

$$\widehat{H} = \text{P. V.}\left(\frac{1}{2\pi i\omega}\right) + \frac{1}{2}\delta.$$

Then the convolution theorem gives that for all $\phi \in \mathcal{S}(\mathbb{R})$, we have

$$c\pi\left\langle \text{P. V.}\left(\frac{\hat{r}(2\cdot/c)}{2\pi i\omega}\right) + \frac{\hat{r}(0)}{2}\delta, \hat{\phi}\right\rangle = c\pi\langle\widehat{H}, \hat{r}(2\cdot/c)\hat{\phi}\rangle = \frac{c^2}{4}\langle H, r(c\cdot/2) * \phi\rangle = \frac{c^2}{4}\langle H * r(c\cdot/2), \phi\rangle$$

Hence, if we recall our assumption that r is supported away from zero, we can conclude that since δ only takes values at the origin, we have

$$d(t) = -\frac{c^2}{4}H(t) * r(ct/2) = -\frac{c^2}{4}\int_{-\infty}^{t} r(cs/2)\,\mathrm{d}s.$$

Then introducing the assumption that $s \geq 0$ completes the proof. □

Note that we selected $x_0 = 0$ for ease of computation, but one may deduce the data function in the general case as well.

2.1.2 Inverse Scattering

Now, having solved the forward scattering problem, we turn to the inverse scattering problem:

Theorem 14. *For $r \in C_c^{\infty}(\mathbb{R})$, measuring the data from the left allows us to recover the scattering potential as*

$$\boxed{r(x) = -\frac{2}{c}\,d'(2x/c)} \tag{2.10}$$

Proof. We can recover r directly from the previous lemma. In particular, we may deduce the following:

$$\begin{aligned} & d(t) = -\frac{c^2}{4}\int_0^t r\left(\frac{cs}{2}\right)\,\mathrm{d}s \\ \iff & \int_0^t r\left(\frac{cs}{2}\right)\,\mathrm{d}s = -\frac{4}{c^2}d(t) \\ \iff & \frac{\mathrm{d}}{\mathrm{d}t}\int_0^t r\left(\frac{cs}{2}\right)\,\mathrm{d}s && = -\frac{4}{c^2}d'(t) \\ \iff & \frac{2}{c}\frac{\mathrm{d}}{\mathrm{d}t}\int_0^{\frac{cs}{2}} r(\eta)\,\mathrm{d}\eta = -\frac{4}{c^2}d'(t), && \text{where } \eta = \frac{cs}{2} \\ \iff & r\left(\frac{ct}{2}\right) = -\frac{2}{c}d'(t) \\ \iff & r(x) = -\frac{2}{c}d'\left(\frac{2x}{c}\right), && \text{where } x = \frac{ct}{2}, \end{aligned}$$

which is precisely what we wanted to prove. □

Remark. *Alternatively, we may have considered the plane wave from the other direction; that is,*

$$\hat{u}_{sc}^{-}(\omega,0) = -\frac{ic}{2\omega}R_{-}(\omega) = -\frac{ic}{2\omega}\hat{r}(-2\omega/c), \tag{2.11}$$

and similarly, we would have deduced that

$$d(t) = -\frac{c^2}{4}\int_0^t r(-cs/2)\,\mathrm{d}s. \tag{2.12}$$

Hence

$$r(x) = -\frac{2}{c}\, d'(-2x/c). \tag{2.13}$$

This is known as the overshoot: where the left and right limits both exist but are not equal.

The formula for the scattering potential which we derived above is more typically obtained in physics literature using the Marchenko or Gelfand-Levitan integral equations. For the interested reader, we refer to reference [8]. We will state the Gelfand-Levitan equation in §3.1, as it is from this equation that the all-important layer stripping algorithms are derived.

Layer Stripping

An alternative method to obtaining r is by using the aforementioned *layer stripping algorithm*. Note that, as stated, in later chapters we will provide a more explicit and complete description of the algorithm. Indeed, it is computationally *less expensive* than the more conventional integral equation based method described above.

In particular, we may recover r by a single pass of the layer stripping approach by solving the boundary value problem

$$\begin{cases} \left(\dfrac{\partial}{\partial x} - \dfrac{1}{c}\dfrac{\partial}{\partial t}\right) v(t,x) = 0, \\ v(t,0) = \dfrac{2}{c} d'(t), \end{cases} \tag{2.14}$$

where $v : \mathbb{R}_+ \times \mathbb{R} \to \mathbb{R}$ is called the velocity wave field.

Proposition 15. *We may retrieve the scattering potential via the velocity wave field as*

$$r(x) = -\frac{2}{c} v(x/c, x) \tag{2.15}$$

for all $x \in \mathbb{R}$.

Proof. For (2.15), we have general solutions of the form

$$v(t,x) = f(x+ct), \qquad f \in C^1(\mathbb{R}). \tag{2.16}$$

Then we compute

$$\begin{aligned} d'(t) &= -\frac{c^2}{4}\frac{\mathrm{d}}{\mathrm{d}t}\int_0^t r(cs/2)\,\mathrm{d}s \\ &= -\frac{c^2}{4}\frac{\mathrm{d}}{\mathrm{d}t}\int_0^{ct/2} r(\eta)\frac{2}{c}\,\mathrm{d}\eta, \qquad \text{where } \eta = \frac{cs}{2} \\ &= -\frac{c}{2}\frac{\mathrm{d}}{\mathrm{d}t}\int_0^{ct/2} r(\eta)\,\mathrm{d}\eta \\ &= -\frac{c^2}{4} r(ct/2). \end{aligned}$$

We have the boundary condition

$$v(t,0) = f(x+ct) = -\frac{2}{c}\cdot\frac{c^2}{4} r(ct/2) = -\frac{c}{2} r(ct/2).$$

Therefore

$$v(t,x) = f(x+ct) = -\frac{c}{2} r\left(\alpha x + \frac{ct}{2}\right),$$

for some $\alpha \in \mathbb{R}$ yet to be determined. If we plug this solution back into the equation (2.14), then it is easy to see that we must have $\alpha = \frac{1}{2}$.

Hence we may write the solution to the differential equation in terms of the scattering potential as

$$v(t,x) = -\frac{c}{2} r\left(\frac{x+ct}{2}\right).$$

Then we can retrieve the scattering potential as

$$r(x) = -\frac{2}{c} v(x/c, x).$$

□

For computer implementations of analytically deduced algorithms for the inverse scattering problem, one must also be able to recover the scattering potential from discretely sampled data.

Single Pass of Layer Stripping Algorithm

Step 1: Initialise algorithm with time domain $\mathbb{T} \subset \mathbb{R}_+$ and spatial domain $\mathbb{X} \subset \mathbb{R}$ and solve plasma wave equation.

for all $t \in \mathbb{T}$ **do**

Fix an observation position $x_0 \in \mathbb{X}$ and derive the data as $d(t) = \tilde{u}(t, x_0)$, where $\tilde{u}$ solves the plasma wave equation

end for $t_0 = \sup \mathbb{T}$

Step 2: Initialise with $v(t, 0) = 2d'(t)$

for all $n = t_0, ..., 1$ **do**

Solve backward advection equation with a backward in time, forward in space scheme

end for $n = 1$

Step 3: Retrieve scattering potential

Interpolate time grid $\mathbb{T}$ to spatial grid $\mathbb{X}$

for all $x \in \mathbb{X}$ **do**

Recover scattering potential as $r(x) = -\frac{2}{c} v(x/c, x)$.

end for $x_N = \sup \mathbb{X}$

We now provide a numerical example of two layer stripping methods. In the first example, we update in time, t, and in the second example we update in space, x.

Example 16 (Updating in t)**.** Let $c = 1$ and also let $r \in C_c^\infty(\mathbb{R})$ be given by

$$r(x) = \psi(x - 2)\psi(-x - 1), \tag{2.17}$$

where $\psi \in C^\infty(\mathbb{R})$ is defined as

$$\psi(x) = \begin{cases} e^{-1/x^2}, & x > 0, \\ 0, & x \leq 0. \end{cases} \tag{2.18}$$

Then we consider the problem

$$\begin{cases} \left(\dfrac{\partial}{\partial x} - \dfrac{\partial}{\partial t} \right) v(t, x) = 0, \\ v(t_0, x) = \operatorname{sinc}\left(\dfrac{x - x_0}{\Delta x} \right), \\ v(t, 0) = 2d'(t), \end{cases} \tag{2.19}$$

where $t_0 > 0$ is the terminal time that the data is recorded. Since we cannot numerically implement plane wave incident fields, we opt for sinc function initial/terminal conditions, since $\lim_{\Delta x \downarrow 0} \operatorname{sinc}(x/\Delta x) = \delta_x$ and we generally choose $\Delta x \ll 1$.[2]

In order to initialise the algorithm with the boundary value $v(t, 0)$, we must also solve the plasma wave equation. To this end, may discretise the Laplace operator $\Delta : C^k(\mathbb{R}) \to C^{k-2}(\mathbb{R})$, $k \geq 2$, in space using a finite difference approximation to get

$$\begin{aligned} \Delta u(t, x) &= \frac{u(t, x + \Delta x) - 2u(t, x) + u(t, x - \Delta x)}{\Delta x^2} + \mathcal{O}(\Delta x^2) \qquad \Delta x \downarrow 0 \\ &\sim \frac{u_{\ell+1}(t) - 2u_\ell(t) + u_{\ell-1}(t)}{\Delta x^2} \\ &=: \mathrm{L} u_\ell(t) \end{aligned}$$

on the lattice $\Delta x \mathbb{Z} \subset \mathbb{R}$, where u_ℓ is the value of the wave field on the ℓ-th point on the spatial grid and $\mathrm{L} \in \mathbb{R}^{M \times M}$, with M being the total number of spatial steps, is the matrix operator:

$$\mathrm{L} = \frac{1}{\Delta x^2} \begin{pmatrix} -2 & 1 & & & 0 \\ 1 & -2 & 1 & & \\ & \ddots & \ddots & \ddots & \\ & & 1 & -2 & 1 \\ 0 & & & 1 & -2 \end{pmatrix}.$$

[2] http://tediousderivations.blogspot.nl/2013/07/dirac-delta-function-sinc-representation.html

Clearly $\Delta x > 0$ refers to the spatial step.

Note that the matrix L is Toeplitz, with

$$\tau_{-N+1} = \cdots = \tau_{-2} = 0, \qquad \tau_{-1} = 1, \qquad \tau_0 = -2, \qquad \tau_1 = 1, \qquad \tau_2 = \cdots = \tau_{N-1} = 0.$$

Thus the spatially discretised plasma wave equation is given by

$$\frac{\mathrm{d}^2}{\mathrm{d}t^2} u_\ell(t) = \left(r - \frac{1}{\Delta x^2} \mathrm{L} \right) u_\ell(t),$$

or more explicitly,

$$\frac{\mathrm{d}^2}{\mathrm{d}t^2} \begin{pmatrix} u_1(t) \\ u_2(t) \\ \vdots \\ u_{N-1}(t) \\ u_N(t) \end{pmatrix} = \left[\begin{pmatrix} r_1 & & & & 0 \\ & r_2 & & & \\ & & \ddots & & \\ & & & r_{N-1} & \\ 0 & & & & r_N \end{pmatrix} - \frac{1}{\Delta x^2} \begin{pmatrix} -2 & 1 & & & 0 \\ 1 & -2 & 1 & & \\ & \ddots & \ddots & \ddots & \\ & & 1 & -2 & 1 \\ 0 & & & 1 & -2 \end{pmatrix} \right] \begin{pmatrix} u_1(t) \\ u_2(t) \\ \vdots \\ u_{N-1}(t) \\ u_N(t) \end{pmatrix}$$

where $N \gg 0$ sufficiently large refers to the total number of time steps.

Then an application of the Leapfrog scheme yields

$$\boldsymbol{u}^{n+1} = 2\boldsymbol{u}^n - \boldsymbol{u}^{n-1} + \Delta t^2 (r - \mathrm{L}) \boldsymbol{u}^n.$$

Thus for a fixed $x_0 \in \mathbb{R}$, the above scheme is the generating equation for the data.

We would like to solve the partial differential equation backward in time and forward in space, thus we may first discretise the equation in space to get

$$\begin{aligned} \frac{\mathrm{d}}{\mathrm{d}t} v_\ell(t) &= \left(\frac{\partial v}{\partial x} \right)_\ell (t) \\ &= \underbrace{\frac{v_{\ell+1}(t) - v_\ell(t)}{\Delta x}}_{F_\ell(t)} + \mathcal{O}(\Delta x), \qquad \Delta x \downarrow 0, \end{aligned}$$

where we have taken the forward finite difference approximation of the spatial derivative.

Now, an application of the Crank-Nicolson scheme, going backwards in time, yields

$$\begin{aligned} & - \frac{v_\ell^{n-1} - v_\ell^n}{\Delta t} = \frac{1}{2} [F_\ell(t^{n-1}) + F_\ell(t^n)] \\ \iff & - \frac{v_\ell^{n-1} - v_\ell^n}{\Delta t} = \frac{v_{\ell+1}^{n-1} - v_\ell^{n-1} + v_{\ell+1}^n - v_\ell^n}{2\Delta x} \\ \iff & - v_\ell^{n-1} = -v_\ell^n + \frac{\mu}{2} (v_{\ell+1}^{n-1} - v_\ell^{n-1} + v_{\ell+1}^n - v_\ell^n) \\ \iff & v_\ell^{n-1} + \frac{\mu}{2} (v_{\ell+1}^{n-1} - v_\ell^{n-1}) = v_\ell^n - \frac{\mu}{2} (v_{\ell+1}^n - v_\ell^n) \end{aligned}$$

Hence we get

$$\boldsymbol{v}^{n-1} = \left(\mathrm{I} + \frac{\mu}{2} \mathrm{A} \right)^{-1} \left(\mathrm{I} - \frac{\mu}{2} \mathrm{A} \right) \boldsymbol{v}^n, \tag{2.20}$$

where $\mu = \Delta t / \Delta x$, I is the identity matrix and $\mathrm{A} \in \mathbb{R}^{M \times M}$ is the banded matrix given by

$$\mathrm{A} = \begin{pmatrix} -1 & 1 & & 0 \\ & -1 & 1 & \\ & & \ddots & \ddots \\ 0 & & & \end{pmatrix}$$

where M represents the total number of spatial steps.

Now we consider two numerical implementations:

(a) In order to acquire the data, we must first solve the following initial value problem:

$$\begin{cases} \left(\Delta + \dfrac{\partial^2}{\partial t^2}\right) u(t,x) = r(x)u(t,x) \\ u(0,x) = \dfrac{\partial}{\partial t} u(0,x) = \operatorname{sinc}\left(\dfrac{x - x_0}{\Delta x}\right). \end{cases} \tag{2.21}$$

If we measure the data at $x_0 = 0$, then we use the Leapfrog scheme to numerically solve the above problem and we get the following data plot which we plot below, with $\Delta t = 10^{-3}$ and $\Delta x = 10^{-2}$:

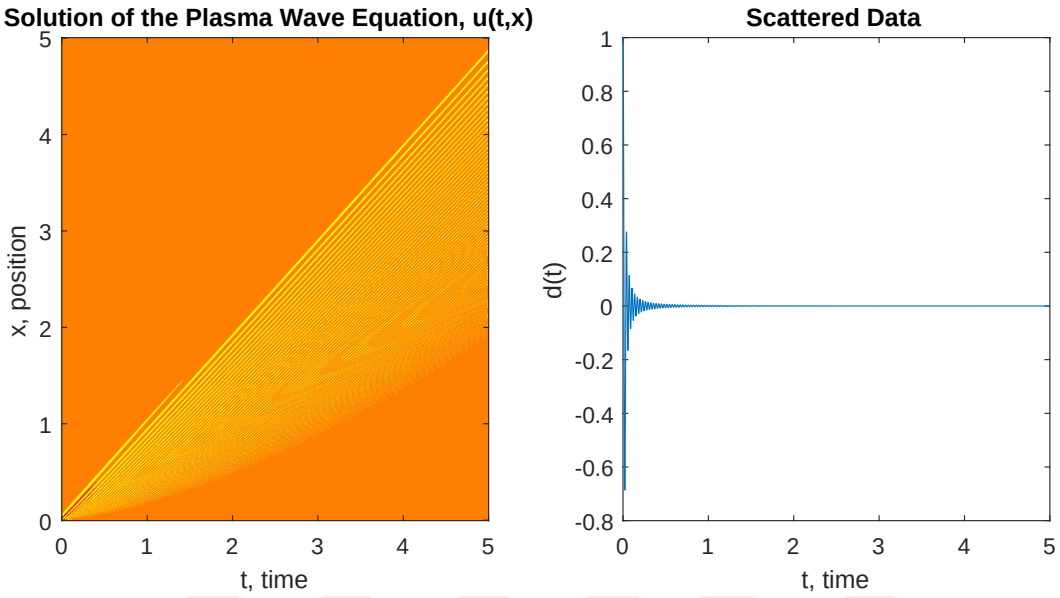

Figure 2.2: Data generated from the plasma wave equation at fixed position $x_0 = 0$.

Now, recalling that

$$r(x) = -2v(x,x),$$

we may numerically retrieve the potential as

$$\mathrm{r} = -2\,\mathrm{diag}\,\mathrm{v},$$

where $\mathrm{v} \in \mathbb{R}^{M \times M}$.

Note that with the A defined above, the solution of the backward advection equation (i.e. 2.14 solved numerically by 2.20) turn out to be unstable. However, using the finite difference matrix A' in place of A, which we define as

$$\mathrm{A}' = \begin{pmatrix} 1 & & & 0 \\ -1 & 1 & & \\ & \ddots & \ddots & \\ 0 & & -1 & 1 \end{pmatrix}$$

yields stable solutions. This, in particular, would imply a backward in space scheme. We provide a plot of the solution $v(t,x)$:

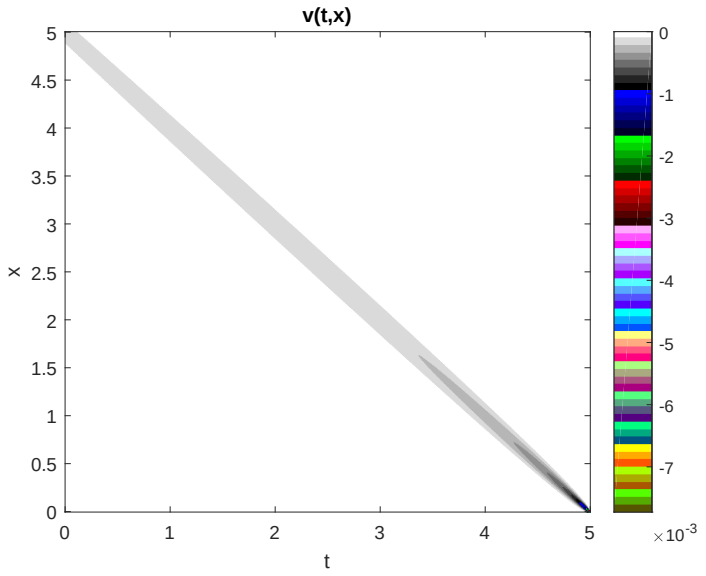

Figure 2.3: Solution of the backward advection equation via (2.20) from data measured at $x_0 = 0$ scattered with potential r.

Indeed, the data from the diagonal above allows us to plot the resulting reconstruction below:

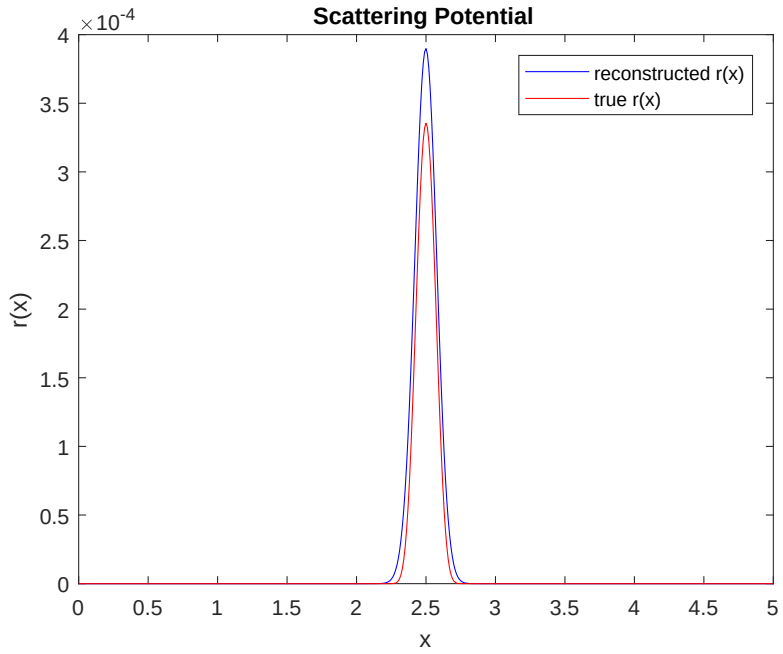

Figure 2.4: Reconstruction of r from data measured at $x_0 = 0$ using the scheme given by (2.20).

Note since $N \neq M$, where N and M represent the total number of time and spatial steps respectively, we have linearly interpolated the time samples onto the spatial grid.

(b) Suppose, instead, that we record the data at $x_0 = 2$; then the respective scattered data is plotted below:

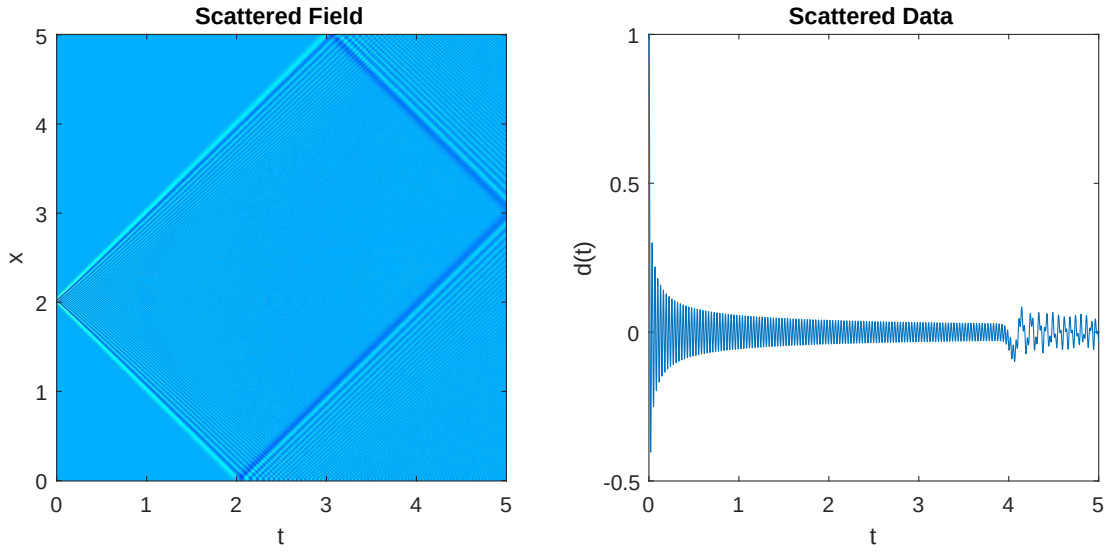

Figure 2.5: Data generated from the plasma wave equation for fixed position $x_0 = 2$.

Then a single pass of the layer stripping yields the following results:

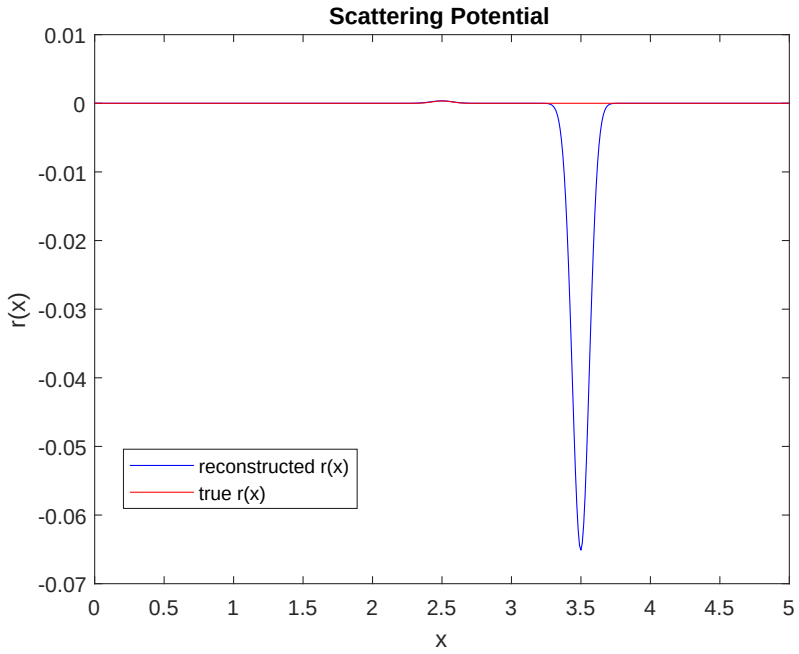

Figure 2.6: Reconstruction attempt of scattering potential from data recorded at $x_0 = 2$.

In this reconstruction, we observe that the on $\mathbb{R} \setminus (3, 4)$, we have a reasonably accurate reconstruction of the scattering potential. However, in the region $(3, 4)$, the reconstruction of the scattering potential is far removed from the true scattering potential. Below we plot $v(t, x)$ with initial condition depending on the data measured at $x_0 = 2$:

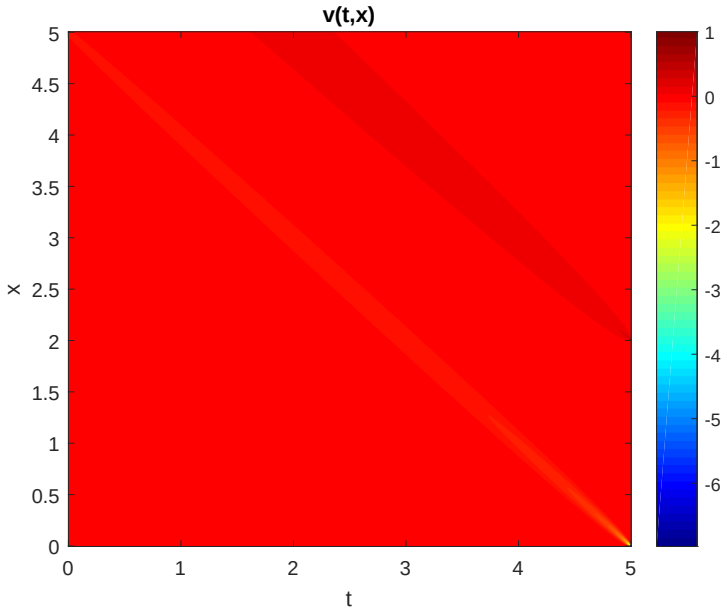

Figure 2.7: Solution of the backward advection equation with boundary condition given by data recorded at $x_0 = 2$.

Indeed, one may observe in the above plot that on $v(x, x)$, there exist relatively large positive values which contribute to the negative spike in our reconstruction plot.

Sinc Interpolation

One may make use of "sinc based"interpolation formulae which reconstruct continuous functions from their discretely sampled analogues provided that certain criterion are satisfied.

Definition 17 (Sampled Function)**.** *Suppose we want to reconstruct $f \in \mathcal{S}(\mathbb{R})$ from its values sampled at the points of the lattice $\Delta t\mathbb{Z}$ in $\mathbb{R}$ for $\Delta t \geq 0$. Then we may sample f via*

$$f_{samp} := \sum_{n=-\infty}^{\infty} \text{Ш}_{\Delta t} f(n\Delta t) \in \mathcal{S}'(\mathbb{R}),$$

where we define the Dirac comb (also called the Shah distribution) $\text{Ш}_{\Delta t} \in \mathcal{S}'(\mathbb{R})$ by

$$\text{Ш}_{\Delta t} := T_{n\Delta t *}\delta_t,$$

where $T_{n\Delta t} : \mathbb{R} \to \mathbb{R}$ is the translation operator which maps $t \mapsto t - n\Delta t$ and $\delta_t : \mathcal{S}(\mathbb{R}) \to \mathbb{C}$ is the Dirac measure at the point $t \in \mathbb{R}$ which maps $\phi \mapsto \phi(t)$, represents an impulse train with the amplitudes of the impulses equal to the samples of f at intervals spaces Δt.

Definition 18 (Band-Limited Function)**.** *A function $f : \mathbb{R}^n \to \mathbb{R}$ is called band-limited with bandwidth B if its Fourier transform is locally integrable and vanishes almost everywhere outside the ball of radius B.*

Proposition 19 (Shannon-Nyquist Sampling Theorem)**.** *If $f(t)$ is a bandlimited signal, i.e. $\hat{f}(\omega) = 0$ for $|\omega| > B$, then $f(t)$ is uniquely determined by its samples, $f(n\Delta t)$, for $n \in \mathbb{Z}$, provided that the sampling rate exceeds twice the maximum frequency of the bandlimited signal, i.e. $\omega_s > 2B$.*

The minimum sampling frequency in this case is called the *Nyquist rate*, which we denote as $\omega_s = 1/\Delta t$, where Δt represents our *sampling period*. The *Nyquist frequency* is half the Nyquist rate.

Note that the bulwark of the techniques involved here can be lumped under *signal processing*. For an in-depth overview of signal processing from a mathematical perspective, we refer the reader to reference [5].

A convenient interpolation formula for reconstructing a continuous function from its discrete samples provided that the conditions of the Shannon-Nyquist sampling theorem are satisfied is given below

Lemma 20 (Whitaker-Shannon interpolation formula)**.** *When the sampled function has bandlimit B satisfies the Shannon-Nyquist Sampling theorem, i.e. $\omega_s = \frac{1}{\Delta t} > 2B$, then the Whitaker-Shannon interpolation formula:*

$$f(t) = \sum_{n=-\infty}^{\infty} f(n\Delta t) \cdot \operatorname{sinc}\left(\frac{t - n\Delta t}{\Delta t}\right), \tag{2.22}$$

is the perfect reconstruction of the original function.

Proof. Since $\hat{f}$ vanishes on the complement of $[-\frac{1}{\Delta t}, \frac{1}{\Delta t}]$, it follows that the Fourier expansion of $\hat{f}$ in this region is given by

$$\hat{f}(\omega) = \Delta t \sum_{n=-\infty}^{\infty} f(n\Delta t) e^{in\Delta t\omega} \qquad \text{in } L^2([-1/\Delta t, 1/\Delta t]).$$

If we multiply the above by $\mathbb{1}_{[-\frac{1}{\Delta t}, \frac{1}{\Delta t}]}$, then we get

$$\hat{f}(\omega) = \Delta t \sum_{n=-\infty}^{\infty} f(n\Delta t) \mathbb{1}_{[-\frac{1}{\Delta t}, \frac{1}{\Delta t}]}(\omega) e^{in\Delta t\omega} \qquad \text{in } L^2(\mathbb{R}).$$

This series converges in $L^2(\mathbb{R})$, so we can take the inverse Fourier transform, term by term, which yields the desired result.[2] □

Corollary 21. *We may construct the scattering potential via*

$$\boxed{r_{const}(x) = -\frac{2}{c} \sum_{n=-\infty}^{\infty} d[n] \frac{\mathrm{d}}{\mathrm{d}x} \operatorname{sinc}\left(\frac{\frac{2x}{c} - n\Delta t}{\Delta t}\right)} \tag{2.23}$$

where $d[n] := d(n\Delta t)$.

Proof. Recall that we deduced the following equation which expressed the scattering potential in terms of the data, namely:

$$r(x) = -\frac{2}{c} d'\left(\frac{2x}{c}\right). \tag{2.24}$$

Thus an application of the aforementioned interpolation formula of the previous lemma provides us with the construction formula for the scattering potential.

We can summarise the above to form the following algorithm: □

Shannon Sampling Algorithm

Step 1: Initialise algorithm with $d(t) = -\frac{c^2}{4} \int_0^t r(cs/2)\,\mathrm{d}s$ & $\omega_s = 1/\Delta t > 0$ for $t > 0$ and sample
  for all n **do**
    discretise $d(t)$ as $d(n\Delta t)$
  end for $n = t/\Delta t$
Step 2:
  Interpolate
  for all n **do**
    Compute $-\frac{2}{c} \sum_n d(n\Delta t) \frac{\mathrm{d}}{\mathrm{d}x} \operatorname{sinc}\left(\frac{\frac{2x}{c} - n\Delta t}{\Delta t}\right)$
  end for $n = t/\Delta t$

Example 22. Let $r \in C_c^\infty(\mathbb{R})$ be as defined previously in Example 17. Then we can generate the data as

$$\begin{aligned} d(t) &= -\frac{c^2}{4} \int_0^t \psi(s)\psi(1-s)\,\mathrm{d}s, \\ &= -\frac{c^2}{4} \int_0^t e^{-1/s^2} e^{-1/(1-s)^2}\,\mathrm{d}s. \end{aligned} \tag{2.25}$$

Suppose $c = 2$. Then performing analogue sampling with $\Delta t = 1/20$ yields

$$\begin{aligned} d[n] = d(n\Delta t) &= -\int_0^{n\Delta t} e^{-1/s^2} e^{-1/(1-s)^2}\,\mathrm{d}s \\ &= -\int_0^{n/20} e^{-1/s^2} e^{-1/(1-s)^2}\,\mathrm{d}s. \end{aligned} \tag{2.26}$$

The discrete-time Fourier transform is given in terms of the frequency ω as:

$$D(\omega) = \sum_{n=0}^{N-1} d[n] e^{-2\pi i \omega n/N}, \tag{2.27}$$

and we plot the result as:

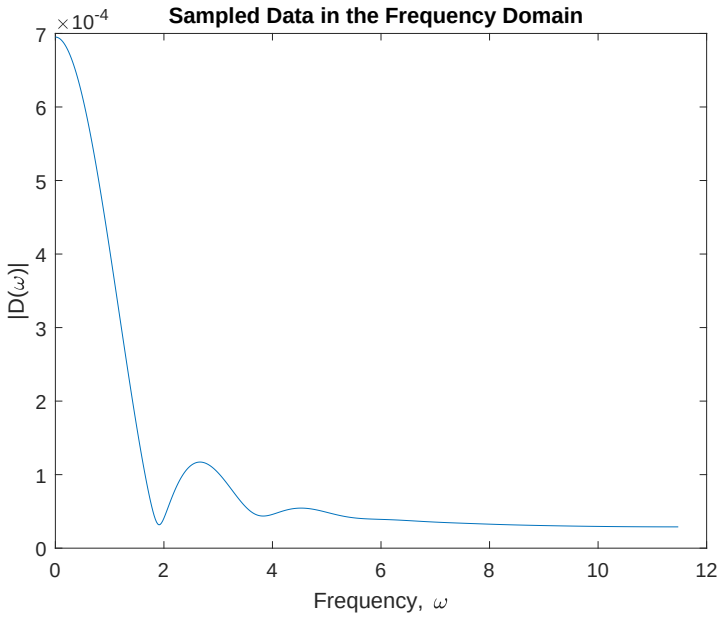

Figure 2.8: The discrete Fourier transform of the data function

In particular, we may observe that the data function is not band-limited. We can see this analytically by computing the continuous Fourier transform

$$\begin{aligned}
\hat{d}(\omega) &= \int_0^\infty d(t) e^{i\omega t} \, \mathrm{d}t \\
&= -\int_0^\infty \int_0^t e^{\frac{1}{-1+2s-2s^2}} \, \mathrm{d}s \cdot e^{i\omega t} \, \mathrm{d}t \\
&= -\frac{i}{\omega} \int_0^t e^{\frac{1}{-1+2s-2s^2}} \, \mathrm{d}s \to 0 \text{ as } \omega \to \infty.
\end{aligned}$$

Thus, in this setting we do not have a Nyquist rate and we choose arbitrary $\omega_s = 23$ so that $\Delta t = 1/23$. Then, recording the data up to $t = 1$, the interpolation formula

$$\begin{aligned}
r_{\text{const}}(x) &= -\sum_{n=-\infty}^{\infty} d[n] \frac{\mathrm{d}}{\mathrm{d}x} \operatorname{sinc}\left(\frac{x - n\Delta t}{\Delta t}\right) \\
&= -\sum_{n=-\infty}^{\infty} d[n] \frac{\mathrm{d}}{\mathrm{d}x} \operatorname{sinc}\left(\frac{x - \frac{n}{23}}{\frac{1}{23}}\right),
\end{aligned}$$

yields the following results, which are plotted below:

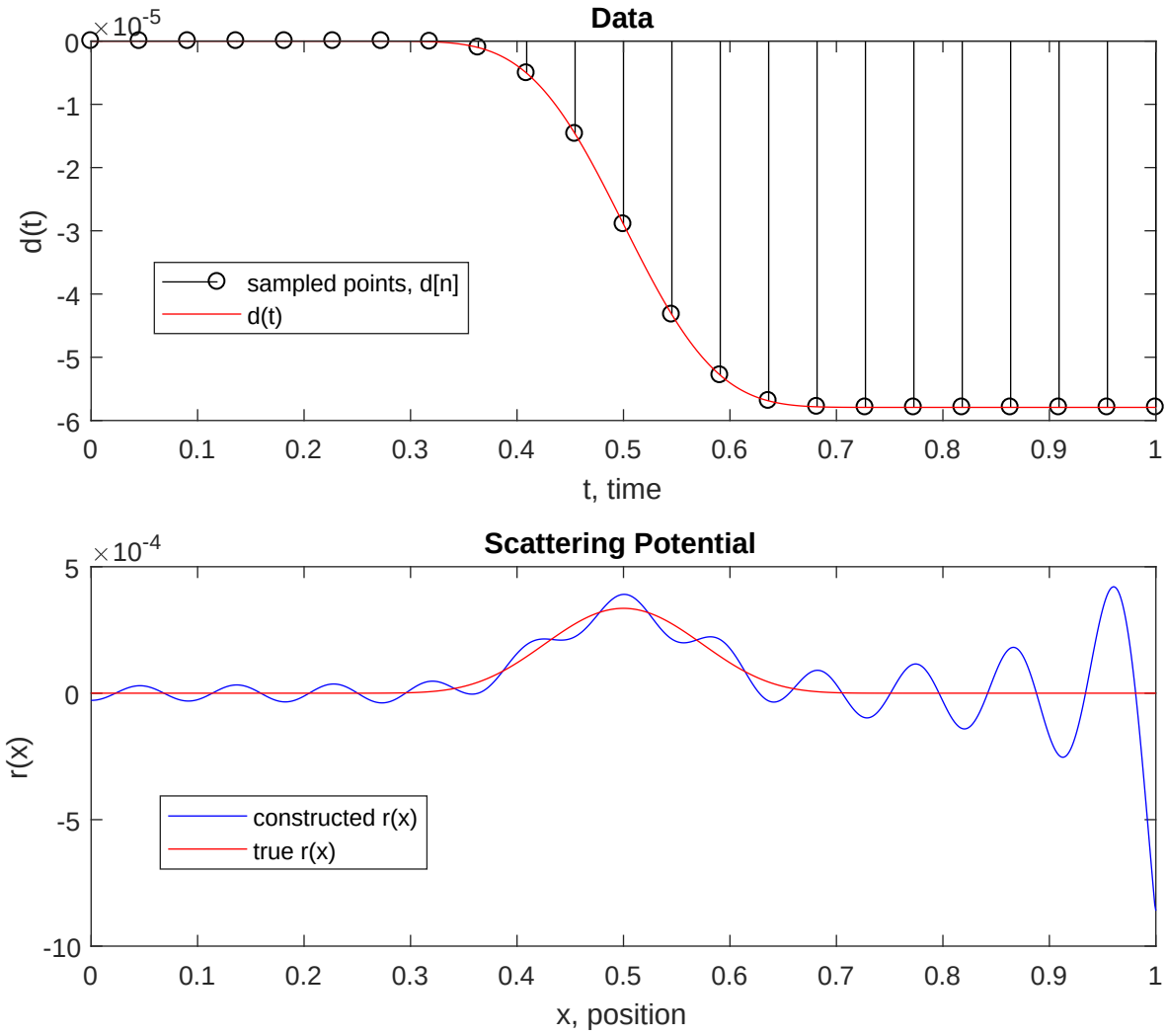

Figure 2.9: The sampled data points and the resulting reconstruction of the scattering potential

Note that we used the following *Matlab* function, which we provide below:

```
function interpolated = getscattering(ts,dn,x)
T = ts(2)-ts(1); % sampling period
F = 1/(x(2)-x(1));
% interpolate r
interpolated = 0;
for n=1:length(ts)
    interpolated = interpolated+dn(n)*gradient(sinc((x-(n-1).*T)./T))*F;
end
```

One may observe in the code that we utilised the built-in Matlab function `gradient` to calculate the *central difference*

$$\begin{aligned}\delta_{\Delta x}\{\text{sinc}\}\left(\frac{x-n\Delta t}{n\Delta t}\right) &= \text{sinc}\left(\frac{x-n\Delta t}{n\Delta t}+\frac{1}{2}\Delta x\right)-\text{sinc}\left(\frac{x-n\Delta t}{n\Delta t}-\frac{1}{2}\Delta x\right)\\ &\approx \frac{\mathrm{d}}{\mathrm{d}x}\,\text{sinc}\left(\frac{x-n\Delta t}{n\Delta t}\right),\end{aligned}$$

since the derivative of sinc is highly oscillatory and therefore derivative of $d(t)$ via the interpolated expression will not resemble its true derivative.

One can record for $t = 2$ and take sampling rates $\omega_s = 10$, $\omega_s = 50$, $\omega_s = 200$, for which we respectively plot the results below:

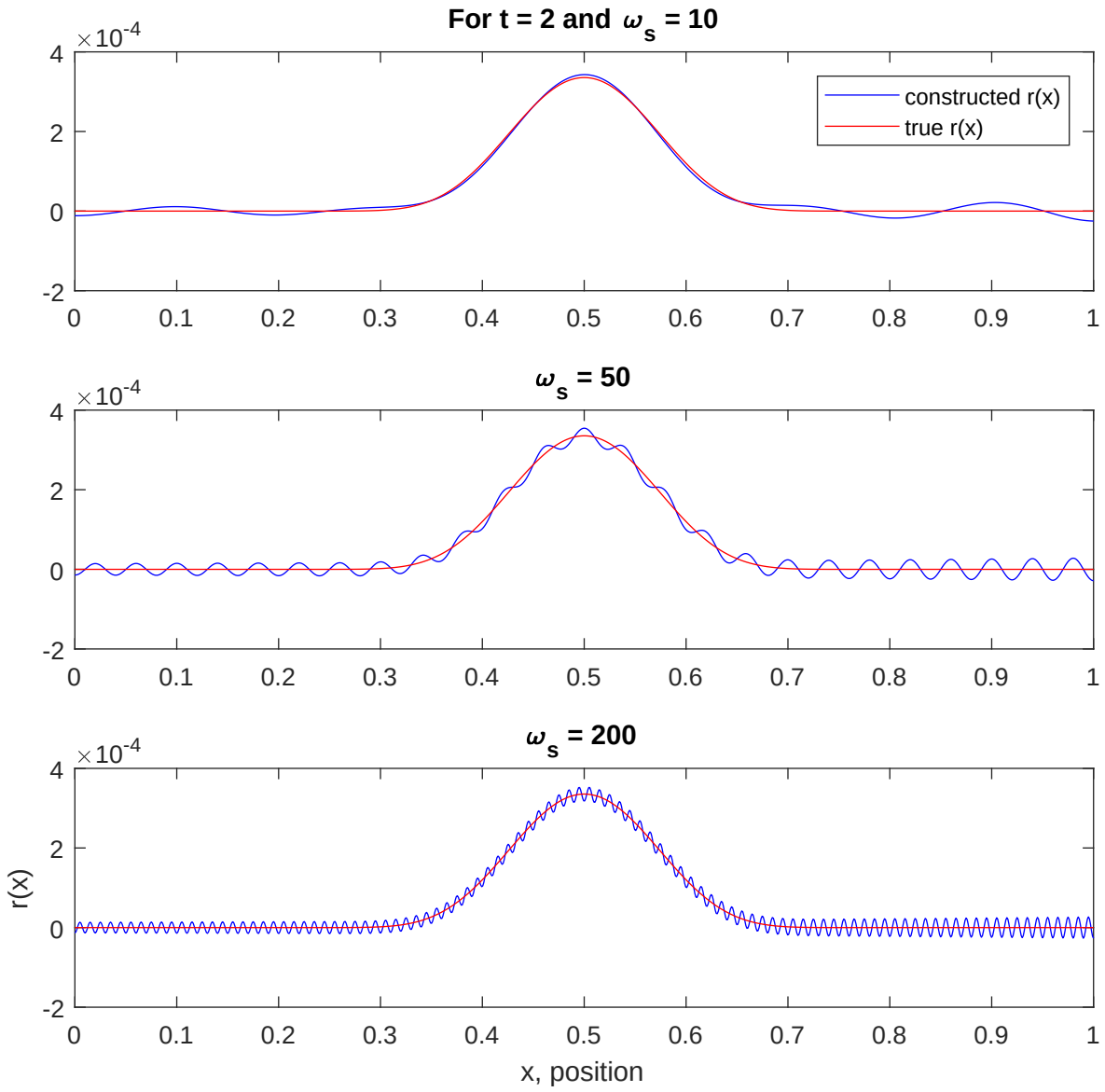

Figure 2.10: Reconstructed scattering potential for increasing sampling rate

We may also fix the sampling rate $\omega_s = 20$ and then record for $t = 2$, $t = 5$ and $t = 15$. Again, we plot the results below:

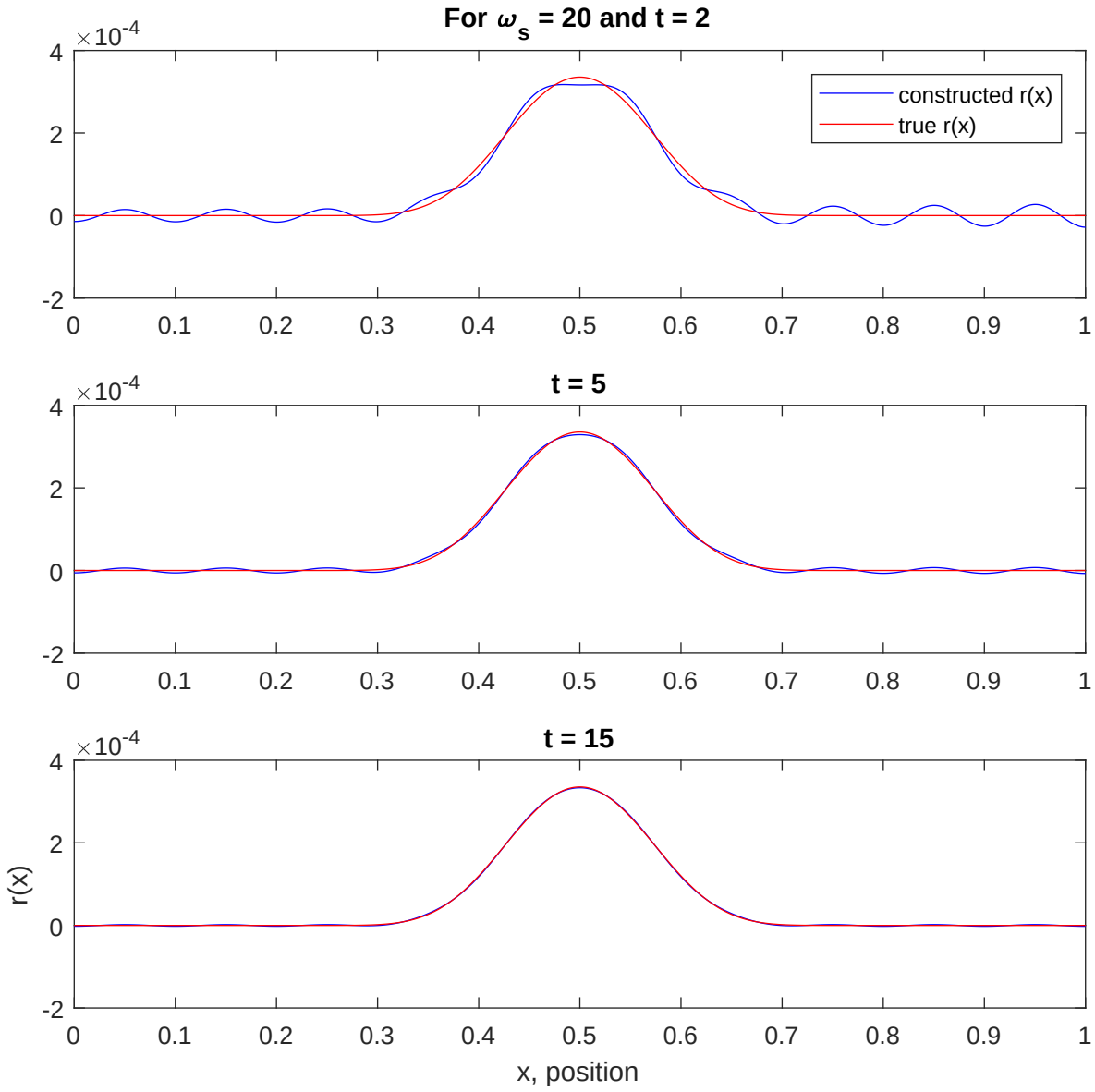

Figure 2.11: Reconstructed scattering potential for increased recording time

Finally, if we sample very finely and record to t very large, then we see that

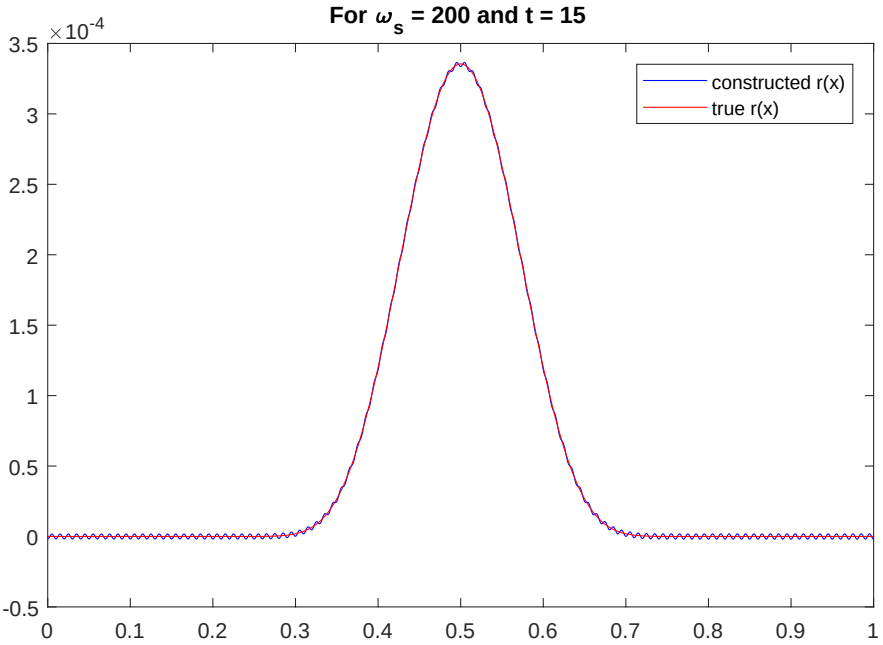

Figure 2.12: Reconstructed scattering potential from finely sampled data recorded for substantial time

As with the initial plot, we notice the rippling of the reconstructed function. This is caused by the sinc function, which is the impulse response of a perfect low-pass filter. In particular, the ideal low-pass filter inherently causes ringing artefacts in the time domain.

We examine the pointwise convergence of $r_{\text{const}}(x)$ to $r(x)$ by determining the ℓ^2 norm of the difference of their sampled versions $r_{\text{const}}(n\Delta x)$ and $r(n\Delta x)$. That is

$$\|r - r_{\text{const}}\|_2 := \left(\sum_{n=1}^{k} |r(n\Delta x) - r_{\text{const}}(n\Delta x)|^2 \right)^{\frac{1}{2}}, \tag{2.28}$$

where the n indexes the elements of the respective vector arrays and k is the maximum number of elements of the array of points on the lattice $\Delta x\mathbb{Z}$ in $\mathbb{R}$ for $\Delta x > 0$. In particular:

Definition 23. *We say that the constructed scattering potential array $r_{const} \to r$ pointwise if and only if $\|r - r_{const}\|_2 \to 0$ as $\omega_s \to \infty$ (i.e. we sample more finely) and/or $t \to \infty$ (i.e. we record the data for a longer time period).*

Indeed, we compute (2.25) for increasing ω_s and t, which we list in the table below:

ℓ^2 norm of $r - r_{\text{const}}$			
Sampling Rate	$t = 2$	$t = 5$	$t = 15$
$\omega_s = 10$	2.9555×10^{-4}	7.5574×10^{-5}	1.3834×10^{-4}
$\omega_s = 20$	4.4997×10^{-4}	1.4442×10^{-4}	4.5×10^{-5}
$\omega_s = 50$	4.532×10^{-4}	1.4404×10^{-4}	4.4521×10^{-5}
$\omega_s = 200$	4.2813×10^{-4}	1.3553×10^{-4}	4.1842×10^{-5}

One can also determine the *uniform convergence* of r_{const} to r by computing the ℓ^∞ norm of the difference of their respectively sampled versions. In particular:

$$\|r - r_{\text{const}}\|_\infty := \max\{|r(\Delta x) - r_{\text{const}}(\Delta x)|, ..., |r(k\Delta x) - r_{\text{const}}(k\Delta x)|\}, \tag{2.29}$$

for $n, k \in \mathbb{N}$ defined as before.

Definition 24. *We say that $r_{const} \to r$ uniformly if and only if $\|r - r_{const}\|_\infty \to 0$ as ω_s or $t \to \infty$.*

As before, we provide a table listing the ℓ^∞ norm of $r - r_{\text{const}}$ for various sampling rates and time the data is measured:

ℓ^∞ norm of $r - r_{\text{const}}$			
Sampling Rate	$t = 2$	$t = 5$	$t = 15$
$\omega_s = 10$	2.4983×10^{-5}	4.9221×10^{-6}	9.2952×10^{-6}
$\omega_s = 20$	2.8194×10^{-5}	7.189×10^{-6}	2.0637×10^{-6}
$\omega_s = 50$	2.8527×10^{-5}	7.1911×10^{-6}	2.0587×10^{-6}
$\omega_s = 200$	2.7×10^{-5}	6.7677×10^{-6}	1.9348×10^{-6}

From the above data, we may observe that, in general, r_{const} appears to diverge from r as the sampling rate is increased whereas the constructed potential converges somewhat more towards the true potential as the sampling time increases.

2.2 Homogeneous media in three dimensions

As stated in reference [1], *due to the greater number of degrees of freedom afforded by the greater number of dimensions, the three dimensional problem has somewhat added richness. For instance, a greater number of possible recording geometries and phenomena exist due to the higher dimensional variation of the background propogation speed.* However, we proceed as in the one dimensional case by deriving first an inversion formula assuming a constant-background wave speed, from which much insight will be gained.[1] With this in mind, we take $m(\boldsymbol{x}) = c^{-2} > 0$ for all $\boldsymbol{x} = (x, y, z) \in \mathbb{R}^3$.

Here $\hat{u} : \mathbb{R}_+ \times \mathbb{R}^3 \times \mathbb{S}^2 \to \mathbb{R}$, given by $(\omega, \boldsymbol{x}, \boldsymbol{\xi}) \mapsto \hat{u}(\omega, \boldsymbol{x}, \boldsymbol{\xi})$ will describe a plane wave $\hat{u}_{\text{inc}}(\omega, \boldsymbol{x}, \boldsymbol{\xi})$ sent in the direction of the unit vector $\boldsymbol{\xi}$ towards the *scattering centre*, together with an outgoing wave $\hat{u}_{\text{sc}}(\omega, \boldsymbol{x}, \boldsymbol{\xi})$ which describes the response of this centre, where $\boldsymbol{\xi} \in \mathbb{R}^3$ and $\|\boldsymbol{\xi}\| = 1$. Note that we will regard $\boldsymbol{\xi}$ as both in $\mathbb{R}^3$ and $\mathbb{S}^2$.

In a three dimensional homogeneous medium, we have the following boundary value problem

$$\begin{cases} u = u_{\text{inc}} + u_{\text{sc}} \\ \left(\Delta + \dfrac{\omega^2}{c^2}\right) \hat{u}_{\text{inc}}(\omega, \boldsymbol{x}, \boldsymbol{\xi}) = 0, \\ \left(\Delta + \dfrac{\omega^2}{c^2}\right) \hat{u}_{\text{sc}}(\omega, \boldsymbol{x}, \boldsymbol{\xi}) = r(\boldsymbol{x}) \hat{u}(\omega, \boldsymbol{x}, \boldsymbol{\xi}), \\ \|\boldsymbol{x}\| \left(\dfrac{\partial}{\partial \|\boldsymbol{x}\|} \hat{u}_{\text{inc}}(\omega, \boldsymbol{x}, \boldsymbol{\xi}) - \dfrac{ic}{\omega} \hat{u}_{\text{inc}}(\omega, \boldsymbol{x}, \boldsymbol{\xi})\right) \to 0 \quad \text{as } \|\boldsymbol{x}\| \to \infty, \\ \|\boldsymbol{x}\| \left(\dfrac{\partial}{\partial \|\boldsymbol{x}\|} \hat{u}_{\text{sc}}(\omega, \boldsymbol{x}, \boldsymbol{\xi}) - \dfrac{ic}{\omega} \hat{u}_{\text{sc}}(\omega, \boldsymbol{x}, \boldsymbol{\xi})\right) \to 0 \quad \text{as } \|\boldsymbol{x}\| \to \infty, \end{cases} \tag{2.30}$$

uniformly in all directions $\boldsymbol{\xi} \in \mathbb{S}^2$.

Moreover, the Green's function for the Helmholtz operator in three dimensional homogeneous media is given by

$$\begin{cases} \widehat{G}(\omega, \boldsymbol{x}) = -\dfrac{e^{i\omega\|\boldsymbol{x}\|/c}}{4\pi\|\boldsymbol{x}\|}, \\ \|\boldsymbol{x}\| \left(\dfrac{\partial}{\partial \|\boldsymbol{x}\|} \widehat{G}(\omega, \boldsymbol{x}) - \dfrac{ic}{\omega} \widehat{G}(\omega, \boldsymbol{x})\right) \to 0 \quad \text{as } \|\boldsymbol{x}\| \to \infty, \end{cases} \tag{2.31}$$

uniformly in all directions $\boldsymbol{\xi}$, which we derive via Proposition 6, using the property that $n + 1/2$ order Hankel functions are related to spherical Bessel functions.

2.2.1 Forward Scattering

Thus, with knowledge of the Green's function, we may thus write the scattered wave field as

$$\hat{u}^{\pm}_{\text{sc}}(\omega, \boldsymbol{x}, \boldsymbol{\xi}) = -\frac{1}{4\pi} \int_{\mathbb{R}^3} r(\boldsymbol{x}') \frac{e^{i\omega\|\boldsymbol{x}-\boldsymbol{x}'\|/c} \hat{u}^{\pm}(\omega, \boldsymbol{x}, \boldsymbol{\xi})}{\|\boldsymbol{x} - \boldsymbol{x}'\|} \, \mathrm{d}\boldsymbol{x}'. \tag{2.32}$$

We probe the medium with the incident wave field $\hat{u}^{\pm}_{\text{inc}}(\omega, \boldsymbol{x}, \boldsymbol{\xi}) = e^{\pm i\omega\boldsymbol{\xi}\boldsymbol{x}/c}$, which satisfies the Helmholtz equation. We may therefore rewrite the scattered field as

$$\begin{aligned} \hat{u}^{\pm}_{\text{sc}}(\omega, \boldsymbol{x}, \boldsymbol{\xi}) &= -\frac{1}{4\pi} \int_{\mathbb{R}^3} r(\boldsymbol{x}') \frac{e^{i\omega\|\boldsymbol{x}-\boldsymbol{x}'\|/c} \hat{u}^{\pm}_{\text{inc}}(\omega, \boldsymbol{x}, \boldsymbol{\xi})}{\|\boldsymbol{x} - \boldsymbol{x}'\|} \, \mathrm{d}\boldsymbol{x}', \\ &= -\frac{1}{4\pi} \int_{\mathbb{R}^3} r(\boldsymbol{x}') \frac{e^{i\omega\|\boldsymbol{x}-\boldsymbol{x}'\|/c} e^{\pm i\omega\boldsymbol{\xi}\boldsymbol{x}'/c}}{\|\boldsymbol{x} - \boldsymbol{x}'\|} \, \mathrm{d}\boldsymbol{x}', \end{aligned} \tag{2.33}$$

where we have made the Born approximation.

Consequently, the Lippmann-Schwinger equation is given by

$$\hat{u}^{\pm}(\omega, \boldsymbol{x}, \boldsymbol{\xi}) = e^{\pm i\omega \boldsymbol{\xi}\cdot\boldsymbol{x}/c} - \frac{1}{4\pi}\int_{\mathbb{R}^3} r(\boldsymbol{x}')\frac{e^{i\omega\|\boldsymbol{x}-\boldsymbol{x}'\|/c}e^{\pm i\omega\boldsymbol{\xi}\cdot\boldsymbol{x}'/c}}{\|\boldsymbol{x}-\boldsymbol{x}'\|}\,\mathrm{d}\boldsymbol{x}'. \tag{2.34}$$

We take measurements in the *far field*; that is, we suppose that our observation position $\boldsymbol{x} \in \mathbb{R}^3 \setminus \mathbb{D}$ is located "far away"from the scatterer. We take this into account by letting $\|\boldsymbol{x}\| \to \infty$. Thus we sample the scattered wave field on a sphere with radius $\|\boldsymbol{x}\| = R \gg 0$.

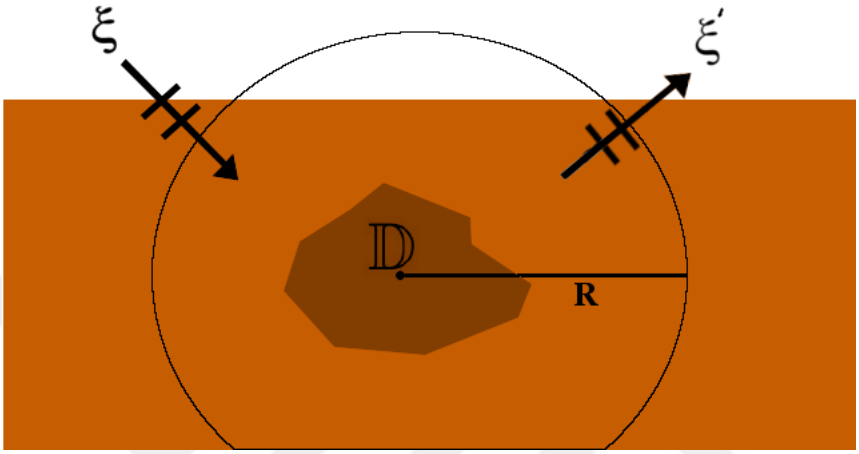

Figure 2.13: A 2D illustration of the far-field data acquisition configuration

Proposition 25. *Measuring from the + direction, with a far-field approximation, i.e.* $\|\boldsymbol{x}\| \gg \|\boldsymbol{x}'\|$ *and* $\|\boldsymbol{x}\| \gg \omega\|\boldsymbol{x}'\|^2$*, the scattered data is given by the asymptotic expansion*

$$\boxed{\hat{d}(\omega, \boldsymbol{\xi}, \boldsymbol{\xi}') \sim -\frac{e^{i\omega R/c}}{4\pi R}\hat{r}(\omega(\boldsymbol{\xi}'-\boldsymbol{\xi})/c)} \tag{2.35}$$

as $R \to \infty$*, where* $\boldsymbol{\xi} \in \mathbb{S}^2$*.*

Proof. We may do the following asymptotic expansion

$$\begin{aligned}
\|\boldsymbol{x}-\boldsymbol{x}'\| &= \sqrt{\|\boldsymbol{x}\| - 2\boldsymbol{x}\cdot\boldsymbol{x}' + \|\boldsymbol{x}'\|^2} \\
&= \|\boldsymbol{x}\|\sqrt{1 - 2\frac{\boldsymbol{\xi}'\cdot\boldsymbol{x}'}{\|\boldsymbol{x}\|} + \frac{\|\boldsymbol{x}'\|^2}{\|\boldsymbol{x}\|^2}} \\
&\sim \|\boldsymbol{x}\|\left(1 - \frac{\boldsymbol{\xi}'\cdot\boldsymbol{x}'}{\|\boldsymbol{x}\|} + \frac{1}{2}\frac{\|\boldsymbol{x}'\|^2}{\|\boldsymbol{x}\|^2} + \cdots\right) \\
&= \|\boldsymbol{x}\| - \boldsymbol{\xi}'\cdot\boldsymbol{x}' + \frac{1}{2}\frac{\|\boldsymbol{x}'\|}{\|\boldsymbol{x}\|} + \cdots
\end{aligned}$$

where $\boldsymbol{\xi}' := \boldsymbol{x}/R \in \mathbb{S}^2$ is the outgoing wave vector (and consequently, the $\boldsymbol{\xi} \in \mathbb{S}^2$ will denote the incoming wave vectors).

Therefore

$$e^{i\omega\|\boldsymbol{x}-\boldsymbol{x}'\|/c} = e^{i\omega\|\boldsymbol{x}\|/c}e^{-i\omega\boldsymbol{\xi}'\cdot\boldsymbol{x}'/c}\left(1 + \mathcal{O}\left(\frac{\omega\|\boldsymbol{x}'\|^2}{\|\boldsymbol{x}\|}\right)\right),$$

and

$$\frac{1}{\|\boldsymbol{x}-\boldsymbol{x}'\|} = \frac{1}{\|\boldsymbol{x}\|}\left(1 + \mathcal{O}\left(\frac{\|\boldsymbol{x}'\|}{\|\boldsymbol{x}\|}\right)\right), \qquad \|\boldsymbol{x}\| \to \infty.$$

As a result, in the far field we have

$$\frac{e^{i\omega\|\boldsymbol{x}-\boldsymbol{x}'\|/c}}{4\pi\|\boldsymbol{x}-\boldsymbol{x}'\|} \sim \frac{e^{i\omega\|\boldsymbol{x}\|/c}}{4\pi\|\boldsymbol{x}\|}e^{-i\omega\boldsymbol{\xi}'\cdot\boldsymbol{x}'}, \qquad \|\boldsymbol{x}\| \to \infty.$$

Thus, recalling that

$$\hat{u}_{\mathrm{sc}}^{+}(\omega,\boldsymbol{x},\boldsymbol{\xi}) = -\frac{1}{4\pi}\int_{\mathbb{R}^3} r(\boldsymbol{x}')\frac{e^{i\omega\|\boldsymbol{x}-\boldsymbol{x}'\|/c}e^{i\omega\boldsymbol{\xi}\boldsymbol{x}'/c}}{\|\boldsymbol{x}-\boldsymbol{x}'\|}\,\mathrm{d}\boldsymbol{x}',$$

we see, with the help of the above, that $\hat{u}_{\mathrm{sc}}^{+}$ has asymptotic behaviour

$$\hat{u}_{\mathrm{sc}}^{+}(\omega,\boldsymbol{x},\boldsymbol{\xi}) = \frac{e^{i\omega\|\boldsymbol{x}\|/c}}{\|\boldsymbol{x}\|}\hat{u}_{\infty}(\omega,\boldsymbol{x},\boldsymbol{\xi}) + \mathcal{O}\left(\frac{1}{\|\boldsymbol{x}\|^2}\right), \qquad \|\boldsymbol{x}\|\to\infty,$$

where the *far field pattern* $\hat{u}_\infty : \mathbb{R}_+ \times \mathbb{R}^3 \times \mathbb{S}^2 \to \mathbb{R}$ is given by

$$\hat{u}_{\infty}(\omega,\boldsymbol{x},\boldsymbol{\xi}) := -\frac{1}{4\pi}\int_{\mathbb{R}^3} r(\boldsymbol{x}')\hat{u}(\omega,\boldsymbol{x}',\boldsymbol{\xi})e^{-i\omega\boldsymbol{\xi}\cdot\boldsymbol{x}'/c}\,\mathrm{d}\boldsymbol{x}' \tag{2.36}$$

and replacing $\hat{u}$ by $\hat{u}_{\mathrm{inc}}$ in this procedure with the Born approximation, this becomes

$$\hat{u}_{\infty}(\omega,\boldsymbol{x},\boldsymbol{\xi}) \approx -\frac{1}{4\pi}\int_{\mathbb{R}^3} r(\boldsymbol{x}')e^{i\omega\boldsymbol{\xi}'\cdot\boldsymbol{x}'/c}e^{-i\omega\boldsymbol{\xi}\cdot\boldsymbol{x}'/c}\,\mathrm{d}\boldsymbol{x}'. \tag{2.37}$$

Consequently

$$\begin{aligned}
\hat{u}_{\mathrm{sc}}^{+}(\omega,\boldsymbol{x},\boldsymbol{\xi}) &\sim -\frac{1}{4\pi\|\boldsymbol{x}\|}\int_{\mathbb{R}^3} r(\boldsymbol{x}')e^{i\omega\|\boldsymbol{x}\|/c}e^{-i\omega\boldsymbol{\xi}'\cdot\boldsymbol{x}'/c}e^{i\omega\boldsymbol{\xi}\cdot\boldsymbol{x}'/c}\,\mathrm{d}\boldsymbol{x}' \\
&= -\frac{e^{i\omega R/c}}{4\pi R}\int_{\mathbb{R}^3} r(\boldsymbol{x}')e^{i\omega\boldsymbol{\xi}'\cdot\boldsymbol{x}'/c}e^{-i\omega\boldsymbol{\xi}\cdot\boldsymbol{x}'/c}\,\mathrm{d}\boldsymbol{x}' \\
&= -\frac{e^{i\omega R/c}}{4\pi R}\int_{\mathbb{R}^3} r(\boldsymbol{x}')e^{i\omega(\boldsymbol{\xi}'-\boldsymbol{\xi})\cdot\boldsymbol{x}'/c}\,\mathrm{d}\boldsymbol{x}' \\
&= -\frac{e^{i\omega R/c}}{4\pi R}\hat{r}(\omega(\boldsymbol{\xi}'-\boldsymbol{\xi})/c)
\end{aligned}$$

as $R\to\infty$.

Hence, the result follows by defining the data in the frequency domain $\hat{d}(\omega,\boldsymbol{\xi},\boldsymbol{\xi}')$ as $\hat{u}_{\mathrm{sc}}^{+}$ for fixed $\boldsymbol{x}_0\in\mathbb{R}^3$. □

Remark. *Note that* $\boldsymbol{\xi} = R\cdot(\cos\varphi,\sin\varphi)$ *and* $\boldsymbol{\xi}' = R\cdot(\cos\theta,\sin\theta)$ *for* $\varphi,\theta\in\mathbb{S}^1$*, so that*

$$\hat{d}(\omega,\boldsymbol{\xi},\boldsymbol{\xi}') = \hat{d}(\omega,\theta,\varphi) \sim -\frac{e^{i\omega R/c}}{4\pi R}\hat{r}\left(\frac{R}{c}\omega(\cos\theta-\cos\varphi,\sin\theta-\sin\varphi)\right). \tag{2.38}$$

2.2.2 Inverse Scattering

As in the one dimensional case, we are interested in deriving the scattering potential from discretely sampled data. Note that the techniques involved here will essentially fall under the category of *multidimensional signal processing*.

Fixing $\boldsymbol{\xi} = \boldsymbol{\xi}_0$

We can restrict our parameters to so that we essentially restrict our problem to a two dimensional framework. However, the medium is still three dimensional and the 3D Helmholtz equation is still the governing equation for the problem, so this method may be referred to as *2.5D inversion*.

If we fix our incoming wave vector $\boldsymbol{\xi} = \boldsymbol{\xi}_0$, then we can sample for all outgoing wave vectors $\boldsymbol{\xi}'\in\mathbb{S}^2$ and frequencies $\omega\in\mathbb{R}$. Then, abusing notation by writing "="in place of "$\sim$", we get

$$\hat{d}(\omega,\boldsymbol{\xi}') = -\frac{e^{i\omega R/c}}{4\pi R}\hat{r}(\omega(\boldsymbol{\xi}'-\boldsymbol{\xi}_0)/c). \tag{2.39}$$

and fixing $\varphi_0 = \pi/2$ yields

$$\boxed{\hat{d}(\omega,\theta) = -\frac{e^{i\omega R/c}}{4\pi R}\hat{r}\left(\frac{R}{c}\omega(\cos\theta,\sin\theta-1)\right)} \tag{2.40}$$

We would like to sample (2.42) in tangent-circular coordinates, in particular, the lattice $(\Delta\rho\mathbb{Z},\Delta\psi\mathbb{Z})$ on the Euclidean plane $\mathbb{R}^2$, for $\rho\in\mathbb{R}_+$ and $\psi\in\mathbb{S}^1$, which we plot below

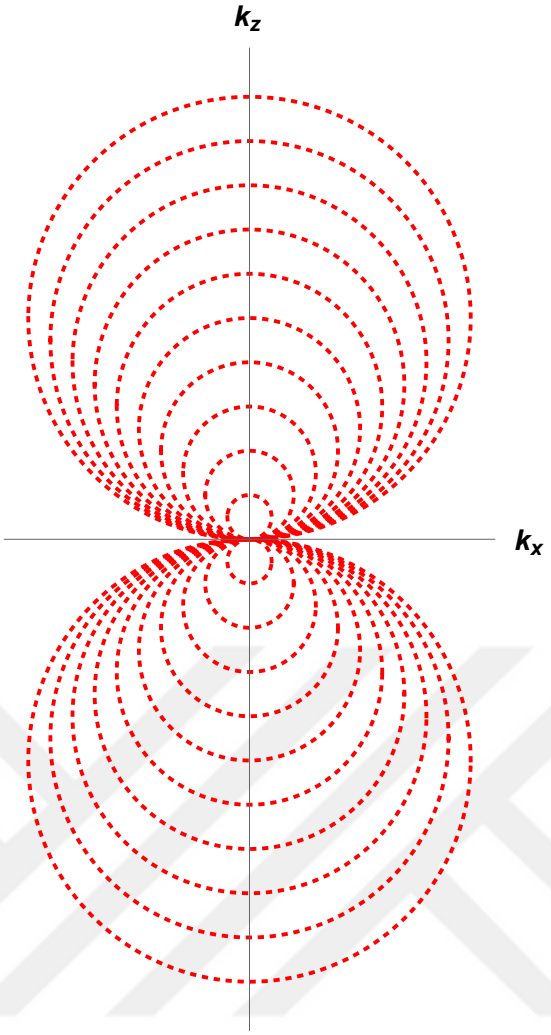

Figure 2.14: Tangent-circular sampling scheme in the spatial frequency domain

The following proposition gives the coordinate transformation map to go from (ω, θ) coordinates to the tangent-circular coordinates:

Proposition 26. *The coordinate transformation map* $\Lambda^{-1} : (\rho, \psi) \mapsto (\omega(\rho, \psi), \theta(\rho, \psi))$ *is given by*

$$(\omega(\rho,\psi),\theta(\rho,\psi)) = \left(-\frac{c\rho(\cos^2\psi + (\sin\psi+1)^2)}{2R(\sin\psi+1)}, \operatorname{atan2}\left(-\frac{2\cos\psi(\sin\psi \pm 1)}{\cos^2\psi + (\sin\psi\pm 1)^2}, \frac{\cos^2\psi - (\sin\psi\pm 1)^2}{\cos^2\psi + (\sin\psi\pm 1)^2}\right)\right),$$

where we have the $+$ *sign for* $k_z < 0$ *and the* $-$ *sign for* $k_z > 0$.

Proof. The tangent circles satisfy the equations

$$\begin{cases} \sqrt{k_x^2 + (k_z^2+\rho)^2} = \rho, & k_z > 0, \\ \sqrt{k_x^2 + (k_z^2-\rho)^2} = \rho, & k_z < 0, \end{cases} \tag{2.41}$$

which we may solve for $\rho \geq 0$ to get the function

$$\rho := \rho(k_x, k_z) = \begin{cases} \dfrac{k_x^2+k_z^2}{2k_z}, & k_z < 0, \\ -\dfrac{k_x^2+k_z^2}{2k_z}, & k_z > 0. \end{cases} \tag{2.42}$$

Then we may determine $\psi(k_x, k_z) \in \mathbb{S}^1$ to get the function

$$\psi := \psi(k_x, k_z) = \operatorname{atan2}\left(k_z + \frac{k_x^2+k_z^2}{2k_z}, k_x \right), \qquad k_z \neq 0.$$

Hence, with the above equations, we may transform from the Euclidean coordinates (k_x, k_z) to the tangent-circular coordinates (ρ, ψ) via

$$\begin{aligned}\Xi : \mathbb{R} \times \mathbb{R} &\to \mathbb{R}_+ \times \mathbb{S}^1 \\ (k_x, k_z) &\mapsto (\rho(k_x, k_z), \psi(k_x, k_z)).\end{aligned}$$

Hence we observe

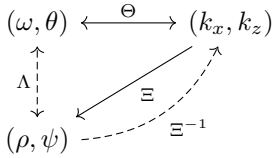

$(\star)$

where

$$\begin{aligned}\Theta : \mathbb{R}_+ \times \mathbb{S}^1 &\to \mathbb{R} \times \mathbb{R} \\ (\omega, \theta) &\mapsto (k_x(\omega, \theta), k_z(\omega, \theta)) = \left(\frac{R}{c}\omega\cos\theta, \frac{R}{c}\omega(\sin\theta - 1)\right)\end{aligned}$$

Now, we may solve the linear system of equations

$$\begin{cases} k_x = \dfrac{R}{c}\omega\cos\theta, \\ k_z = \dfrac{R}{c}\omega(\sin\theta - 1), \end{cases}$$

to deduce

$$\begin{aligned}\Theta^{-1} : \mathbb{R} \times \mathbb{R} &\to \mathbb{R}_+ \times \mathbb{S}^1 \\ (k_x, k_z) &\mapsto (\omega(k_x, k_z), \theta(k_x, k_z)) = \left(-\frac{c(k_x^2 + k_z^2)}{2Rk_z}, \operatorname{atan2}\left(-\frac{2k_xk_z}{k_x^2 + k_z^2}, \frac{k_x^2 - k_z^2}{k_x^2 + k_z^2}\right)\right)\end{aligned}$$

where $\operatorname{atan2} : \mathbb{R} \times \mathbb{R} \to \mathbb{R}$ is the four quadrant inverse tangent function.

Observe that $(\star)$ is a diagram of coordinate transformations. The solid arrows represent the transformations, Θ, Θ^{-1} and Ξ, which have already been determined whilst the dashed arrows are the ones which are yet to be determined (e.g. $\Xi^{-1} : \mathbb{R}_+ \times \mathbb{S}^1 \to \mathbb{R} \times \mathbb{R}$). We may observe that once the transformation $\Xi^{-1} : (\rho, \psi) \mapsto (\rho(k_x, k_z), \psi(k_x, k_z))$ has been established then the diagram will commute and consequently the transformations from $\Lambda : (\omega, \theta) \mapsto (\rho(\omega, \theta), \psi(\omega, \theta))$ and its inverse $\Lambda^{-1} : (\rho, \psi) \mapsto (\omega(\rho, \psi), \theta(\rho, \psi))$ will be a composition of transformations:

$$\begin{aligned}\Lambda = \Theta \circ \Xi : \mathbb{R}_+ \times \mathbb{S}^1 &\to \mathbb{R}_+ \times \mathbb{S}^1 \\ (\omega, \theta) &\mapsto ((\rho \circ k_x)(\omega, \theta), (\psi \circ k_z)(\omega, \theta))\end{aligned}$$

and

$$\begin{aligned}\Lambda^{-1} = \Xi^{-1} \circ \Theta^{-1} : \mathbb{R}_+ \times \mathbb{S}^1 &\to \mathbb{R}_+ \times \mathbb{S}^1 \\ (\rho, \psi) &\mapsto ((\omega \circ k_x)(\rho, \psi), (\theta \circ k_z)(\rho, \psi)).\end{aligned}$$

To this end, let $\Omega : \mathbb{R}_+ \times \mathbb{S}^1 \to \mathbb{R} \times \mathbb{R}$ defined by $(\rho, \vartheta) \mapsto (k_x(\rho, \vartheta), k_z(\rho, \vartheta)) = (\rho\cos\vartheta, \rho\sin\vartheta)$ be the transformation map from polar to Cartesian coordinates. Then one can observe that $\vartheta = \psi$ and

$$\begin{aligned}\Xi^{-1} : \mathbb{R}_+ \times \mathbb{S}^1 &\to \mathbb{R} \times \mathbb{R} \\ (\rho, \psi) &\mapsto (k_x(\rho, \psi), k_z(\rho, \psi)) = \begin{cases} \Omega(\rho, \psi) \oplus (0, -\rho), & k_z > 0, \\ \Omega(\rho, \psi) \oplus (0, \rho), & k_z < 0. \end{cases}\end{aligned}$$

Note that the tangent circular lattice on $\mathbb{R}^2$ is $(\Delta\rho\mathbb{Z}, \Delta\psi\mathbb{Z})$. We may thus write

$$\begin{aligned}\Lambda^{-1}(\omega, \theta) &= \Xi^{-1}(\Theta^{-1}(\omega, \theta)) \\ &= (\omega(k_x(\rho, \psi), k_z(\rho, \psi)), \theta(k_x(\rho, \psi), k_z(\rho, \psi))) \\ &= \begin{cases} (\omega(\rho\cos\psi, \rho\sin\psi - \rho), \theta(\rho\cos\psi, \rho\sin\psi - \rho)), & k_z > 0, \\ (\omega(\rho\cos\psi, \rho\sin\psi + \rho), \theta(\rho\cos\psi, \rho\sin\psi + \rho)), & k_z < 0. \end{cases} \\ &= \begin{cases} \left(-\dfrac{c\rho(\cos^2\psi + (\sin\psi - 1)^2)}{2R(\sin\psi - 1)}, \operatorname{atan2}\left(-\dfrac{2\cos\psi(\sin\psi - 1)}{\cos^2\psi + (\sin\psi - 1)^2}, \dfrac{\cos^2\psi - (\sin\psi - 1)^2}{\cos^2\psi + (\sin\psi - 1)^2}\right)\right), & k_z > 0, \\ \left(-\dfrac{c\rho(\cos^2\psi + (\sin\psi + 1)^2)}{2R(\sin\psi + 1)}, \operatorname{atan2}\left(-\dfrac{2\cos\psi(\sin\psi + 1)}{\cos^2\psi + (\sin\psi + 1)^2}, \dfrac{\cos^2\psi - (\sin\psi + 1)^2}{\cos^2\psi + (\sin\psi + 1)^2}\right)\right), & k_z < 0, \end{cases}\end{aligned}$$

□

Proposition 27. *For $(\rho, \psi) \in \mathbb{R}_+ \times \mathbb{S}^1$, we may retrieve the scattering potential in the frequency domain as*

$$\hat{r}(\rho,\psi) = -4\pi R \cdot \hat{d}\left[-\frac{c\rho(\cos^2\psi + (\sin\psi+1)^2)}{2R(\sin\psi+1)}, \operatorname{atan2}\left(-\frac{2\cos\psi(\sin\psi\pm 1)}{\cos^2\psi+(\sin\psi\pm1)^2}, \frac{\cos^2\psi-(\sin\psi\pm1)^2}{\cos^2\psi+(\sin\psi\pm1)^2}\right)\right] \cdot \exp\left(\frac{\rho(\cos^2\psi+(\sin\psi\pm1)^2)}{2(\sin\psi\pm1)}\right).$$

Proof. The result follows quite easily from a change of coordinates via the previous proposition. □

Corollary 28. *We may recover the scattering potential in Cartesian coordinates as*

$$\boxed{r(x,z) = (\mathcal{F}^{-1} \circ \hat{r})((\rho,\psi) \circ \Xi^{-1})}$$

Proof. From Proposition 28, switch to Cartesian coordinates via Ξ^{-1} and apply an inverse Fourier transform. □

Corollary 29. *We may regularly sample the data in the frequency domain in the tangent circle lattice $(\Delta\rho\mathbb{Z}, \Delta\psi\mathbb{Z}) \subset \mathbb{R}^2$ via*

$$\hat{d}(n\Delta\rho, m\Delta\psi) = -\frac{e^{i\omega(n\Delta\rho, m\Delta\psi)R/c}}{4\pi R}\hat{r}\left(\frac{R}{c}\omega(n\Delta\rho, m\Delta\psi)(\cos(\theta(n\Delta\rho, m\Delta\psi)), \sin(\theta(n\Delta\rho, m\Delta\psi)) - 1)\right),$$

for $\Delta\rho, \Delta\psi > 0$ and $\omega : \mathbb{R}_+ \times \mathbb{S}^1 \to \mathbb{R}_+$ and $\theta : \mathbb{R}_+ \times \mathbb{S}^1 \to \mathbb{S}^1$ defined as before.

Conjecture 30. *One may reconstruct the scattering potential $r(x,z)$ from data sampled on the lattice $(\Delta\rho\mathbb{Z}, \Delta\psi\mathbb{Z})$.*

Remark. *The above conjecture remains an open problem.*

In computerised tomography, one often reconstructs data from polar samples. In particular, one fires x-rays at an object measures its "shadow"at the other end. In the proceeding section, we explore these methods for the seismic problem.

Measurements at $\boldsymbol{\xi}' = -\boldsymbol{\xi}$

One scenario in which uniform polar sampling can be used is the scenario whereby we sample the scattered wave field at $\boldsymbol{\xi}' = -\boldsymbol{\xi}$; in particular, where $\hat{d}(\omega, \boldsymbol{\xi}, \boldsymbol{\xi}') = \hat{d}(\omega, \boldsymbol{\xi}, -\boldsymbol{\xi})$. We get that

$$\hat{d}(\omega, \boldsymbol{\xi}) = -\frac{e^{i\omega R/c}}{4\pi R}\hat{r}(2\omega\boldsymbol{\xi}/c), \tag{2.43}$$

i.e.

$$\boxed{\hat{d}(\omega,\theta) = -\frac{e^{i\omega R/c}}{4\pi R}\hat{r}\left(\frac{2R}{c}\omega(\cos\theta, \sin\theta)\right)} \tag{2.44}$$

One can sample in polar coordinates (ρ, ϑ), with $\rho \in \mathbb{R}_+$ and $\vartheta \in \mathbb{S}^1$, which yields the polar lattice $(\Delta\omega\mathbb{Z}, \Delta\theta\mathbb{Z})$ on the Euclidean plane $\mathbb{R}^2$. We plot this below on the Cartesian plane in the spatial frequency domain (k_x, k_z):

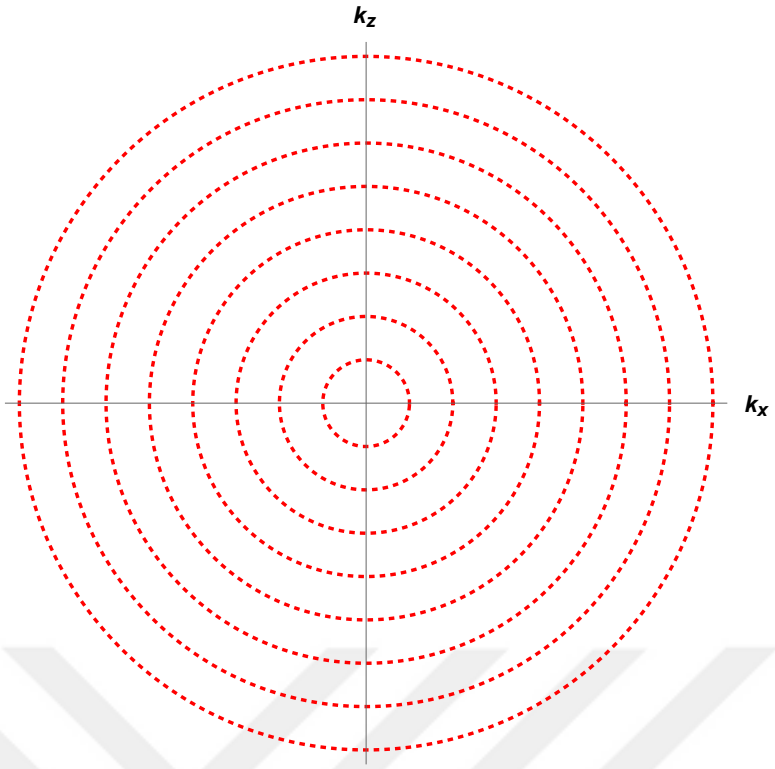

Figure 2.15: Polar sampling scheme in spatial frequency domain

Theorem 31. *Taking measurements at $\boldsymbol{\xi}' = -\boldsymbol{\xi}$, for all $x, z \in \mathbb{R}$, we may retrieve the scattering potential in the frequency domain as*

$$\boxed{\hat{r}(\rho,\vartheta) = -4\pi R \cdot \hat{d}\left(\frac{c}{2R}\rho,\vartheta\right) e^{-i\rho/2}} \qquad (\rho,\vartheta) \in \mathbb{R}_+ \times \mathbb{S}^1 \tag{2.45}$$

Proof. We may deduce via some simple algebraic manipulation that

$$\hat{r}(\underbrace{2R\omega\cos(\theta)/c}_{k_x}, \underbrace{2R\omega\sin(\theta)/c}_{k_z}) = -4\pi R \cdot \hat{d}(\omega,\theta)e^{-i\omega R/c}.$$

Then in order to write $\hat{r}(\rho,\vartheta)$, we note that the maps from polar to Cartesian coordinates and vice versa are given by the maps

$$\begin{aligned}\Upsilon : \mathbb{R}\times\mathbb{R} &\to \mathbb{R}_+ \times \mathbb{S}^1 \\ (k_x,k_z) &\mapsto (\rho(k_x,k_z),\vartheta(k_x,k_z)) = (\rho\cos\vartheta, \rho\sin\vartheta)\end{aligned}$$

and

$$\begin{aligned}\Upsilon^{-1} : \mathbb{R}_+\times\mathbb{S}^1 &\to \mathbb{R}\times\mathbb{R} \\ (\rho,\vartheta) &\mapsto (k_x(\rho,\vartheta),k_z(\rho,\vartheta)) = (\sqrt{k_x^2+k_z^2}, \operatorname{atan2}(k_z,k_x))\end{aligned}$$

Thus, we may compute

$$\rho := \rho(k_x,k_z) = \sqrt{k_x^2+k_z^2} = 2\frac{R}{c}\omega\sqrt{\cos^2\theta+\sin^2\theta} = \frac{2R}{c}\omega$$

and

$$\vartheta := \vartheta(k_x,k_z) = \operatorname{atan2}(k_z,k_y) = \theta,$$

Then it is easy to see that the map from polar coordinates to (ω,θ) is given by

$$\begin{aligned}\Psi : \mathbb{R}_+\times\mathbb{S}^1 &\to \mathbb{R}_+\times\mathbb{S}^1 \\ (\rho,\vartheta) &\mapsto (\omega(\rho,\vartheta),\theta(\rho,\vartheta)) = \left(\frac{c}{2R}\rho,\vartheta\right).\end{aligned}$$

Hence, in polar coordinates, we may write the scattering potential in the Fourier domain as

$$\hat{r}(\rho,\vartheta) = -4\pi R \cdot \hat{d}\left(\frac{c}{2R}\rho,\vartheta\right) e^{-i\rho/2} \tag{2.46}$$

□

Since we would like to construct the scattering potential from data regularly sampled in polar coordinates in the frequency domain, we state the following lemma:

Lemma 32. *Let $f(x,y)$ be space-limited to $2A$ and $\hat{f}(\omega,\theta)$ be angularly band-limited to K. Then $\hat{f}(\omega,\theta)$ can be reconstructed from its polar samples via*

$$\hat{f}(\omega,\theta)=\sum_{n=-\infty}^{\infty}\sum_{k=0}^{N-1}\tilde{\hat{f}}\left(\frac{n}{2A},\frac{2\pi k}{N}\right)\operatorname{sinc}\left[\frac{(\omega-\frac{n}{2A})}{\frac{1}{2A}}\right]\cdot D_N\left(\theta-\frac{2\pi k}{N}\right), \tag{2.47}$$

where N is even,

$$D_N(\theta)=\frac{\sin\left[\frac{1}{2}(N-1)\theta\right]}{N\sin\left(\frac{\theta}{2}\right)},$$

is a function similar to the Dirichlet kernel and

$$\tilde{\hat{f}}\left(\frac{n}{2A},\frac{2\pi k}{N}\right)=\begin{cases}\hat{f}\left(\frac{n}{2A},\frac{2\pi k}{N}\right), & n\geq 0,\\ \hat{f}\left(-\frac{n}{2A},\frac{2\pi k}{N}+\pi\right), & n<0.\end{cases} \tag{2.48}$$

[4]

Remark. *In the above lemma, the sampling rates have been taken to be $\Delta\omega=\frac{1}{2A}$ and $\Delta\theta=\frac{2\pi}{N}$.*

Corollary 33. *We may construct the scattering potential from the data regularly sampled in polar coordinates as*

$$\boxed{\begin{aligned}r_{const}(x,z)=-4\pi R\sum_{n=-\infty}^{\infty}\sum_{m=0}^{N-1}\tilde{\hat{d}}(n\Delta\omega,m\Delta\theta)\int_{-\infty}^{\infty}\int_{-\infty}^{\infty}\operatorname{sinc}\left(\frac{\frac{c}{2R}\sqrt{k_x^2+k_z^2}-n\Delta\omega}{\Delta\omega}\right)\\ \cdot D_N\left[\operatorname{atan2}(k_z,k_x)-m\Delta\theta\right]e^{-i\sqrt{k_x^2+k_z^2}/2}\cdot e^{-i(k_x\cdot x+k_z\cdot z)}\,\mathrm{d}k_x\,\mathrm{d}k_z\end{aligned}} \tag{2.49}$$

Proof. We may sample on the polar lattice $(\Delta\omega\mathbb{Z},\Delta\theta\mathbb{Z})\subset\mathbb{R}^2$ and then apply the previous lemma which allows us to deduce

$$\hat{r}_{\text{const}}(\rho,\vartheta)=-4\pi R\sum_{n=-\infty}^{\infty}\sum_{m=0}^{N-1}\tilde{\hat{d}}(n\Delta\omega,m\Delta\theta)\operatorname{sinc}\left(\frac{\frac{c}{2R}\rho-n\Delta\omega}{\Delta\omega}\right)\cdot D_N(\vartheta-m\Delta\theta)e^{-i\rho/2},$$

where

$$\tilde{\hat{d}}(n\Delta\omega,m\Delta\theta)=\begin{cases}\hat{d}(n\Delta\omega,m\Delta\theta), & n\geq 0,\\ \hat{d}(-n\Delta\omega,m\Delta\theta+\pi), & n<0,\end{cases}$$

for $N\in\mathbb{N}$ even and $D_N:\mathbb{S}^1\to\mathbb{C}$ is the function similar to the Dirichlet kernel, defined as before.

Thus switching to Cartesian coordinates yields

$$\hat{r}_{\text{const}}(k_x,k_z)=-4\pi Re^{-i\sqrt{k_x^2+k_z^2}/2}\sum_{n=-\infty}^{\infty}\sum_{m=0}^{N-1}\tilde{\hat{d}}(n\Delta\omega,m\Delta\theta)\operatorname{sinc}\left(\frac{\frac{c}{2R}\sqrt{k_x^2+k_z^2}-n\Delta\omega}{\Delta\omega}\right)\cdot D_N\left[\operatorname{atan2}(k_z,k_x)-m\Delta\theta\right].$$

Finally, taking the inverse Fourier transform gives us what we want. □

We can summarise the reconstruction steps proven above in the form of an algorithm:

Sinc Interpolation Algorithm in Frequency Domain

Step 1: Initialise algorithm with data measured in the frequency domain, $\hat{d}(\omega, \theta)$ and $N \in \mathbb{N}$, even.
  for all n & m **do**
    Sample the data in the frequency domain to get $\hat{d}(n\Delta\omega, m\Delta\theta)$
  end for $n = \omega/\Delta\omega$ & $m = \theta/\Delta\theta$
Step 2: Interpolate the data
  for all $n \in \mathbb{Z}$ & $m \in \mathbb{Z}_+$ **do**
    Write $\hat{d}(n\Delta\omega, m\Delta\theta)\,\mathrm{sinc}\left(\frac{\omega - n\Delta\omega}{\Delta\omega}\right) D_N[\theta - m\Delta\theta]e^{-R\omega/c}$
    Step 2.1: Write $\omega = \frac{c}{2R}\rho$.
    Step 2.2: Switch to Cartesian coordinates: $\rho = \sqrt{k_x^2 + k_z^2}$ & $\theta = \mathrm{atan2}(k_z, k_x)$.
    Step 2.3: Compute $\hat{r}(k_x, k_z) = -4\pi R e^{-i\sqrt{k_x^2+k_z^2}/2} \sum_{n=-\infty}^{\infty} \sum_{m=0}^{N-1} \tilde{\hat{d}}(n\Delta\omega, m\Delta\theta)\,\mathrm{sinc}\left(\frac{\frac{c}{2R}\sqrt{k_x^2+k_z^2} - n\Delta\omega}{\Delta\omega}\right) \cdot D_N\left[\mathrm{atan2}(k_z, k_x) - m\Delta\theta\right]$
  end for $m = N - 1$
Step 3: Inverse Fourier transform
Retrieve the scattering potential as $r(x, z) = \mathcal{F}^{-1}\{\hat{r}(\cdot, \cdot)\}(x, z)$

Example 34. To generate example data, we will use the scattering potential $r = s \otimes s \in C_c^\infty(\mathbb{R} \times \mathbb{R})$, where

$$\begin{aligned} s : \mathbb{R} &\to \mathbb{R} \\ x &\mapsto \psi(x)\psi(1-x), \end{aligned} \tag{2.50}$$

with $\psi \in C^\infty(\mathbb{R})$ defined as in (2.28).

We plot $r(x, z)$ below:

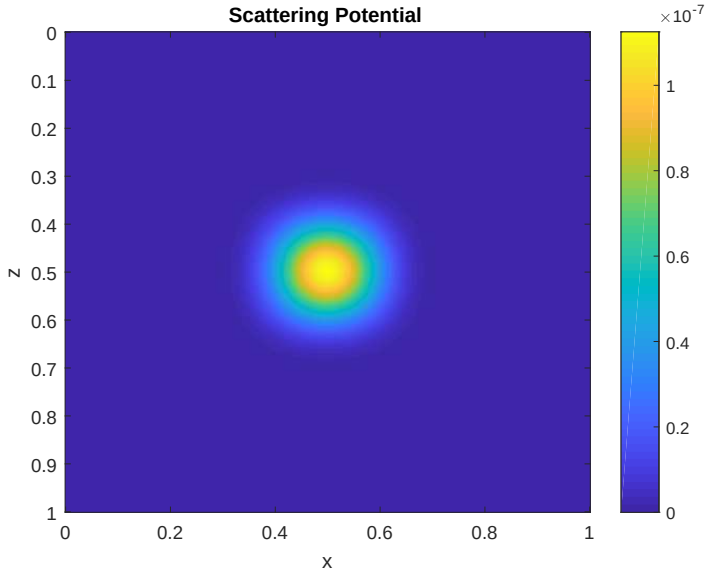

Figure 2.16: Example scattering potential

We will generate the example data from this scattering potential and then apply our formulae to see whether we can reconstruct it again to exact precision.

Recall that the data in the frequency domain $\hat{d} : \mathbb{R}_+ \times \mathbb{S}^1 \to \mathbb{C}$, with measurements at $\boldsymbol{\xi}' = -\boldsymbol{\xi}$, was given by

$$\begin{aligned} \hat{d}(\omega, \theta) &= -\frac{e^{10i\omega}}{40\pi} \hat{r}(20\omega(\cos\theta, \sin\theta)) \\ &= -\frac{e^{10i\omega}}{40\pi} \int_{-\infty}^{\infty} \int_{-\infty}^{\infty} r(x, z) e^{20i\omega(x\cdot\cos\theta + z\cdot\sin\theta)}\,\mathrm{d}x\,\mathrm{d}z, \end{aligned} \tag{2.51}$$

where we have set $c = 1$ and $R = 10$.

Since the equation for the data involves a Fourier transform, it is complex valued. Below we plot the real, imaginary and absolute values, $\mathrm{Re}\{\hat{d}(\omega,\theta)\}$, $\mathrm{Im}\{\hat{d}(\omega,\theta)\}$ and $|\hat{d}(\omega,\theta)|$ respectively:

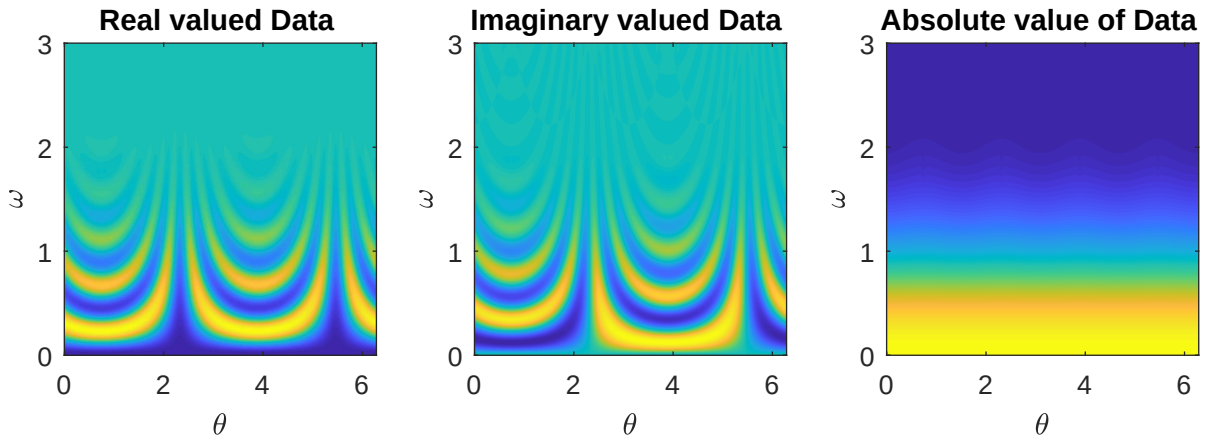

Figure 2.17: Data plots in polar frequency domain

The sampled data is then given by

$$\begin{aligned}\hat{d}(n\Delta\omega, m\Delta\theta) &= -\frac{e^{10in\Delta\omega}}{40\pi}\hat{r}(20n\Delta\omega(\cos(m\Delta\theta),\sin(m\Delta\theta))) \\ &= -\frac{e^{10in\Delta\omega}}{40\pi}\int_0^\infty\int_0^\infty r(x,z)e^{20in\Delta\omega(\cos(m\Delta\theta)\cdot x+\sin(m\Delta\theta)\cdot z)}\,\mathrm{d}x\,\mathrm{d}z,\end{aligned}$$

We determined that one may construct the scattering potential using the equation

$$\begin{aligned}r_{\text{const}}(x,z) = -40\pi\sum_{n=-\infty}^{\infty}\sum_{m=0}^{N-1}\tilde{\hat{d}}(n\Delta\omega, m\Delta\theta)\int_{-\infty}^{\infty}\int_{-\infty}^{\infty}\operatorname{sinc}\left(\frac{\frac{1}{20}\sqrt{k_x^2+k_z^2}-n\Delta\omega}{\Delta\omega}\right) \\ \cdot D_N\left[\operatorname{atan2}(k_z,k_x)-m\Delta\theta\right]e^{-i\sqrt{k_x^2+k_z^2}/2}\cdot e^{-i(k_x\cdot x+k_z\cdot z)}\,\mathrm{d}k_x\,\mathrm{d}k_z,\end{aligned}$$

However, our subsequent attempts to implement the above formula were in vain, so this would be a path for further research.

Reconstruction via Interpolation onto the Cartesian frame

Alternatively, having retrieved the scattering potential given data in polar coordinates, we may sample on the polar lattice $(\Delta\rho\mathbb{Z}, \Delta\vartheta\mathbb{Z}) \subset \mathbb{R}^2$ and through Theorem 33, get a uniformly sampled version of the scattering potential in polar coordinates in the Fourier domain:

$$\hat{r}(n\Delta\rho, m\Delta\vartheta) = -4\pi R\cdot\hat{d}\left(\frac{c}{2R}n\Delta\rho, m\Delta\vartheta\right)e^{-in\Delta\rho/2}. \tag{2.52}$$

We can then interpolate onto the Cartesian coordinate frame, (k_x, k_z), using *Matlab's* built-in `interp2` function to get $\hat{r}(k_x, k_z)$. In particular, we will utilise and compare the following two interpolation methods:

Definition 35 (Nearest Neighbour Interpolation)**.** *For each point of the polar lattice $(\Delta\rho\mathbb{Z}, \Delta\vartheta\mathbb{Z})$, the nearest neighbour interpolation algorithm simply selects the value of the nearest point on the Euclidean plane $\mathbb{R}^2$, where "nearest point"here is with respect to Euclidean distance.*

Or, to be more precise, one may define nearest neighbourhood interpolation as an embedding

$$\mathcal{N} : (\Delta\rho\mathbb{Z}, \Delta\vartheta\mathbb{Z}) \hookrightarrow \mathbb{R}^2.$$

Definition 36 (Bilinear Interpolation)**.** *Let $f : \mathbb{R}_+ \times \mathbb{S}^1 \to \mathbb{R}$ be a function and let (ρ_1, ϑ_1), (ρ_1, ϑ_2), (ρ_2, ϑ_1), $(\rho_2, \vartheta_2) \in \mathbb{R}_+ \times \mathbb{S}^1$ be points on the Euclidean plane. Then bilinear interpolation is the result of linear interpolation with respect to ρ and ϑ. Note that it does not matter which variable we choose to linearly interpolate with respect to first.*

Finally, we may retrieve $r(x, z)$ using the discrete Fourier transform. For this, we may in fact use the inverse of the fast Fourier transform (FFT), which is also a built-in Matlab function, `ifft`.

Linear/Nearest Neighbourhood Interpolation Algorithm in Frequency Domain

---

Step 1: Initialise algorithm with $\hat{r}(n\Delta\rho, m\Delta\vartheta) = -4\pi R \cdot \hat{d}\left(\frac{c}{2R} n\Delta\rho, m\Delta\vartheta\right) e^{-in\Delta\rho/2}$

for all n & m **do**

Interpolate $(n\Delta\rho, m\Delta\vartheta) \hookrightarrow (n\Delta k_x, m\Delta k_z)$ using either linear interpolation or nearest neighbourhood interpolation.

end for $n = \omega/\Delta\omega$ & $m = \theta/\Delta\theta$

Step 2: Retrieve the scattering potential in discrete space by the inverse Fast Fourier transform

---

Example 37. Define $r \in C_c^\infty(\mathbb{R}^2)$ as in previous examples. Below we plot the $\mathrm{Re}\{\hat{r}(n\Delta\rho, m\Delta\vartheta)\}$ derived via nearest neighbourhood interpolation and bilinear interpolation respectively from $\hat{r}(n\Delta k_x, m\Delta k_z)$:

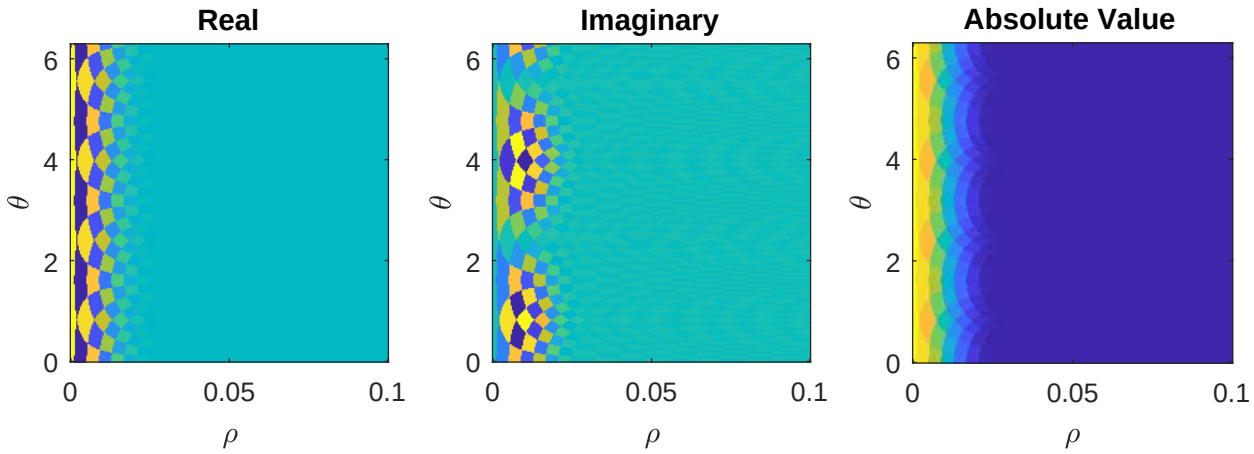

Figure 2.18: Approximate value of $\hat{r}(n\Delta\rho, m\Delta\vartheta)$ after nearest neighbourhood interpolation

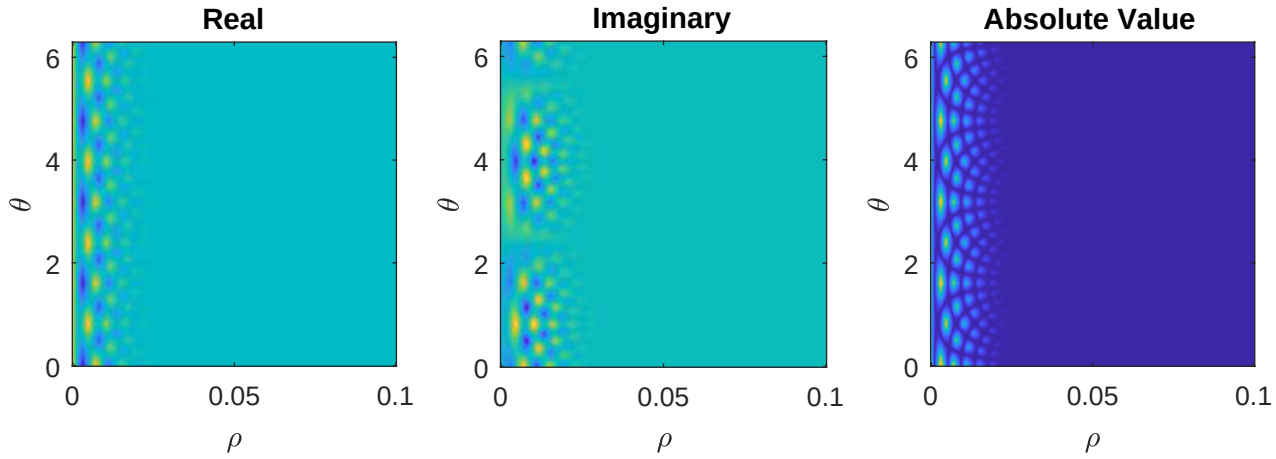

Figure 2.19: Approximate value of $\hat{r}(n\Delta\rho, m\Delta\vartheta)$ after bilinear interpolation

Next we plot the reconstructed scattering potential $r_{\text{const}}(x, z)$ which have been acquired by an inverse

fast Fourier transform of the data given by nearest neighbourhood interpolation and bilinear interpolation respectively:

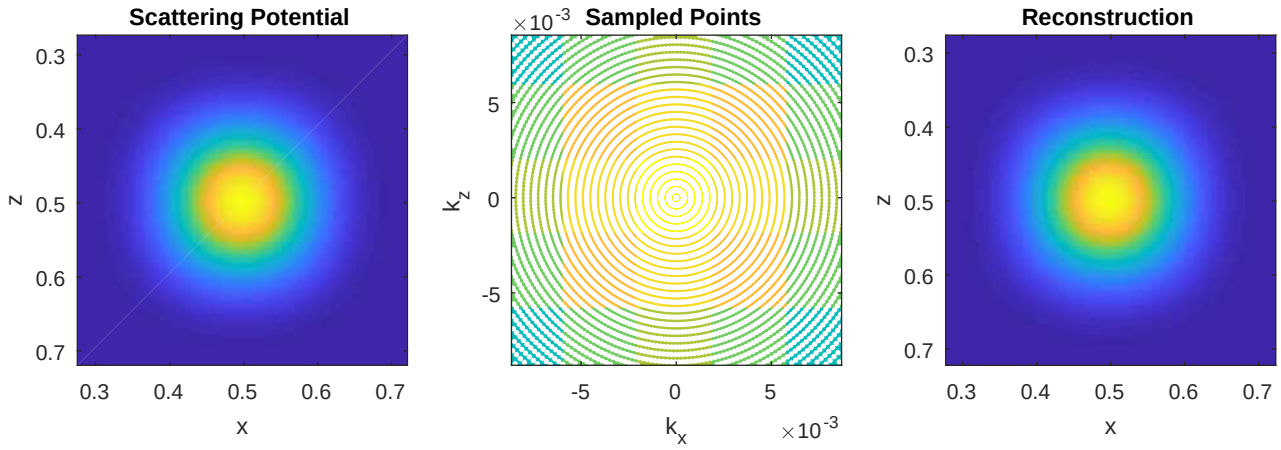

Figure 2.20: $r_{\text{const}}(x, z)$ reconstructed via nearest neighbourhood interpolation

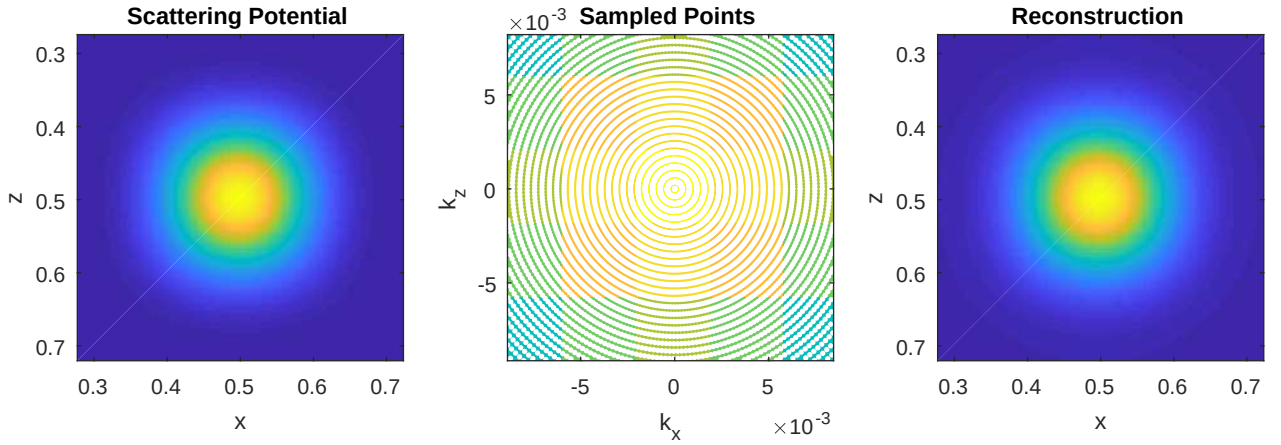

Figure 2.21: $r_{\text{const}}(x, z)$ reconstructed via bilinear interpolation

Now we examine the pointwise and uniform convergence of the reconstructed scattering potential to the actual scattering potential. We set $\mathrm{R} = r(n\Delta x, m\Delta z)$ as the discrete scattering matrix and $\mathrm{R}^{\text{near}}_{\text{const}} \in \mathbb{C}^{N\times M}$ and $\mathrm{R}^{\text{lin}}_{\text{const}} \in \mathbb{C}^{N\times M}$ for $n = 1, .., N$ and $m = 1, ..., M$ as the matrices of the reconstructions via nearest neighbourhood and bilinear interpolation respectively.

Definition 38 (L^{pq} and Hilbert-Schmidt norm)**.** *Let* A *be an* $N \times M$ *matrix. Then for* $p, q \geq 1$*, we may define its* L^{pq} *norm as*

$$\|\mathrm{A}\|_{p,q} = \left(\sum_{n=1}^{N} \left(\sum_{m=1}^{M} |a_{nm}|^p \right)^{q/p} \right)^{1/q},$$

where $a_{nm} \in \mathbb{C}^{N\times M}$ *represents the entries of the matrix.*

If $p = q = 2$ *then we have the Hilbert-Schmidt norm*

$$\|\mathrm{A}\|_{HS} = \left(\sum_{m=1}^{M} \sum_{n=1}^{N} |a_{nm}|^2 \right)^{1/2}$$

We compute

$$\|\mathrm{R} - \mathrm{R}^{\mathrm{near}}_{\mathrm{const}}\|_{\mathrm{HS}} = 9.5295 \times 10^{-16},$$

$$\|\mathrm{R} - \mathrm{R}^{\mathrm{lin}}_{\mathrm{const}}\|_{\mathrm{HS}} = 3.0682 \times 10^{-7}.$$

Hence we deduce reconstruction via nearest neighbourhood interpolation yields a closer reconstruction to the true scattering potential than via bilinear interpolation. Indeed, from an observation of the above plots we may see that the reconstruction via bilinear interpolating produces a ringing artefact.

2.2.3 Depth Migration

Depth migration is applied to seismic data in depth, which is calculated from seismic data in time coordinates. This method requires a velocity model. Here, $v : \mathbb{R}_+ \times \mathbb{R}_+ \times \mathbb{R}^2 \to \mathbb{C}$ represents the velocity wave field.

We introduce the coordinate system $\boldsymbol{x} = (z, \boldsymbol{y})$ where $z \in \mathbb{R}_+$ is the *depth* coordinate and $\boldsymbol{y} \in \mathbb{R}^2$ denotes the lateral coordinate.

Double Square Root Equation

Suppose that we have a continuum of geophones (i.e. receivers) along the $\boldsymbol{y}$-axis, then we want an equation which, instead of describing a downward extrapolation for a wavefield, describes a downward extrapolation equation for our geophones. It would therefore retrieve the data which would have been recorded had our geophones been buried beneath the surface. The equation which does this is the *double square root equation*, which may be derived from the acoustic wave equation.[3]

If we consider our shots and geophones and being continuously distributed along the $\boldsymbol{y}$-axis, our data will be a function of $\boldsymbol{y}' \in \mathbb{D}$ (the location of the scatterer) and $\boldsymbol{y} \in \mathbb{R}^3 \setminus \mathbb{D}$ (the location of the geophones). These data can be Fourier transformed over space to become a function of $\boldsymbol{k_y}'$ and $\boldsymbol{k_y}$ in the Fourier domain. The extrapolation of geophones can be achieved with $\boldsymbol{k_y}$ and similarly, the extrapolation of shots is achieved with $\boldsymbol{k_y}'$. Finally, the simultaneous downward extrapolation is achieved by adding phase shifts, thus yielding the double square root equation:

$$\frac{\partial}{\partial z}\hat{v}(\omega, z, \boldsymbol{k_y}, \boldsymbol{k_y}') = -i\frac{\omega}{c}\left[\sqrt{1 - \left(\frac{c\boldsymbol{k_y}}{\omega}\right)^2} + \sqrt{1 - \left(\frac{c\boldsymbol{k_y}'}{\omega}\right)^2}\right]\hat{v}(\omega, z, \boldsymbol{k_y}, \boldsymbol{k_y}'), \tag{2.53}$$

where the first square root is cosine of the arrival angle of the ray and the second square root is the cosine of the take-off angle from the source.

Measurements at $z = 0$

In this setting, we have one sided measurements at $z = 0$ for various incoming plane waves. Thus in order to retrieve the scattering potential, we can solve the boundary value problem

$$\begin{cases} \dfrac{\partial}{\partial z}\hat{v}(\omega, z, \boldsymbol{k_y}, \boldsymbol{k_y}') = -i\dfrac{\omega}{c}\left[\sqrt{1 - \left(\dfrac{c\boldsymbol{k_y}}{\omega}\right)^2} + \sqrt{1 - \left(\dfrac{c\boldsymbol{k_y}'}{\omega}\right)^2}\right]\hat{v}(\omega, z, \boldsymbol{k_y}, \boldsymbol{k_y}') \\ \hat{v}(\omega, 0, \boldsymbol{k_y}, \boldsymbol{k_y}') = \hat{d}(\omega, \boldsymbol{k_y}, \boldsymbol{k_y}'). \end{cases} \tag{2.54}$$

and apply inverse Fourier transforms on each of the variables in order to obtain the image $\mathcal{I}(z, \boldsymbol{y}) = v(0, z, \boldsymbol{y}, \boldsymbol{y'})$ with $\boldsymbol{x} = (z, \boldsymbol{y})$.

Proposition 39. *The image $\mathcal{I} : \mathbb{R}_+ \times \mathbb{R}^2 \to \mathbb{C}$ is given by*

$$\mathcal{I}(z, \boldsymbol{y}) = \frac{1}{128\pi^6 R}\int_0^\infty e^{i\omega R/c}\Bigg(\int_{\mathbb{R}^2}\int_{\mathbb{R}^2}\hat{r}(\omega(\boldsymbol{k_y}' - \boldsymbol{k_y})/c) \cdot \exp\left\{-iz\frac{\omega}{c}\left[\sqrt{1 - \left(\frac{c\boldsymbol{k_y}}{\omega}\right)^2} + \sqrt{1 - \left(\frac{c\boldsymbol{k_y}'}{\omega}\right)^2}\right]\right\} \cdot e^{-i(\boldsymbol{y}\cdot\boldsymbol{k_y} + \boldsymbol{y'}\cdot\boldsymbol{k_y}')}\,\mathrm{d}\boldsymbol{k_y}\,\mathrm{d}\boldsymbol{k_y}'\Bigg)\,\mathrm{d}\omega.$$

Proof. For (2.61), we have general solutions of the form

$$\hat{v}(\omega, z, \boldsymbol{k_y}, \boldsymbol{k_y}') = C\exp\left\{-iz\frac{\omega}{c}\left[\sqrt{1 - \left(\frac{c\boldsymbol{k_y}}{\omega}\right)^2} + \sqrt{1 - \left(\frac{c\boldsymbol{k_y}'}{\omega}\right)^2}\right]\right\}, \tag{2.55}$$

for some constant $C > 0$. Then our boundary conditions gives us that

$$\hat{v}(\omega, 0, \boldsymbol{k_y}, \boldsymbol{k_y}') = \hat{d}(\omega, \boldsymbol{k_y}, \boldsymbol{k_y}') = C,$$

so that in fact the solution is given by

$$\hat{v}(\omega, z, \boldsymbol{k_y}, \boldsymbol{k_y}') = \hat{d}(\omega, \boldsymbol{k_y}, \boldsymbol{k_y}') \exp\left\{-iz\frac{\omega}{c}\left[\sqrt{1-\left(\frac{c\boldsymbol{k_y}}{\omega}\right)^2} + \sqrt{1-\left(\frac{c\boldsymbol{k_y}'}{\omega}\right)^2}\right]\right\}. \tag{2.56}$$

We recall that

$$\hat{d}(\omega, \boldsymbol{\xi}, \boldsymbol{\xi}') = -\frac{e^{i\omega R/c}}{4\pi R}\hat{r}(\omega(\boldsymbol{\xi} - \boldsymbol{\xi}')/c).$$

Then, since, for $\boldsymbol{\xi} = (\xi_z, \boldsymbol{\xi_y})$, we have $\boldsymbol{k_y} = \boldsymbol{\xi_y}$; it follows in fact that

$$\hat{v}(\omega, z, \boldsymbol{k_y}, \boldsymbol{k_y}') = -\frac{e^{i\omega R/c}}{4\pi R}\hat{r}(\omega(\boldsymbol{k_y}' - \boldsymbol{k_y})/c) \exp\left\{-iz\frac{\omega}{c}\left[\sqrt{1-\left(\frac{c\boldsymbol{k_y}}{\omega}\right)^2} + \sqrt{1-\left(\frac{c\boldsymbol{k_y}'}{\omega}\right)^2}\right]\right\}$$

Thus, recalling that

$$\mathcal{I}(z, \boldsymbol{y}) = v(0, z, \boldsymbol{y}, \boldsymbol{y}') = \frac{1}{2\pi}\int_0^\infty \hat{v}(\omega, z, \boldsymbol{y}, \boldsymbol{y}')\,\mathrm{d}\omega, \tag{2.57}$$

and

$$\begin{aligned}\hat{v}(\omega, z, \boldsymbol{y}, \boldsymbol{y}') &= \frac{1}{(2\pi)^4}\int_{\mathbb{R}^2}\int_{\mathbb{R}^2} \hat{v}(\omega, z, \boldsymbol{k_y}, \boldsymbol{k_y}') e^{-i(\boldsymbol{y}\cdot\boldsymbol{k_y} + \boldsymbol{y}'\cdot\boldsymbol{k_y}')}\,\mathrm{d}\boldsymbol{k_y}\,\mathrm{d}\boldsymbol{k_y}' \\ &= -\frac{e^{i\omega R/c}}{64\pi^5 R}\int_{\mathbb{R}^2}\int_{\mathbb{R}^2} \hat{r}(\omega(\boldsymbol{k_y}' - \boldsymbol{k_y})/c) \exp\left\{-iz\frac{\omega}{c}\left[\sqrt{1-\left(\frac{c\boldsymbol{k_y}}{\omega}\right)^2} + \sqrt{1-\left(\frac{c\boldsymbol{k_y}'}{\omega}\right)^2}\right]\right\} \\ &\quad \cdot e^{-i(\boldsymbol{y}\cdot\boldsymbol{k_y} + \boldsymbol{y}\cdot\boldsymbol{k_y}')}\,\mathrm{d}\boldsymbol{k_y}\,\mathrm{d}\boldsymbol{k_y}',\end{aligned}$$

we get, in fact, that

$$\begin{aligned}\mathcal{I}(z, \boldsymbol{y}) = -\frac{1}{128\pi^6 R}\int_0^\infty e^{i\omega R/c}\Bigg(\int_{\mathbb{R}^2}\int_{\mathbb{R}^2} \hat{r}(\omega(\boldsymbol{k_y}' - \boldsymbol{k_y})/c) \\ \cdot \exp\left\{-iz\frac{\omega}{c}\left[\sqrt{1-\left(\frac{c\boldsymbol{k_y}}{\omega}\right)^2} + \sqrt{1-\left(\frac{c\boldsymbol{k_y}'}{\omega}\right)^2}\right]\right\} \cdot e^{-i(\boldsymbol{y}\cdot\boldsymbol{k_y} + \boldsymbol{y}'\cdot\boldsymbol{k_y}')}\,\mathrm{d}\boldsymbol{k_y}\,\mathrm{d}\boldsymbol{k_y}'\Bigg)\,\mathrm{d}\omega.\end{aligned}$$

□

In order to retrieve the scattering potential from the equation above, one may use asymptotic methods such as the method of stationary phase. Indeed, there is room for further research in this direction as our subsequent attempts to retrieve $r(x, z)$ were unfruitful. Certainly, retrieving the scattering potential via the double square root equation is done within the context of the acoustic wave equation; but it is another question of whether this is possible for the Schrödinger equation.

Chapter 3

Multiple Scattering

Recall the Lippmann-Schwinger equation with the Born approximation, which is given by:

$$\hat{u} = \hat{u}_{\text{inc}} + \widehat{G} *_x r\hat{u}_{\text{inc}}. \tag{3.1}$$

We wish to formulate an expression which gives a more explicit representation of multiple scattering. With this in mind, we can observe that the wave field u can be expressed in terms of u_{inc} by writing

$$\hat{u} = (1 + \widehat{G} *_x r)^{-1}\hat{u}_{\text{inc}}. \tag{3.2}$$

Writing $(\mathrm{I} + \mathrm{A})^{-1}$ for an operator A yields a solution in the form of a Neumann series $\mathrm{I} - \mathrm{A} + \mathrm{A}^2 - \mathrm{A}^3 + \cdots$ provided $\|\mathrm{A}\| < 1$ for some norm (recall that in finite dimension, all norms are equivalent). In this case we have the *Born series*, which is essentially an iteration of the Lippmann-Schwinger equation:

$$\hat{u} = \hat{u}_{\text{inc}} + \widehat{G} *_x r\hat{u}_{\text{inc}} - \widehat{G} *_x (r\hat{u}_{\text{inc}} \cdot (\widehat{G} *_x r\hat{u}_{\text{inc}})) + \cdots \tag{3.3}$$

i.e.

$$\begin{aligned}
\hat{u}(\omega, x) =& \hat{u}_{\text{inc}}(\omega, x) \\
&\text{(incident wave)} \\
&+ \int_{\mathbb{R}^n} \widehat{G}(\omega, x - x_1')r(x_1')\hat{u}_{\text{inc}}(\omega, x_1')\,\mathrm{d}x_1' \\
&\text{(single scattering)} \\
&- \int_{\mathbb{R}^n} \widehat{G}(\omega, x - x_3')r(x_3')\hat{u}_{\text{inc}}(\omega, x_3')\left(\int_{\mathbb{R}^n} \widehat{G}(\omega, x_2' - x_3')r(x_2')\hat{u}_{\text{inc}}(\omega, x_2')\,\mathrm{d}x_2'\right)\mathrm{d}x_3' \\
&\text{(double scattering)} \\
&+ \cdots
\end{aligned} \tag{3.4}$$

where $x = x_1'$ is the location of the first response, $x = x_2'$ the location of the second, *etcetera*. Note that the convergence of the Born series is based on the *weak scattering condition*, $\|\widehat{G} *_x r\| < 1$. For a proof, we refer the reader to reference [6] which not only provides a mathematical proof but also the physical motivations for why the series should converge. Incidentally, physical understanding of the Born series was achieved before the mathematical understanding of its convergence.

3.1 Homogeneous media in one dimension

Let $m(x) = c^{-2}$ for all $x \in \mathbb{R}$.

Gelfand-Levitan-Marchenko Equation

The Gelfand-Levitan Marchenko equation is given by

$$d(t + x) + K(t, x) + \int_{-\infty}^{x} d(s + t)K(s, x)\,\mathrm{d}s = 0, \tag{3.5}$$

where $K : \mathbb{R} \times \mathbb{R} \to \mathbb{R}$ is the inverse Fourier transform of the Jost solutions. For an overview of its derivation, we refer to [10].

For any fixed $x_0 \in \mathbb{R}$, this is a linear integral equation for K and one may use it to solve from K by inverting the integral operator

$$K(t) \mapsto K(t) + \int_{-\infty}^{x} d(s+t)K(s,x)\,\mathrm{d}x. \tag{3.6}$$

In particular, for a given K, one can recover the scattering potential as

$$r(x) = 2\frac{\mathrm{d}}{\mathrm{d}x}K(x,x). \tag{3.7}$$

The Toeplitz nature integral kernel, $K(s,x)$, which is derived in reference [20], can be exploited to reduce equation (3.5) into a differential equation which is easier to solve. Consequently, we may express the plasma wave equation as the coupled system of partial differential equations which form the essence of the layer stripping method which we state explicitly in the proceeding section.[15].

3.1.1 Layer Stripping

As hinted, the plasma wave equation may be written as the coupled system

$$\begin{cases} \left(\dfrac{\partial}{\partial x} + \dfrac{1}{c}\dfrac{\partial}{\partial t}\right) u(t,x) := v(t,x), \\ \left(\dfrac{\partial}{\partial x} - \dfrac{1}{c}\dfrac{\partial}{\partial t}\right) v(t,x) = r(x)u(t,x). \end{cases} \tag{3.8}$$

for the wave fields which are inhomogeneous forward and backward advection equations with solutions $u, v : \mathbb{R}_+ \times \mathbb{R} \to \mathbb{R}$ respectively.[13]

Then the layer stripping approach amounts to recursively solving this system of partial differential equations. In particular, we may initialise the algorithm with observations of the scattered field and its derivative

$$u(t,0) = d(t), \qquad v(t,0) = \frac{2}{c}d'(t), \tag{3.9}$$

and then we propagate the following equations recursively in x and t, for $t > x$:

$$\begin{cases} \left(\dfrac{\partial}{\partial x} + \dfrac{1}{c}\dfrac{\partial}{\partial t}\right) u(t,x) = v(t,x), \\ \left(\dfrac{\partial}{\partial x} - \dfrac{1}{c}\dfrac{\partial}{\partial t}\right) v(t,x) = r(x)u(t,x), \\ r(x) = -\dfrac{2}{c}v(x/c,x). \end{cases} \tag{3.10}$$

This amounts to successively truncating the potential, where, at each recursion, the region to the left of x is replaced by "free space"$\{r(y) = 0 : y < x\}$. Thus the algorithm is successively reconstructing the scattering potential and then stripping away its effects.

Remark. Note that this algorithm requires $\mathcal{O}(M^2)$ operations to construct $r(x)$ since it must propagate M responses through M steps (where M is the total number of spatial steps). Furthermore, although we do not include noise in our model, the algorithm is rather sensitive to it and the errors grow with time.[16]

3.1.2 The Very Weak Scattering Assumption

In this section, we would like to implement various interpretations of the layer stripping algorithm and also previously determined algorithms and investigate the differences in their reconstruction results for multiply scattered data assuming and without assuming single scattering respectively. In particular, the aforementioned Born approximation constitutes a single scattering approximation and thus assumes *very weak scattering*:

Definition 40 (Very Weak Scattering)**.** *If* $\|\widehat{G} *_x r\| \ll 1$*, then* $\hat{u}_{sc} = \widehat{G} *_x r\hat{u}_{inc}$

In the following example, we make the weak scattering assumption for data which has been multiply scattered:

Example 41. Let $V \in C_c^\infty([0,10])$ be given by $V(x) := r(x-5) + r(x-7)$ for $r \in C_c^\infty([0,10])$ defined as in previous examples. We plot $V(x)$ below:

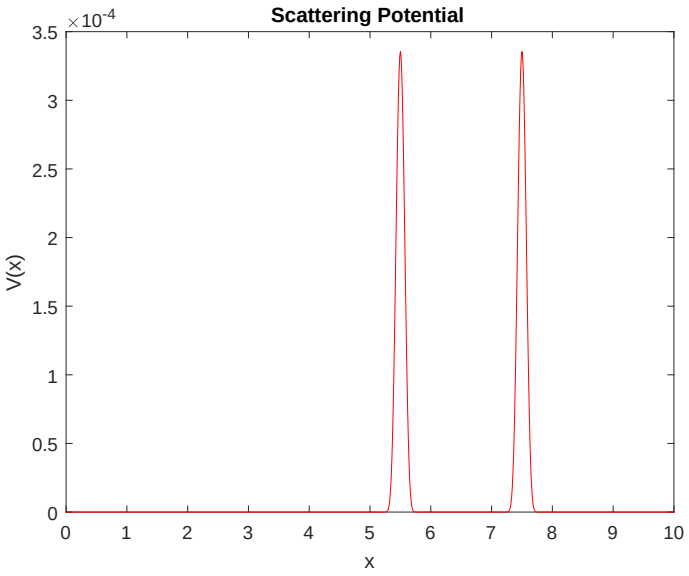

Figure 3.1: Plot of $V(x)$, a linear combination of $r(x)$ used in prior examples.

Then, in *this* example, we compute the data as $d(t) = u_{\text{sc}}(t, x_0)$, where $x_0 \in \mathbb{R}$ is fixed and here $u_{\text{sc}}(t, x)$ is the solution of the difference of the solution of the plasma wave equation and the wave equation, i.e. $u_{\text{sc}}(t, x) = u_p(t, x) - u_w(t, x)$, where $u_p(t, x)$ is the solution of

$$\begin{cases} \left(\Delta + \dfrac{\partial^2}{\partial t^2}\right) u_p(t, x) = V(x) u_p(t, x), \\ u_p(0, x) = \dfrac{\partial}{\partial t} u_p(0, x) = \operatorname{sinc}\left(\dfrac{x - x_0}{\Delta x}\right), \end{cases} \tag{3.11}$$

and $u_w(t, x)$ is the solution of

$$\begin{cases} \left(\Delta + \dfrac{\partial^2}{\partial t^2}\right) u_w(t, x) = 0, \\ u_w(0, x) = \dfrac{\partial}{\partial t} u_w(0, x) = \operatorname{sinc}\left(\dfrac{x - x_0}{\Delta x}\right) \end{cases} \tag{3.12}$$

For the aforementioned scattering potential, we measure the data at $x_0 = 5$ up to $t = 30$ and plot the results below (where we have taken $\Delta t = 10^{-3}$ and $\Delta x = 10^{-2}$):

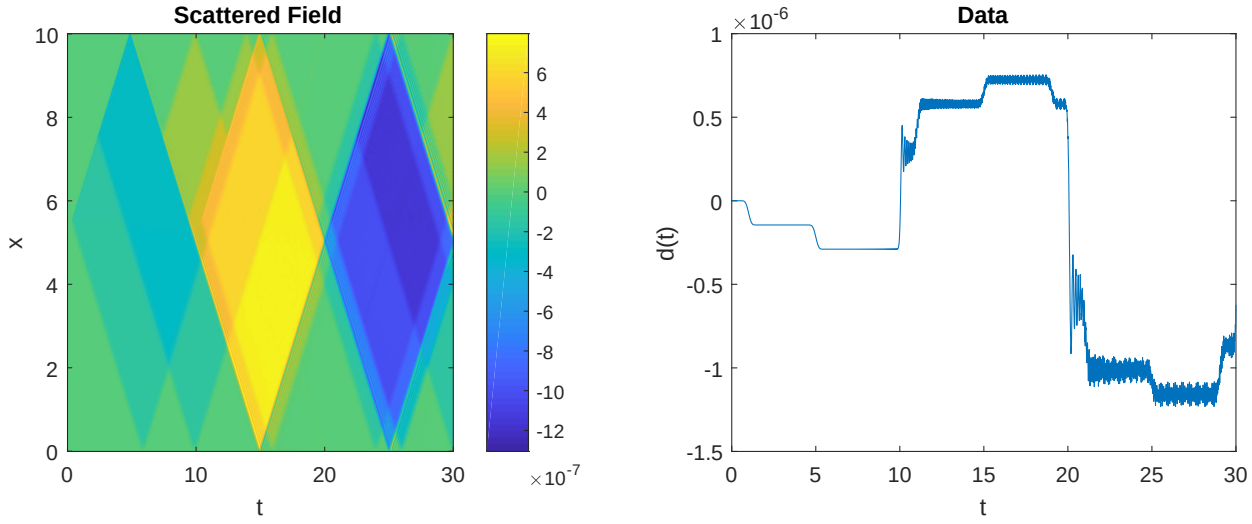

Figure 3.2: Data recorded at $x_0 = 5$ for $t \in [0, 30]$.

From the above data, we attempt to reconstruct the aforementioned scattering potential function with the very weak scattering assumption and otherwise respectively:

- First we *assume* that the data has been singly scattered. Thus an implementation of the layer stripping algorithm would involve just a single pass of the algorithm. We use the data as above and plot $v(t,x)$ which solves

$$\begin{cases} \left(\dfrac{\partial}{\partial x} - \dfrac{\partial}{\partial t}\right) v(t,x) = 0, \\ v(t,0) = 2d'(t), \\ v(t_0,x) = \operatorname{sinc}\left(\dfrac{x-x_0}{\Delta x}\right), \end{cases} \tag{3.13}$$

  where here, $t_0 = 30$ and $x_0 = 5$.

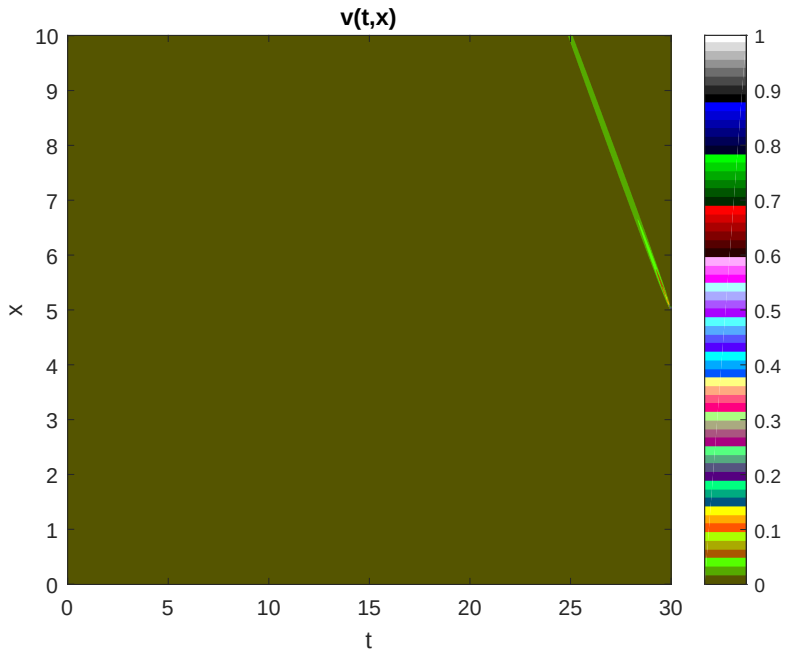

Figure 3.3: Solution of the backward advection equation with data as boundary condition measured at $x_0 = 5$ for $t \in [0, 30]$.

Note that we solve the partial differential equation using the Crank-Nicolson scheme, backward in time (2.20). However, extracting the diagonal elements from the above solution yields a wholly undesirable reconstruction of the scattering potential.

Now, suppose instead that we measure the data at $x_0 = 5$ for time $t \in [0, 2]$; then we get the following values for $v(t,x)$:

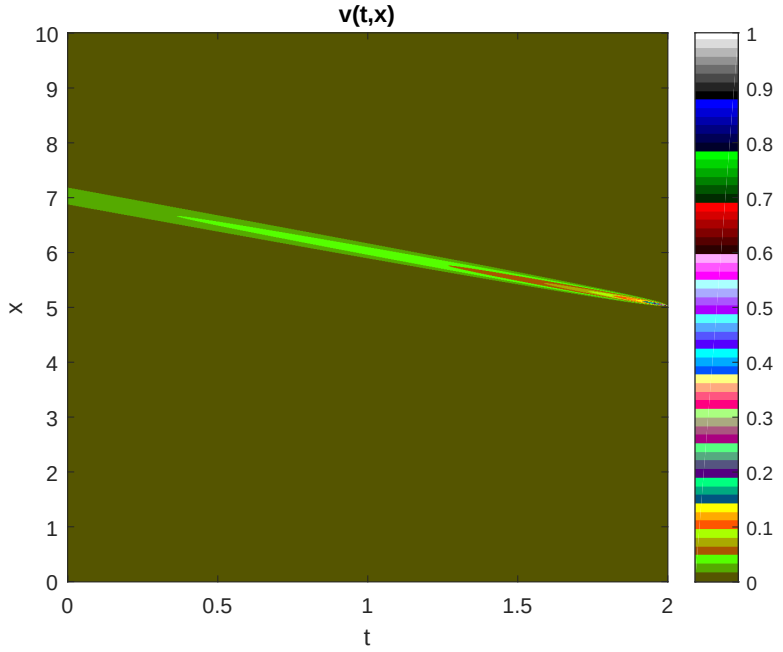

Figure 3.4: Solution of the backward advection equation with data as boundary condition measured at $x_0 = 5$ for $t \in [0, 2]$.

Reconstructing the scattering potential in this way yields:

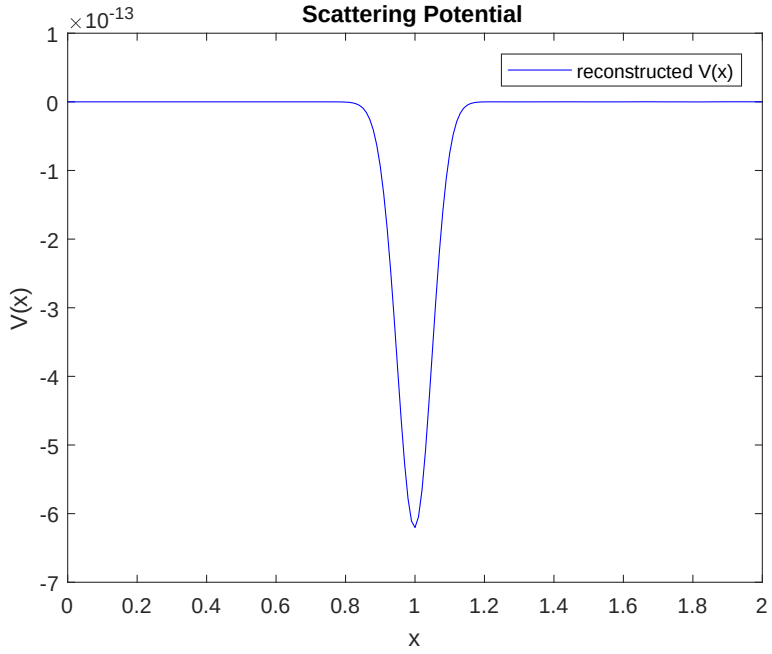

Figure 3.5: Reconstruction of the scattering potential for the aforementioned data.

We thus observe that the reconstructed scattering potential is not an exact reconstruction. Additionally, since the original scattering potential is defined on a larger spatial domain than the time for which the data is measured, the construction of the scattering potential, which involves interpolating the time samples onto the spatial samples, mean that a true reconstruction of the scattering potential in the desired location would have been an implausibility.

- We have thus motivated the need to utilise a full layer stripping algorithm for reconstructing multiply scattered data, rather than using just a single pass of the algorithm.

To this end, we implement layer stripping algorithms for retrieving both r and V respectively.

"Layer Stripping" Algorithm # 1

Step 1: Initialise the algorithm with $x_0 \in \mathbb{R}$ and generate the data with $d(t) = \tilde{u}_{\text{sc}}(t, x_0)$, where $\tilde{u}$ is the solution with the plasma wave equation with initial conditions $\tilde{u}(0,x) = \partial_t \tilde{u}(0,x) = \text{sinc}((x-x_0)/\Delta x)$.
Step 2: Solve the following partial differential equations with initial conditions and boundary values

$$\begin{cases} \left(\dfrac{\partial}{\partial x} + \dfrac{1}{c}\dfrac{\partial}{\partial t}\right) u(t,x) = v(t,x) \\ \left(\dfrac{\partial}{\partial x} - \dfrac{1}{c}\dfrac{\partial}{\partial t}\right) v(t,x) = r(x)u(t,x) \\ u(0,x) = v(0,x) = \text{sinc}\left(\dfrac{x-x_0}{\Delta x}\right) \\ u(t,0) = d(t) \\ v(t,0) = \dfrac{2}{c} d'(t), \end{cases}$$

forward in space, the first forward in time and the second backward in time.
Step 3: Retrieve the scattering potential as $r(x) = -2v(x/c, x)$.

Note that we have included speech marks for "layer stripping", since the above algorithm does not suggest that we solve the forward and backward advection equations alternatingly in true layer stripping fashion so as to remove the effects of the scatterer with each recursion.

(a) Solving the inverse problem for r, with $c = 1$, we employ the above algorithm, solving the first equation, first discretising as

$$\frac{u(t+\Delta t, x+\Delta x) - u(t+\Delta t, x)}{\Delta x} + \frac{1}{c}\frac{u(t+\Delta t, x) - u(t,x)}{\Delta t} = v(t,x),$$

where the above is a forward in time, forward in space finite difference scheme. Notice that the finite difference approximation of the spatial differential operator is evaluated at $t + \Delta t$. We may rewrite this as

$$\begin{aligned} &\frac{u_{\ell+1}^{n+1} - u_\ell^{n+1}}{\Delta x} + \frac{1}{c}\frac{u_\ell^{n+1} - u_\ell^n}{\Delta t} = v_\ell^n \\ \iff &\frac{1}{c\Delta t} u_\ell^{n+1} - \frac{1}{\Delta x} u_\ell^{n+1} + \frac{1}{\Delta x} u_{\ell+1}^{n+1} = \frac{1}{c\Delta t} u_\ell^n + v_\ell^n \\ \iff &\left(\frac{1}{c\Delta t}\mathrm{I} + \frac{1}{\Delta x}\mathrm{D}\right) \boldsymbol{u}^{n+1} = \frac{1}{c\Delta t}\boldsymbol{u}^n + \boldsymbol{v}^n \end{aligned}$$

where A is the banded matrix as before.

Hence

$$\boldsymbol{u}^{n+1} = \left(\frac{1}{c\Delta t}\mathrm{I} + \frac{1}{\Delta x}\mathrm{D}\right)^{-1} \left(\frac{1}{c\Delta t}\boldsymbol{u}^n + \boldsymbol{v}^n\right). \tag{3.14}$$

where $\mathrm{D} \in \mathbb{R}^{N\times N}$ is given by

$$\mathrm{D} = \begin{pmatrix} -1 & 1 & & \\ & -1 & 1 & \\ & & \ddots & \ddots \end{pmatrix}$$

If we set $\Delta t = 10^{-3}$, $\Delta x = 10^{-2}$ and $x_0 = 0$, then we get the following plot:

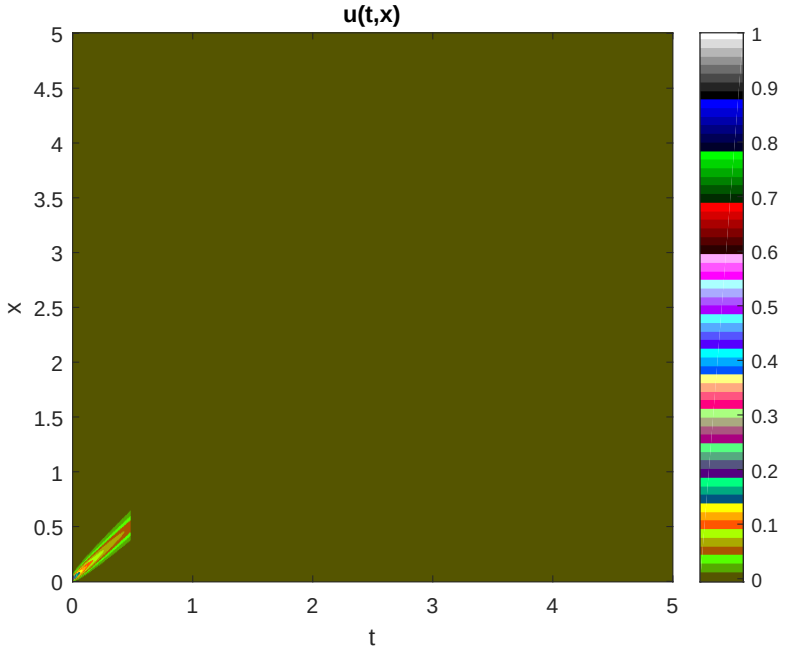

Figure 3.6: Solution of the forward advection equation.

Then to solve the backward advection equation, we may discretise as

$$\frac{v(t-\Delta t, x+\Delta x)-v(t-\Delta t,x)}{\Delta x}-\frac{1}{c}\left(\frac{v(t,x)-v(t-\Delta t,x)}{\Delta t}\right)=r(x)u(t,x),$$

which is backward in time and forward in space. We may rewrite this as

$$\begin{aligned}
&\frac{v_{\ell+1}^{n-1}-v_\ell^{n-1}}{\Delta x}-\frac{1}{c}\left(\frac{v_\ell^n-v_\ell^{n-1}}{\Delta t}\right)=ru_\ell^n\\
\iff &\frac{1}{\Delta x}(v_{\ell+1}^{n-1}-v_\ell^{n-1})+\frac{1}{c\Delta t}v_\ell^{n-1}=\frac{1}{c\Delta t}v_\ell^n+ru_\ell^n\\
\iff &\left(\frac{1}{\Delta x}\mathrm{D}+\frac{1}{c\Delta t}\mathrm{I}\right)\boldsymbol{v}^{n-1}=\frac{1}{c\Delta t}\boldsymbol{v}^n+r\boldsymbol{u}^n
\end{aligned}$$

Hence

$$\boldsymbol{v}^{n-1}=\left(\frac{1}{\Delta x}\mathrm{D}+\frac{1}{c\Delta t}\mathrm{I}\right)^{-1}\left(\frac{1}{c\Delta t}\boldsymbol{v}^n+r\boldsymbol{u}^n\right), \tag{3.15}$$

where $\mathrm{D}\in\mathbb{R}^{N\times N}$ is as before.

We plot the solution below:

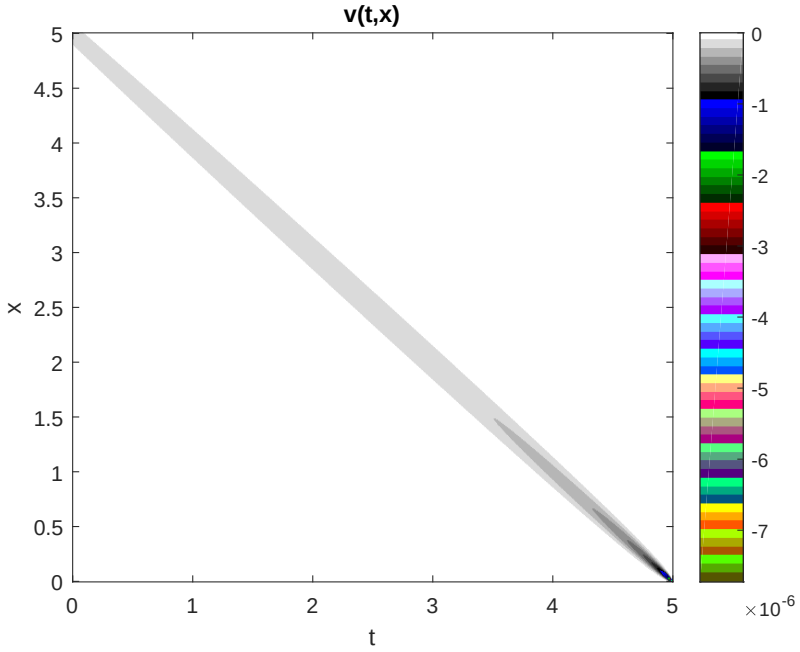

Figure 3.7: Solution of the backward advection equation.

Finally, we would like to retrieve the scattering potential via the formula $r(x) = -2v(x/c, x)$. However, in the context of this numerical derivation, we cannot do this immediately as there exist ten times more time steps than spatial steps. We can interpolate the time grid onto the spatial grid, however, and then taking values from the diagonal of the plot above, we may retrieve r as in the plot below:

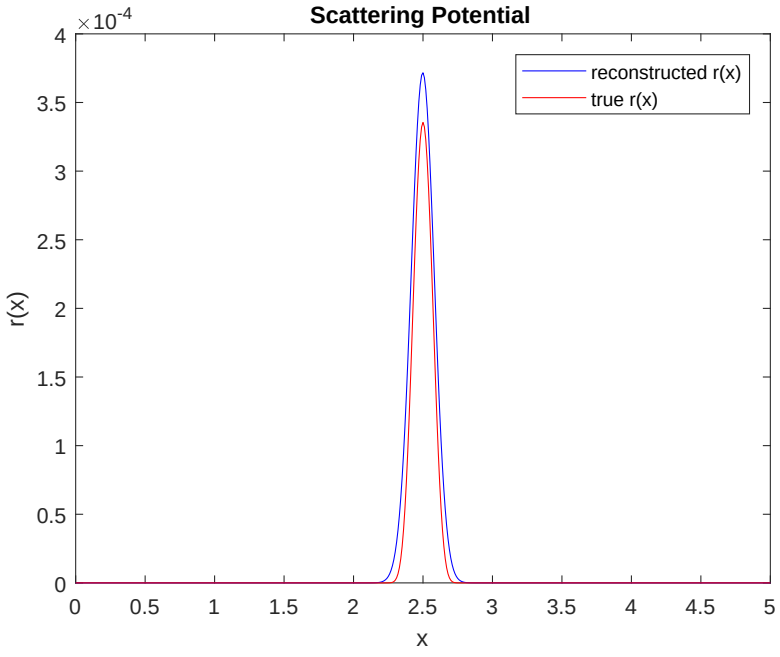

Figure 3.8: Reconstructed scattering potential.

Now, for the sake of another example let $x_0 = 2$ instead. Then we get the following plots for $u(t, x)$ and $v(t, x)$ respectively:

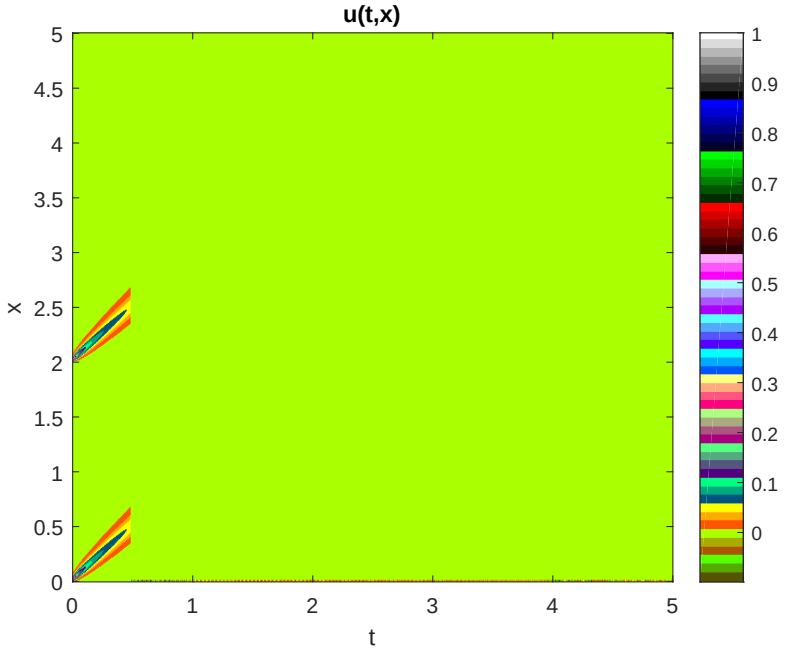

Figure 3.9: Solution of the forward advection equation, with $x_0 = 2$ and $c = 1$.

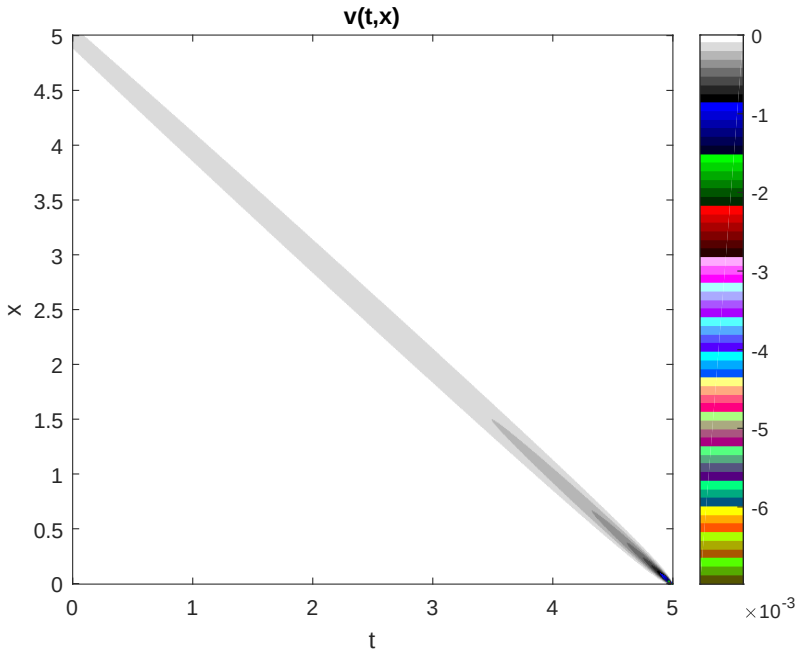

Figure 3.10: Solution of the backward advection equation.

Then we may similarly reconstruct the scattering potential as plotted below:

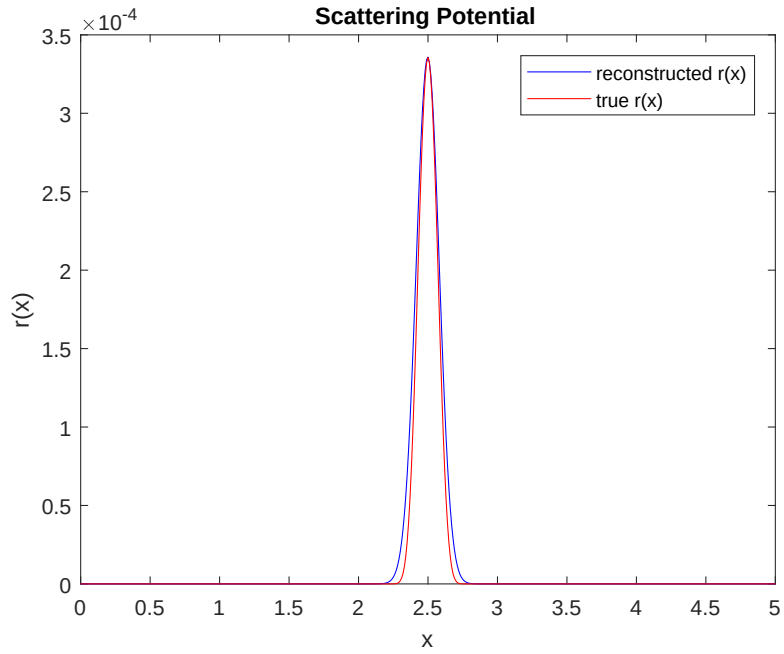

Figure 3.11: Reconstruction of scattering potential from data recorded at position $x_0 = 2$.

We can observe that this appears to be an even closer reconstruction of the true scattering potential.

(b) Now, we increase the size of our spatial domain to $[0, 10] \subset \mathbb{R}$ and let $c = 1$. We employ the above algorithm to reconstruct V. Set $x_0 = 5$; then we get the following solutions and reconstruction:

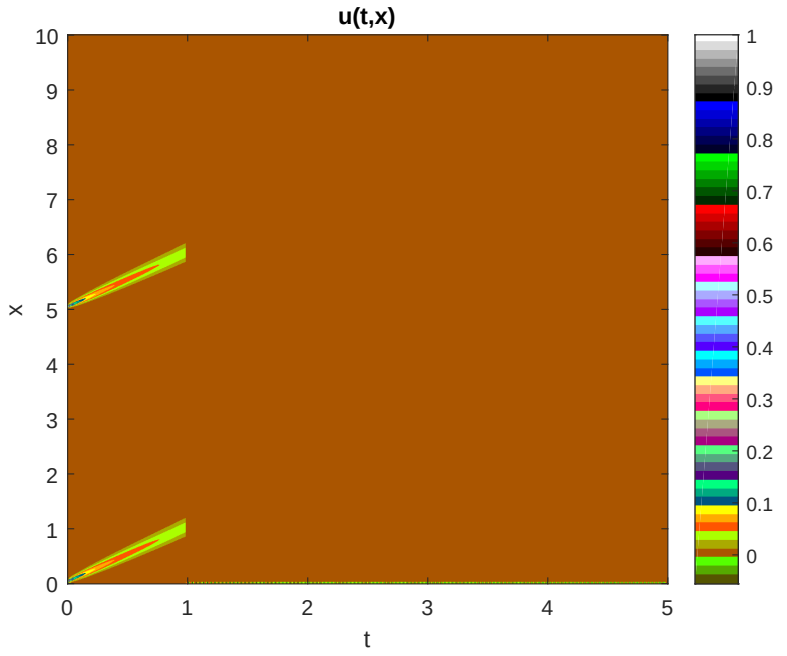

Figure 3.12: Solution of the forward advection equation with $x_0 = 5$.

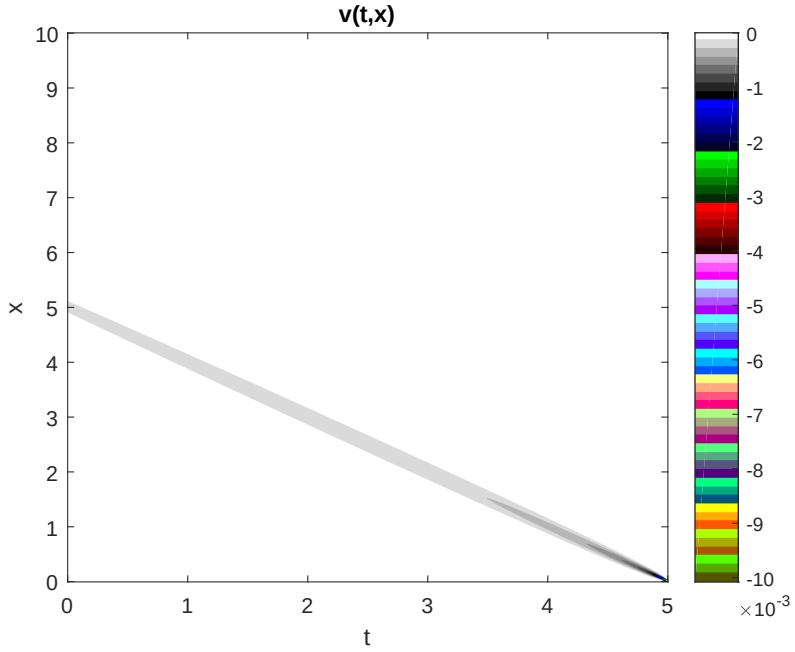

Figure 3.13: Solution of the backward advection equation

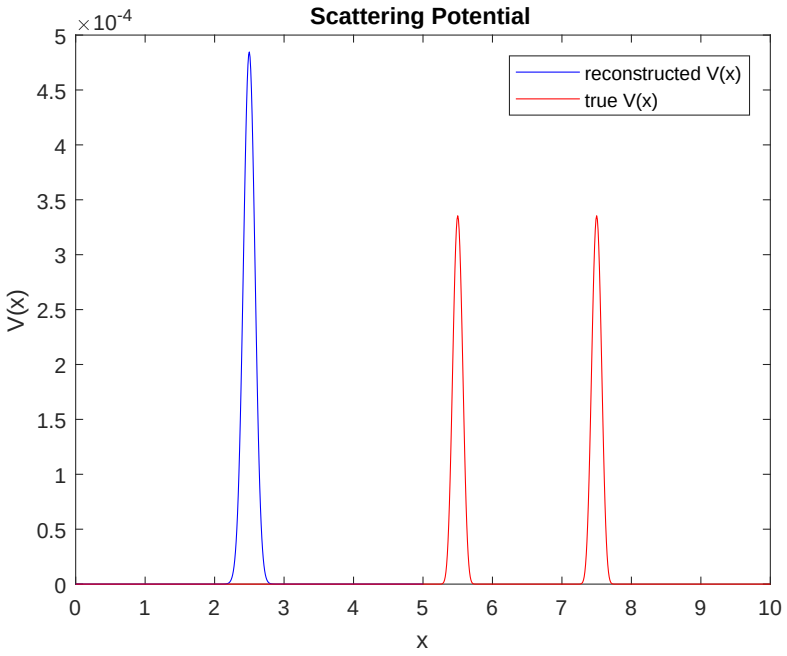

Figure 3.14: Reconstruction of the scattering potential.

One can thus observe that the reconstruction in this case is quite unsatisfactory.

Note that one can also formulate an algorithm which solves the forward advection equation and the backward advection equation alternatingly. This would indeed be closer to the essence of the method suggested in reference [7]. In the case we have a differing number of time and spatial steps, say ten times as many time steps than spatial steps, then one could (in this example) solve the forward advection equation for one time step and then the backward advection equation for ten time steps and so on and so forth. Our subsequent implementations of this method however were to no avail.

In reference [7], a layer stripping algorithm which solves the forward and backward equations alternatingly and updates in space is suggested:

Layer Stripping Algorithm # 2

Step 1: Initialise the algorithm with $u(t,0) = d(t)$ and $v(t,0) = \frac{2}{c}d'(t)$, where $d(t)$ is the data generated from the solution of the plasma wave equation at position $x_0 \in \mathbb{R}$.
Step 2: Solve the following partial differential equations alternatingly

$$\begin{cases} \left(\frac{\partial}{\partial x} + \frac{1}{c}\frac{\partial}{\partial t}\right) u(t,x) = v(t,x) \\ \left(\frac{\partial}{\partial x} - \frac{1}{c}\frac{\partial}{\partial t}\right) v(t,x) = r(x)u(t,x) \end{cases}$$

forward in space, the first forward in time and the second backward in time.
Step 3: Retrieve the scattering potential as $r(x) = -2v(x/c, x)$.

As in the previous simulations, we set $c = 1$, the time and spatial domain as $[0, 5]$ and implement the above algorithm to reconstruct r. Taking the forward difference of the spatial and time derivatives in the forward advection equation yields

$$\frac{u_{\ell+1}^n - u_\ell^n}{\Delta x} + \frac{u_\ell^{n+1} - u_\ell^n}{\Delta t} = v_\ell^n.$$

We can rewrite the above as

$$u_{\ell+1}^n = u_\ell^n - \eta(u_\ell^{n+1} - u_\ell^n) + \Delta x v_\ell^n,$$

i.e.

$$\boldsymbol{u}_{\ell+1} = \mathrm{S}\boldsymbol{u}_\ell + \Delta x \boldsymbol{v}_\ell, \tag{3.16}$$

where $\eta = \Delta x/\Delta t$ and $\mathrm{S} \in \mathbb{R}^{N\times N}$, for N the total number of time steps, is the finite difference matrix given by

$$\mathrm{S} = \begin{pmatrix} 1-\eta & -\eta & & \\ & 1-\eta & -\eta & \\ & & \ddots & \ddots \end{pmatrix}$$

We can then solve the backward advection equation backward in time by taking the conjugate transpose of S, which yields

$$\boldsymbol{v}_{\ell+1} = \mathrm{S}^*\boldsymbol{v}_\ell + \Delta x r_\ell \boldsymbol{u}_\ell. \tag{3.17}$$

Suppose we measure the data from position $x_0 = 0$, then we may implement the above algorithm, yielding the following plots:

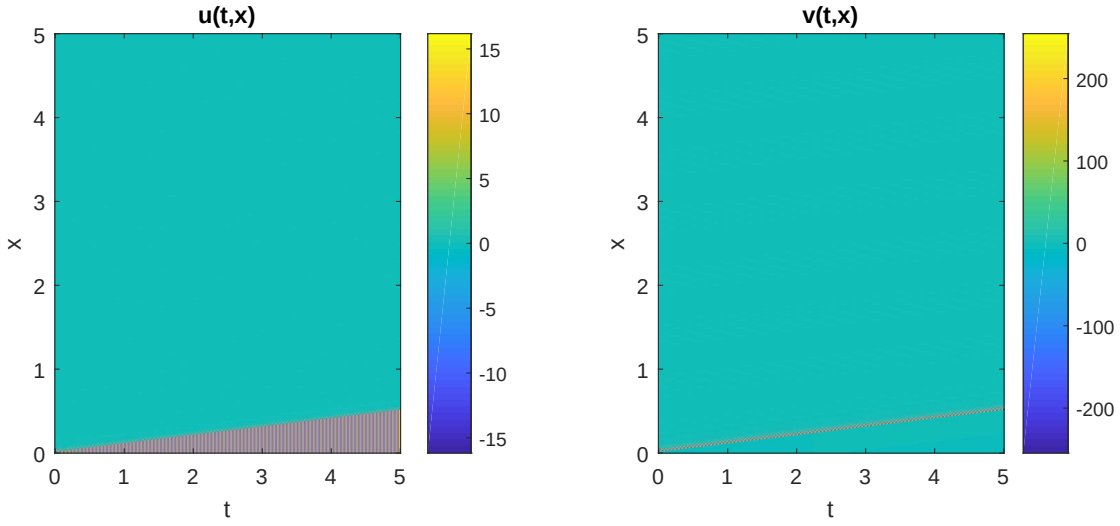

Figure 3.15: The solutions of the forward advection equation (left) and backward advection equation (right) solved alternatingly with boundary conditions given by data measured at $x_0 = 0$ from scattering potential r.

The plot of the solution $v(t,x)$ already alludes to a poor reconstruction of the scattering potential since it takes on very large values and does not appear to have values of magnitude greater than zero along the middle part of the diagonal. In any case, the respective reconstruction of the scattering potential is plotted below

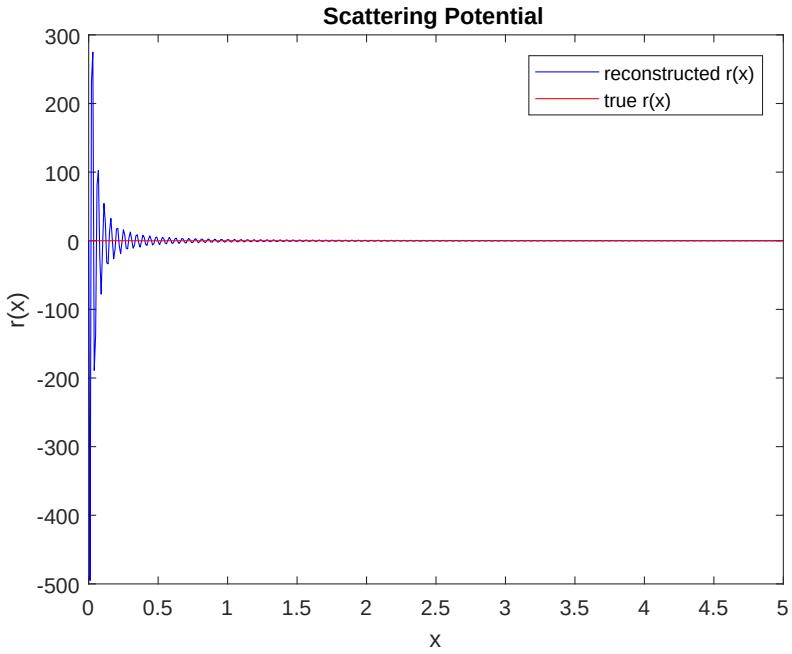

Figure 3.16: Reconstruction of scattering potential

We subsequently observe that the above algorithm completely failed to reconstruct the scattering potential and no useful information can be gathered from the plot above.

Example 42. We may also test the performance of the Shannon interpolation formula on data which has been multiply scattered. To this end, let $c = 1$ and $V \in C_c^\infty(\mathbb{R})$ as in the previous example. Then

$$V_{\text{const}}(x) = -2 \sum_{n=-\infty}^{\infty} d[n] \frac{\mathrm{d}}{\mathrm{d}x} \operatorname{sinc}\left(\frac{2x - n\Delta t}{\Delta t}\right),$$

where $d[n]$ is the sampled data acquired from the difference of the solution of the plasma wave equation and the wave equation for fixed x_0. In particular, this is the same data as in the previous example, with $x_0 = 5$. In this case, measuring up to $t = 30$, we utilise the above formula to reconstruct the scattering potential as below

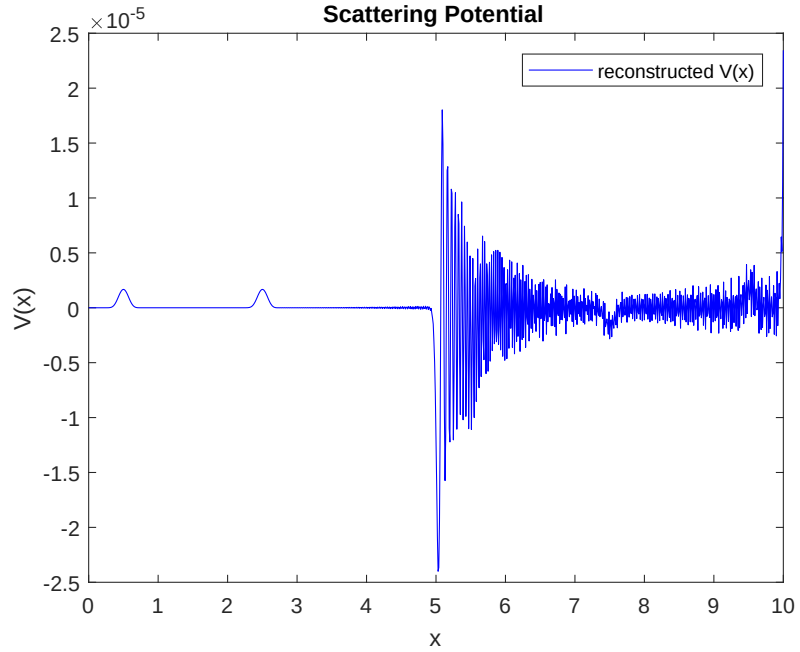

Figure 3.17: Reconstructed scattering potential from data recorded at position $x_0 = 5$ and time $t \in [0, 30]$.

We observe that the above reconstruction is unsatisfactory in this case. In the region $[0, 5]$, it constructs the scattering potential but with far smaller amplitude and translated to the left.

Now, we experiment with various other time measurements, namely: $t = 2$, $t = 10$ and $t = 50$ and compare the results with the previous example.

(a) For $t = 2$:

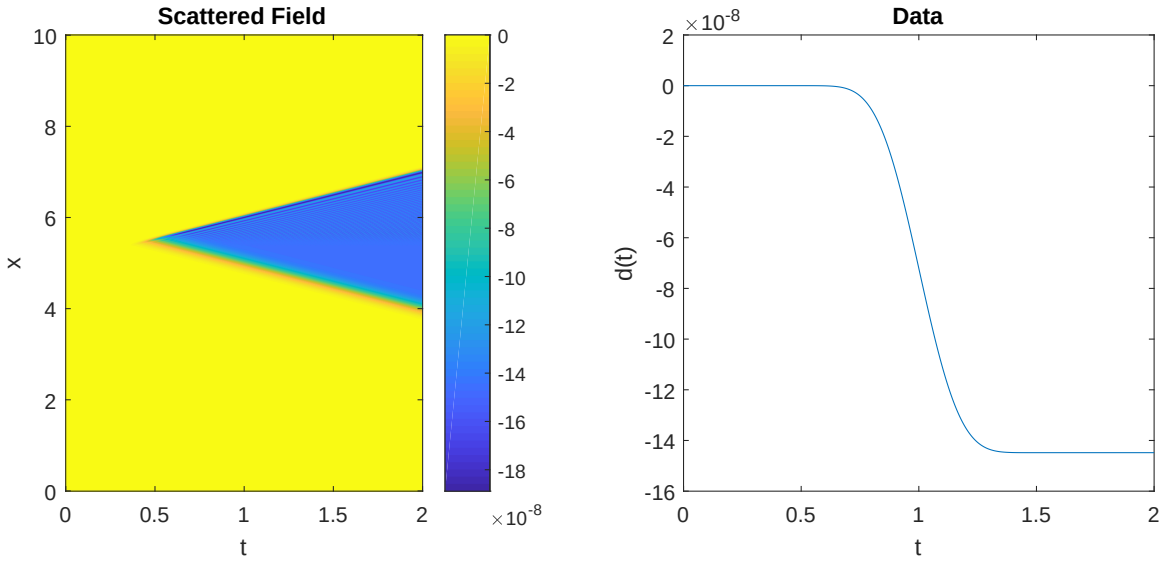

Figure 3.18: Data plots corresponding to $x_0 = 5$ and $t \in [0, 2]$.

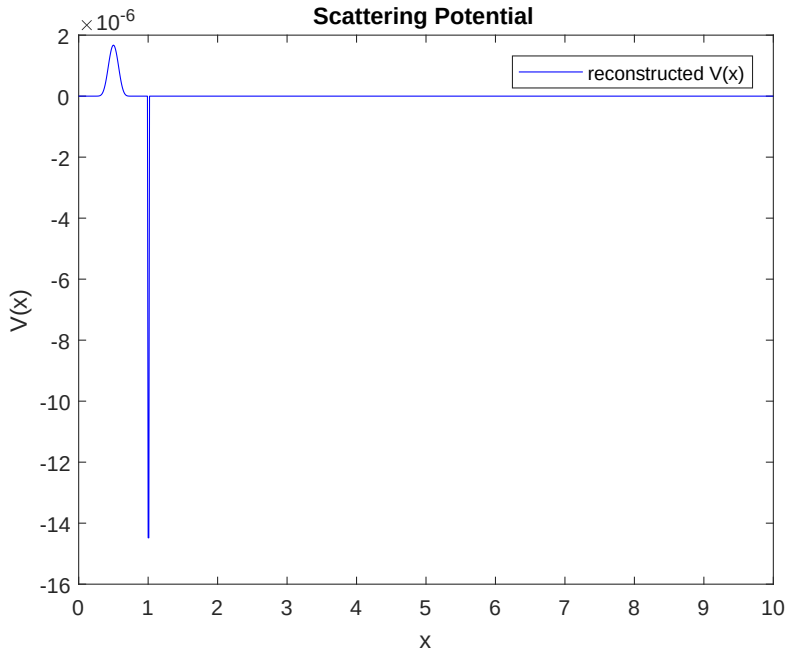

Figure 3.19: Reconstruction of scattering potential

(b) For $t = 10$:

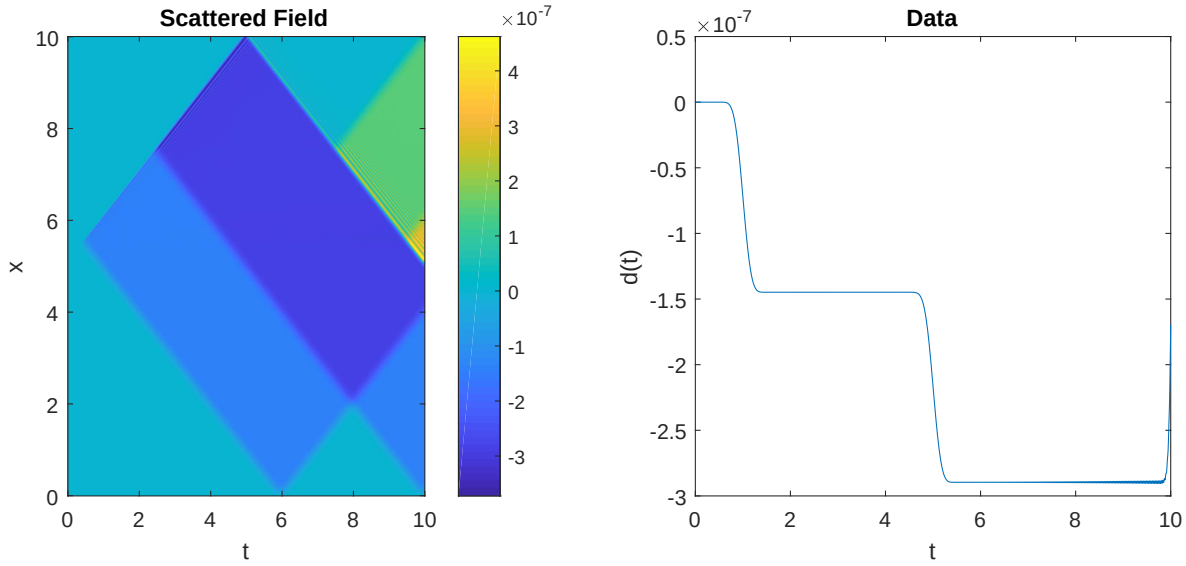

Figure 3.20: Data plots corresponding to $x_0 = 5$ and $t \in [0, 10]$.

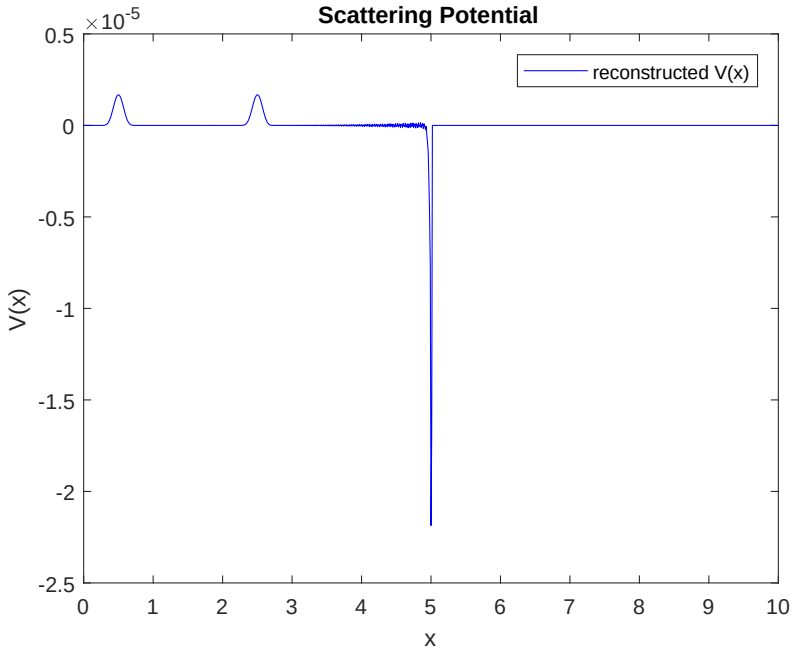

Figure 3.21: Reconstruction of scattering potential

(c) For $t = 50$:

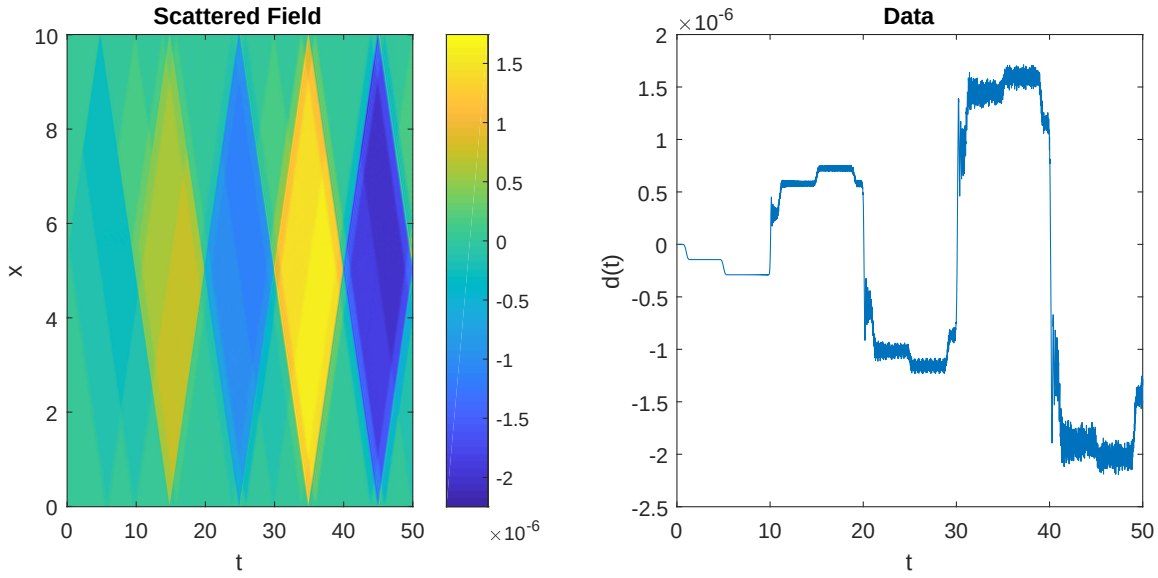

Figure 3.22: Data plots corresponding to $x_0 = 5$ and $t \in [0, 50]$.

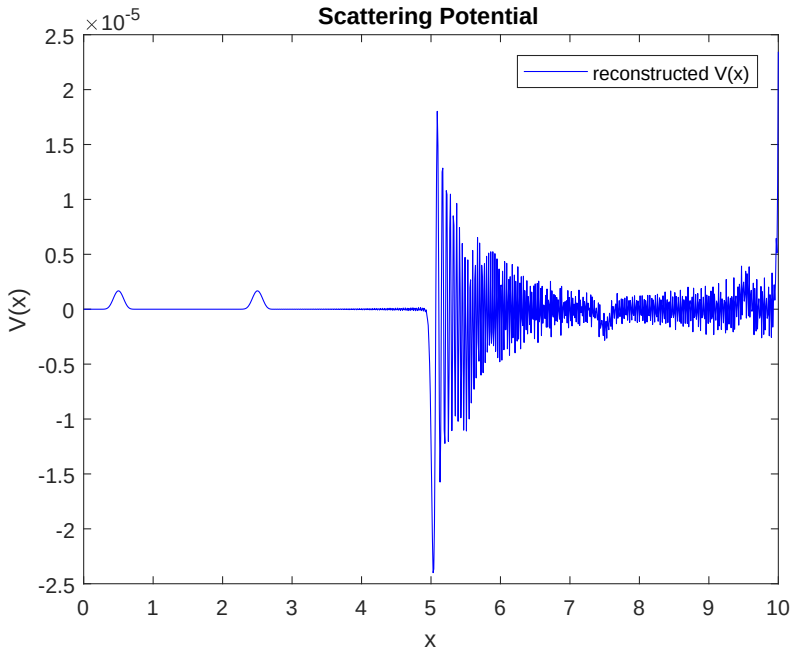

Figure 3.23: Reconstruction of scattering potential

Thus we may observe, comparing with Figure 3.1, that for $t \in [0, t_0]$, the accuracy of the reconstructed scattering potential improves with regards to its amplitude as $t_0 \to \infty$. We subsequently find that experimenting further with different x_0 does not yield more fruitful results.

Chapter 4

Conclusions & Further Questions

In one dimensional homogeneous media, we formulated a number of algorithms for reconstructing the scattering potential. Below we provide a brief summary of their performances:

(a) **Shannon-Whittaker Interpolation**

- **Single Scattering:** The reconstruction results of the algorithm, particularly when the data had been measured for large time values, yielded very desirable results.
- **Multiple Scattering:** For multiple scattering, the algorithm left a lot to be desired.

(b) **Single Pass (in time) of the Layer Stripping Algorithm**

- **Single Scattering:** The algorithm, while seemingly not as accurate as the aforementioned interpolation method, produced strong reconstruction results nonetheless. However, we also tested the algorithm for data measured at differing observation points and found that the reconstruction results varied drastically in this case.
- **Multiple Scattering:** In the instance whereby the data was multiply scattered, the single pass of the layer stripping approach also failed to yield acceptable reconstruction results.

(c) **Single Pass (in space) of the Layer Stripping Algorithm:** The backward advection equation could not be solved numerically using the Euler forward, Euler backward nor Crank-Nicolson scheme, which were all unstable thus a numerical implementation could not be achieved.

(d) **"Layer Stripping" Algorithm (in time)**

- **Single Scattering:** The "layer stripping" algorithm yielded accurate reconstructions of the scattering potential for data measured at differing observation positions.
- **Multiple Scattering:** In the case of multiple scattering, the method was unfruitful and the reconstructed scattering potential resembled the reconstruction obtained from the single scattering example.

(e) **"Layer Stripping" Algorithm (in space):** As a consequence of the failed implementation of the single pass of the layer stripping approach in space, it was not possible to then generalise it to a "layer stripping" algorithm

(f) **Layer Stripping Algorithm (in time):** This algorithm failed to produce results of any substance.

(g) **Layer Stripping Algorithm (in space):** In this case, the algorithm did yield values along a skewed "diagonal" of $v(t, x)$ in a recursive fashion; but, in any case, the reconstruction attempt of the scattering potential was wholly unsatisfactory.

In three dimensional homogeneous media, we attempted to implement the following algorithms, for which we also provide a brief summary of their performances:

(a) **Interpolating Tangent-Circular Samples in the Frequency Domain:** This remains an open problem.

(b) **Interpolating Polar Samples in the Frequency Domain:** Reference [4] provides an interpolation formula for reconstructing functions which have been sampled in polar coordinates in the frequency domain. However, our subsequent attempts to implement the aforementioned formula were to no avail.

Further Research

In light of the summaries above, one can gather that there is indeed room for improvement and further research. In particular, a correct numerical implementation of the layer stripping algorithm (updating in space) in one dimension would be highly desirable. In reference [18], a layer stripping algorithm for the two dimensional inverse Schrödinger scattering problem is numerically implemented, but the numerical implementations of the aforementioned one dimensional case and also the three dimensional problem appear yet to have been enacted. A generalisation of the one dimensional layer stripping algorithm to the three dimensional setting is given in reference [7].

Reconstructing the scattering potential in the frequency domain was also one of our more major ambitions; therefore successfully implementing the interpolation formula given in reference [4] would complete a gap in this thesis. Finally, although the tangent-circular sampling scheme in the frequency domain arises from a more realistic setting (at least, in the context of seismic imaging), overcoming the problem of interpolating from these samples would seem a particularly major hurdle to overcome.

Additionally, as our model assumed only a single incident wave field, one could further generalise the work done in this thesis by including additional incident fields and also receivers, which would thus form an array and draw on techniques from time series analysis. Further paths for generalisations of the methods in this thesis include modelling for one and three dimensional inhomogeneous media and also for partially known or unknown wave speed profiles.

Bibliography

[1] N.Bleistein, J.K. Cohen, J.K. Stockwell, Jr.
Mathematics of Multidimensional Seismic Imaging, Migration and Inversion
Springer-Verlag New York, Inc
2001

[2] F. Natterer
The Mathematics of Computerized Tomography
John Wiley and Sons Ltd and B G Teubner, Stuttgart
1986

[3] Jon F. Claerbout.
Double Square Root Equation
`http://sepwww.stanford.edu/public/docs/sep15`.

[4] Robert J. Marks II.
Advanced Topics in Shannon Sampling and Interpolation Theory
Springer-Verlag New York, Inc.
1993.

[5] Charles L. Bryne.
Signal Processing: a Mathematical Approach
Chapman and Hall/CRC; 2 edition
17 November 2014

[6] Laurent Demanet.
Waves and Imaging
`http://math.mit.edu/icg/resources/notes325.pdf`

[7] Andrew E. Yagle
Multidimensional Inverse Scattering: an Orthogonalization Approach
Communications and Signal Processing Laboratory, Departmental of Electrical Engineering and Computer Science, The University of Michigan, Ann Arbor, Michigan 48109
4 March 1987

[8] Roger G. Newton.
Inverse Schrödinger Scattering in Three Dimensions
Springer Berlin Heidelberg
1989

[9] David Colton, Rainer Kress.
Inverse Acoustic and Electromagnetic Scattering Theory
Third Edition, Springer New York Heidelberg Dordrecht London
2010

[10] Terrence Tao.
Israel Gelfand
`https://terrytao.wordpress.com/2009/10/07/israel-gelfand/#more-2860`

[11] Reese T. Prosser.
Formal Solutions of Inverse Scattering Problems
Journal of Mathematical Physics
1969

[12] J.J. Duistermaat, J.A.C. Kolk
Distributions: Theory and Applications
Springer Science+Business Media,
LLC 2010

[13] Andrew E. Yagle, Bernard C. Levy
Layer-stripping solutions of multidimensional inverse scattering problems
Journal of Mathematical Physics
1986

[14] Arieh Iserles
A First Course in the Numerical Analysis of Differential Equations
Cambridge University Press
1996

[15] B.D.O. Anderson, T. Kailath
Fast Algorithms for the Integral Equations of the Inverse Scattering Problem
Birkhäuser Verlag Basel
Integral Equations and Operator Theory
Vol. 1.1 1978

[16] M. Bertero, E.R. Pike
Inverse Problems in Scattering and Imaging
Adam Hilger, Bristol, Philadelphia, New York
IOP Publishing Limited 1992

[17] D. Colton, R. Kress
Integral Equation Methods in Inverse Scattering Theory
Society for Industrial and Applied Mathematics
20 March 2014

[18] Andrew E. Yagle, Poovendran Raadhakrishnan
Numerical performance of layer stripping algorithms for two-dimensional inverse scattering problems
IOP Publishing Ltd
1992

[19] Mark H. Holmes
Introduction to Perturbation Methods
Springer Science+Business Media New York
2013

[20] T. Kailath, L.Ljung, M. Morf
Generalized Krein-Levinson Equations for the Efficient Computation of Fredholm Resolvents of Nondisplacement Kernels
Surveys in Mathematical Analysis: Essays Dedicated to M.G. Krein, New York: Academic Press,
1978

Appendix

Distributions

In the thesis, with the use of plane waves and Green's functions, it was necessary to employ the theory of distributions (or generalised functions). Our point of reference was [12]; however, for the benefit of the reader, we also provide a brief exposition in the appendix (which is very closely related to the material in the aforementioned reference).

The idea behind distributions is that we consider

$$\langle u, \phi \rangle = \int_{\mathbb{R}^n} u(x)\phi(x)\,\mathrm{d}x$$

as a function of all possible *test functions* $\phi \in C_c^\infty(\mathbb{R}^n)$. In particular, we consider the mapping

$$\begin{aligned} T_u : C_c^\infty(\mathbb{R}^n) &\to \mathbb{C} \\ \phi &\mapsto \int_{\mathbb{R}^n} u(x)\phi(x)\,\mathrm{d}x. \end{aligned}$$

Before we define the space of distributions, we must first give the necessary conditions for convergence in the space of test functions:

Definition 43 (Test Functions)**.** *Let ϕ and $\phi_n \in C_c^\infty(\Omega)$, for $n \in \mathbb{N}$ and $\Omega \subset \mathbb{R}^n$ open. Then $\lim_{n\to\infty} \phi_n = \phi$ in $C_0^\infty(\Omega)$ if and only if*

(a) there exists a compact subset $K \subset \Omega$ such that $\operatorname{supp} \phi_n \subset K$ for all $n \in \mathbb{N}$;

(b) for every $\alpha \in \mathbb{N}^n$, $\partial^\alpha \phi_n \to \partial^\alpha \phi$ uniformly on Ω.

Now we are ready to define the class of distributions:

Definition 44 (Distributions)**.** *Let Ω be an open subset of $\mathbb{R}^n$. A distribution on Ω is a linear functional T on $C_c^\infty(\Omega)$ that is also continuous in the sense that*

$$\lim_{n\to\infty} \langle T, \phi_n \rangle = \langle T, \phi \rangle \qquad \text{as} \qquad \lim_{n\to\infty} \phi_n = \phi \text{ in } C_c^\infty(\Omega).$$

We denote the space of distributions on Ω by $\mathcal{D}'(\Omega)$.

Note that Laurent Schwartz, the founding father of the modern theory of distributions, defined $C_c^\infty(\Omega) =: \mathcal{D}(\Omega)$ and in this way the $\mathcal{D}'$ notation makes sense, since it is the dual space of $\mathcal{D}$.

A more practical way to prove that a linear functional defines a distribution is to utilise the following theorem:

Theorem 45. *A linear functional $T : C_c^\infty(\Omega) \to \mathbb{C}$ belongs to $\mathcal{D}'(\Omega)$ if and only if for every compact subset $K \subset \Omega$ there exists a constant $C_K > 0$ and an order of differentiation $k \in \mathbb{N}_0$ such that*

$$|\langle T, \phi \rangle| \leq C_K \|\phi\|_{C^k} \qquad (\phi \in C_c^\infty(K)),$$

where the C^k norm is defined by

$$\|\phi\|_{C^k} := \sup_{|\alpha| \leq k, x \in \Omega} |\partial^\alpha \phi(x)|.$$

[12]

Theorem 46. *For every $f \in L^1_{loc}(\Omega)$,*

$$\langle T_u, \phi \rangle = \int_\Omega u(x)\phi(x)\,\mathrm{d}x \qquad (\phi \in C_c^\infty(\Omega))$$

defines a distribution $u = T_u$ on Ω.[12]

Example 47 (Principal Value)**.** *The principal value*

$$\mathrm{P.V.}\left(\frac{1}{x}\right) : C_c^\infty(\mathbb{R}) \to \mathbb{C}$$

is the distribution defined by

$$\left\langle \mathrm{P.V.}\left(\frac{1}{x}\right), \phi \right\rangle = \lim_{\varepsilon \downarrow 0} \int_{|x|>\varepsilon} \frac{\phi(x)}{x}\,\mathrm{d}x.$$

We now define another class of test functions:

Definition 48. *Let $(\phi_n)_{n\in\mathbb{N}} \subset C^\infty(\Omega)$ and $\phi \in C^\infty(\Omega)$. Then*

$$\phi_n \xrightarrow{n\to\infty} \phi \text{ in } C^\infty(\Omega)$$

if for all $\alpha \in \mathbb{N}^n$ and $K \subset \Omega$ compact

$$(\partial^\alpha \phi_n) \xrightarrow{n\to\infty} \partial^\alpha \phi \text{ uniformly on } K.$$

In the style of Laurent Schwartz, we may also write $\mathcal{E}(\Omega) := C^\infty(\Omega)$.

Definition 49 (Distributions with Compact Support)**.** *A linear functional $T : C^\infty(\Omega) \to \mathbb{C}$ is continuous if $\langle T, \phi_n \rangle = \langle T, \phi \rangle$ whenever $\phi_n \to \phi$ in $C^\infty(\Omega)$ as $n \to \infty$. We denote the space of all such linear functionals as $\mathcal{E}'(\Omega)$.*

Let $(T_n)_{n\in\mathbb{N}} \subset \mathcal{E}'(\Omega)$ and $T \in \mathcal{E}'(\Omega)$, $T_n \to T$ in $\mathcal{E}'(\Omega)$ as $n \to \infty$ if $\langle T_n, \phi \rangle \to \langle T, \phi \rangle$ in $\mathbb{C}$ for all $\phi \in C^\infty(\Omega)$.[12]

The following theorem provides the justification for referring to the aforementioned linear functionals belonging to $\mathcal{E}'(\Omega)$ as the *distributions with compact support*:

Theorem 50. *Let $T \in \mathcal{D}'(\Omega)$. Then $T \in \mathcal{E}'(\Omega)$ if and only if $\operatorname{supp} T \subset \Omega$ is compact. Moreover, T is of finite order and there exists $C > 0$ and $k \in \mathbb{N}_0$ such that*

$$|\langle T, \phi \rangle| \le C\|\chi\phi\|_{C^k}$$

for all $\phi \in C^\infty(\Omega)$ and $\chi \in C_c^\infty(\Omega)$ such that $\chi = 1$ on an open neighbourhood of $\operatorname{supp} T$.

Proof. For the proof we refer to [12]. □

The following class of test functions we define are the functions of rapid decay, which are also called Schwartz functions:

Definition 51 (Schwartz Functions)**.** *We define the Schwartz functions as*

$$\mathcal{S}(\mathbb{R}^n) := \{\phi \in C^\infty(\mathbb{R}^n) : x \mapsto x^\beta \partial^\alpha \phi(x) \text{ is bounded for all } \alpha, \beta \in \mathbb{N}^n\}.$$

Let $(\phi_n)_{n\in\mathbb{N}} \subset \mathcal{S}(\mathbb{R}^n)$ and $\phi \in \mathcal{S}(\mathbb{R}^n)$. Then $\phi_n \to \phi$ in $\mathcal{S}(\mathbb{R}^n)$ as $n \to \infty$ if,

$$(x^\beta \partial^\alpha \phi_n) \xrightarrow{n\to\infty} x^\beta \partial^\alpha \phi \text{ uniformly on } \mathbb{R}^n$$

for all $\alpha, \beta \in \mathbb{N}^n$.

In particular, we may endow $\mathcal{S}(\mathbb{R}^n)$ with the locally convex topology induced by the norms

$$\phi \mapsto \|\phi\|_{\mathcal{S}(k,N)} := \sup_{|\alpha|\le k, |\beta| \le N, x\in\mathbb{R}^n} |x^\beta \partial^\alpha \phi(x)|.$$

Definition 52 (Tempered Distributions)**.** *The tempered distributions on $\mathbb{R}^n$ are the continuous linear functionals $T : \mathcal{S}(\mathbb{R}^n) \to \mathbb{C}$. We denote the space of all tempered distributions by $\mathcal{S}'(\mathbb{R}^n)$.*

In particular, if $(T_n)_{n\in\mathbb{N}} \subset \mathcal{S}'(\mathbb{R}^n)$ and $T \in \mathcal{S}'(\mathbb{R}^n)$, then

$$T_n \xrightarrow{n\to\infty} T \text{ in } \mathcal{S}'(\mathbb{R}^n)$$

if $\langle T_n, \phi \rangle \xrightarrow{n\to\infty} \langle T, \phi \rangle$ in $\mathbb{C}$ for all $\phi \in \mathcal{S}(\mathbb{R}^n)$.

Remark. *Note that*

$$C_c^\infty(\mathbb{R}^n) \hookrightarrow \mathcal{S}(\mathbb{R}^n) \hookrightarrow C^\infty(\mathbb{R}^n)$$

with continuous inclusion maps.

We also have the continuous inclusions

$$\mathcal{E}'(\mathbb{R}^n) \hookrightarrow \mathcal{S}'(\mathbb{R}^n) \hookrightarrow \mathcal{D}'(\mathbb{R}^n).$$

[12]

The following two examples are distributions (or more specifically, tempered distributions), which we employ frequently in the thesis:

Example 53 (Dirac Distribution)**.** *The Dirac delta distribution $\delta \in \mathcal{S}'(\mathbb{R}^n)$ is the tempered distribution defined by*

$$\begin{aligned} \delta : \mathcal{S}(\mathbb{R}^n) &\to \mathbb{C} \\ \phi &\mapsto \phi(0). \end{aligned}$$

Note also that $\operatorname{supp}\delta = \{0\}$.

In particular, the Dirac delta distribution, with support at a single point, represents an impulse within the context of wave propagation at least.

Example 54 (Heaviside Function)**.** *The Heaviside function $H \in \mathcal{S}'(\mathbb{R})$ is defined as the characteristic function of the interval $[0, \infty)$.*

Matlab Code

Below we provide the Matlab code for the single pass of the Layer Stripping algorithm and the full "Layer Stripping"algorithm respectively, updating in time, with example parameters (which may be changed at the convenience of the reader). In particular, these, together with the Whittaker-Shannon interpolation formula (for which we already provided the code), were the more successfully implemented algorithms.

Single Pass of the Layer Stripping Algorithm (in time):

```
%% Parameters

L = 5; % size of domain
T = 5; % measurement time
dx = 1e-2; % position step
dt = 1e-3; % time step
x0 = 0; % point of measurement
c = 1; % wave speed profile

%% More Parameters

t = 0:dt:T; % time vector
x = (0:dx:L)'; % position vector
nt = length(t);
nx = length(x);
mu = dt/dx;
Lx = (1/dx^2)*spdiags(ones(nx,1)*[1 -2 1],-1:1,nx,nx); % Laplacian
I = eye(nx,nx); % identity matrix
A = spdiags(ones(nx,1)*[-1 1 0],-1:1,nx,nx); % finite difference matrix
phi = @(x) (x>0).*exp(-1./x.^2);
R = @(x) phi(x).*phi(1-x); % scattering potential
r = R(x-2); % example scattering potential

%% Solve Plasma Wave Equation and get Data

u = zeros(nx,nt); % preallocate memory
uw = zeros(nx,nt);
```

```
% initial conditions
u(:,1) = sinc((x-x0)/dx);
u(:,2) = sinc((x-x0)/dx);
for k = 2:nt-1
    u(:,k+1) = 2*u(:,k) - u(:,k-1) + dt^2*Lx*u(:,k) - dt^2*r.*u(:,k);
end
data = u(x==x0,:); % acquire data

%% Solve Backwards Advection Equation (via Crank-Nicolson)

v = zeros(nx,nt); % preallocate memory
v(:,nt) = sinc((x-x0)/dx); % final condition
v(1,:) = 2*gradient(data)/dt; % observation of scattered field
for n = nt:-1:2
    v(:,n-1) = (I+(c/2)*mu*A)\(I-(c/2)*mu*A)*v(:,n);
end

%% Reconstruct Scattering Potential

[xq,yq] = meshgrid(x,x); % create mesh grid
vs = interp2(t,x,v,xq,yq); % interpolate t onto x
rc = -2*diag(vs); % reconstructed potential
```

"Layer Stripping" Algorithm (in time):

```
%% Parameters

L = 5; % size of domain
T = 5; % measurement time
dx = 1e-2; % position step
dt = 1e-3; % time step
x0 = 5; % point of measurement
c = 1; % wave speed

%% More Parameters

t = 0:dt:T; % time vector
x = (0:dx:L)'; % position vector
nt = length(t);
nx = length(x);
Lx = (1/dx^2)*spdiags(ones(nx,1)*[1 -2 1],-1:1,nx,nx); % Laplacian
mu = dt/dx;
I = eye(nx,nx); % identity matrix
A = spdiags(ones(nx,1)*[-1 1 0],-1:1,nx,nx); % finite difference matrix
phi = @(x) (x>0).*exp(-1./x.^2);
R = @(x) phi(x).*phi(1-x);
r = R(x-2); % example scattering potential

%% Solve Plasma Wave Equation & Get Data

us = zeros(nx,nt); % preallocate memory
% initial conditions
us(:,1) = sinc((x-x0)/dx);
us(:,2) = sinc((x-x0)/dx);
for k = 2:nt-1
    us(:,k+1) = 2*us(:,k) - us(:,k-1) + dt^2*Lx*us(:,k) - dt^2*r.*us(:,k);
end
data = us(x==x0,:); % sample data

%% Solve Forward Advection Equation

% preallocate memory
```

```
u = zeros(nx,nt);
v = zeros(nx,nt);
% initial conditions in time
u(:,1) = sinc((x-x0)/dx);
v(:,1) = sinc((x-x0)/dx);
u(1,:) = data; % observation of the scattered field
for i = 1:nx-1
    u(:,i+1) = ((1/(c*dt))*I+(1/dx)*A)\((1/(c*dt))*u(:,i)+v(:,i));
end

%% Solve Backwards Advection Equation #2

v = zeros(nx,nt); % preallocate memory
v(1,:) = (2/c)*gradient(data); % observation of scattered field
for j = nt:-1:2
    v(:,j-1) = ((1/dx)*A+(1/(c*dt))*I)\((1/(c*dt))*v(:,j)+r.*u(:,j));
end

%% Construct Scattering Potential

[xq,yq] = meshgrid(x,x); % create mesh grid
vs = interp2(t,x,v,xq,yq); % interpolate t onto x
rn = -2*diag(vs); % reconstructed potential
```

For additional code used in the thesis (for example, the layer stripping algorithm which updates in space), you may contact me via `kemalraik@hotmail.com`.

Notation

Glossary

Symbol	Description
$\mathbb{R}^n$	n-dimensional Euclidean vector space of real numbers
$\mathbb{S}^n$	sphere of dimension $n-1$. Note that $\mathbb{S}$ is the circle and $\mathbb{S}^2$ is the sphere.
$\mathbb{C}$	complex field. In particular, $\mathbb{C} \cong \mathbb{R}^2$
$\mathbb{Z}$	set of integers, i.e. $\mathbb{Z} = \{..., -2, -1, 0, 1, 2, ...\}$
$\mathbb{N}$	set of natural numbers, i.e. $\mathbb{N} = \{1, 2, 3, ...\}$
$\mathbb{R}_+$	the set of positive real numbers
$\mathbb{D}$	the domain of the scattering potential
x	one dimensional real valued vector
i	imaginary unit
$\boldsymbol{x}$	bold symbol refers to a vector of dimension n, where $\boldsymbol{x} = (x_1, x_2, \cdots, x_n)$.
$\lvert\cdot\rvert$	absolute value
$\lVert\cdot\rVert$	Euclidean norm, i.e. $\lVert\boldsymbol{x}\rVert = \sqrt{x_1^2 + \cdots x_n^2}$.
A, B,...	operators
$\lVert\cdot\rVert_{\text{op}}$	operator norm
Ω	open set in $\mathbb{R}^n$
$\mathbb{1}_A$	indicator function which is equal to 1 on the set A and is 0 everywhere else.
$\mathrm{d}^n/\mathrm{d}x^n$	the n-th derivative with respect to x
$\partial^n/\partial x^n$	n-th partial derivative with respect to x
∇	gradient, i.e. $\nabla = \left(\frac{\partial}{\partial x_1}, \cdots \frac{\partial}{\partial x_n}\right)$
Δ	on a function, the Laplace operator, $\Delta = \nabla \cdot \nabla = \sum_{i=1}^n \frac{\partial^2}{\partial x_i}$. On a variable, this is a step
$\otimes$	tensor product, e.g. if $f : X \to \mathbb{C}$, $g : Y \to \mathbb{C}$, then $(f \otimes g)(x, y) = f(x)g(y)$ with $x \in X$, $y \in Y$
$\oplus$	direct sum
$\cdot$	dot product, e.g. $\boldsymbol{x} \cdot \boldsymbol{y} = x_1 y_1 + \cdots + x_n y_n$
$'$	X is a topological vector space, then we denote by X' its dual space. For functions, f' is the derivative
$\cong$	isomorphic to
$\sim$	asymptotically equal to
$\approx$	approximately equal to
$*$	convolution of functions or adjoint of an operator
$\to$	"converges to"for sequences and "to"for functions
$\mapsto$	maps to
$\hookrightarrow$	inclusion map or embedding
$\gg, \ll$	e.g. "$x \gg y$" $\iff \exists C > 0$ large s.t. $x > Cy$
$\hat{}$, $\mathcal{F}$	Fourier transform, with positive complex exponent and no normalising constant
$\check{}$, $\mathcal{F}^{-1}$	inverse Fourier transform, with negative exponent and a normalising constant
$\emptyset$	empty set
σ_p	point/discrete spectrum, i.e. the set of eigenvalues

"Big O"& "Small o"Notation

Since scattering theory is concerned with asymptotics, we must refer to the orders of our asymptotic expansions and for this we employ the $\mathcal{O}$ and o notation ("big O"and "small o"respectively).

We say that $f = \mathcal{O}(\psi)$ as $\varepsilon \downarrow \varepsilon_0$ if there exists constants C and ε_1 (not depending on ε) such that

$$|f(\varepsilon)| \leq C|\psi(\varepsilon)|,$$

for $\varepsilon_0 < \varepsilon < \varepsilon_1$.

Then, $f = o(\psi)$ as $\varepsilon \downarrow \varepsilon_0$ if for all positive $\lambda > 0$ there exists ε_2 (not depending on ε) such that

$$|f(\varepsilon)| \leq \lambda|\psi(\varepsilon)|,$$

for $\varepsilon_0 < \varepsilon < \varepsilon_2$.

For a detailed exposition of asymptotic analysis, we refer the reader to [19].